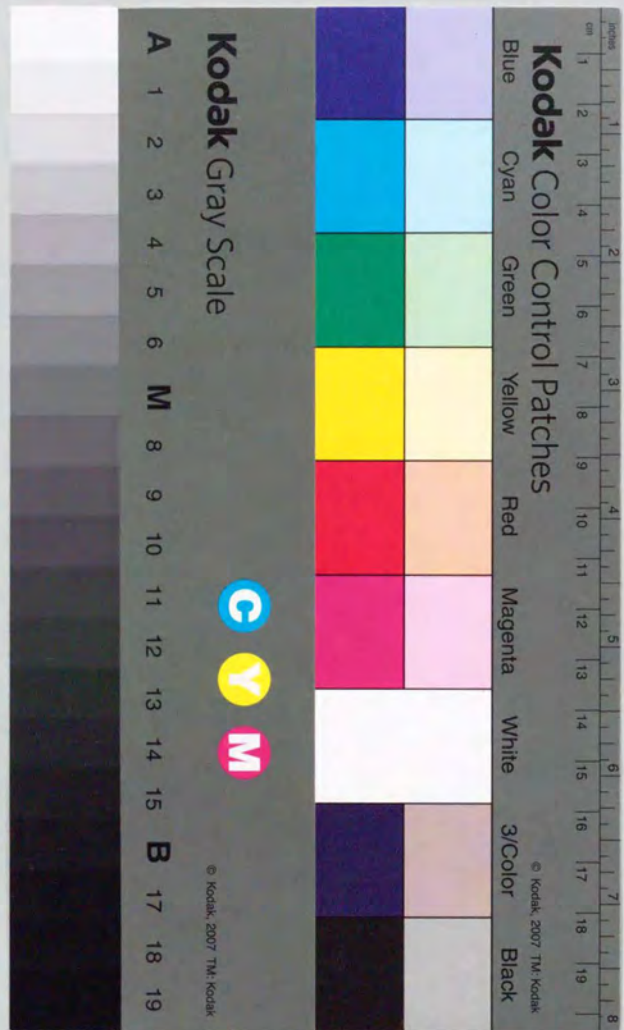

反応性スパッタリングによるTiO2形成プロセスの解析

ANALYSIS OF REACTIVE SPUTTERING DEPOSITION PROCESS OF TiO_2 FILMS

草 野 英 二

ANALYSIS OF REACTIVE SPUTTERING DEPOSITION PROCESS OF TiO_2 FILMS

by

Eiji KUSANO

December 1992

ABSTRACT

Reactive sputtering is a technique to deposit compound films such as oxide, nitride, *etc*. It is well known that in reactive sputtering there are two operation modes:metal mode and compound mode. The transition between the two modes is generally avalanche-like and nonlinear to reactive gas flow rate, and further shows hysteresis versus reactive gas flow rate. The nonlinear transition and hysteresis reduce controllability and reproducibility of the reactive sputtering process when it is operated in the near-transition region. Therefore, it is thought to be crucial to reveal mechanisms involved in mode transition and hysteresis in order to improve stability and reproducibility of reactive sputtering.

In this thesis the formation process of TiO_2 films is investigated and discussed to reveal mechanisms of mode transition and hysteresis. An investigation of the time-dependent process condition is first made. The time-dependent process changes are clearly observed, and effects of pimping speed and Ar/O_2 ratio are discussed. The obtained results show a strong dependence of time-dependent target condition changes on these two factors. Gettering effects are also investigated quantitatively. The role of gettering in the total mass balance changes has been discussed in relation to the evacuation of reactive gas by the vacuum pumping system. Most importantly, effects of pumping speed and sputtering current on mode transition and hysteresis have been discussed. It is shown that hysteresis width decreases at a higher pumping speed or a lower sputtering current. The systematic investigations reveal that the origin of the hysteresis behavior is the difference of gettering capacity between metal mode and compound mode. Throughout the discussion, it is emphasized that reactive gas gettering plays an important role in the total mass balance changes in the reactive sputtering process.

On the basis of discussion of results obtained experimentally, a model simulating mode transition and hysteresis is proposed. The model is based on the physical mechanisms involved in target and wall behaviors. This enables us to calculate time-dependent condition change until the process reach a steady-state without assuming anything how the process reaches a steady-state. Another important feature of the model is that hysteresis can be obtained as a result of the calculations of the time-dependent target condition changes, as an actual process is so. In the time-dependent condition change calculations, changes in target coverage, sputtered flux, and reactive gas partial pressure are clearly shown. Effects of reactive gas mass flow rate, pumping speed, and sputtering current on target coverage changes are also shown as a function of elapsed time. Hysteresis curves are obtained as a consequence of time-dependent calculations as a function of reactive gas mass flow rate. It is further shown by the simulation that the width of hysteresis strongly depends on pumping

speed and sputtering current. Results obtained by the model calculation are in accord with those obtained experimentally, suggesting that the hypothesis used to develop simulation program is appropriate.

The research reveals the important roles of reactive gas gettering in mass balance change and mechanisms of mode transition and hysteresis. In addition, it is theoretically explained that although hysteresis cannot be eliminated as far as there is the difference in sputtering yields of a metallic target and a compound-covered target, it is possible to suppress hysteresis by increasing pumping speed or decreasing sputtering current or power. It is believed that the results obtained in this research are crucial to improve stability and reproducibility of reactive sputtering processes.

ACKNOWLEDGEMENTS

I would like to thank Mr.K.Koizumi and Mr.K.Enjouji for their assistance in progressing the research at Tsukuba Research Laboratory of Nippon Sheet Glass Co., Ltd. and also Mr.H.Nakai, Mr.E.Ogino, Mr.M.Ueda, and Mr.Y.Yamamoto for their fruitful suggestion for me to progress in the research. In addition, I would like to acknowledge Ms.K.Nakamura, who analyzed deposited films to obtain their composition data used in Chapter IV.

In particular, I would like to express my deepest appreciation to John A.Thornton who let me start research in reactive sputtering and taught me not only thin film physics but also physical approach to solve the problems.

Finally, I would like to acknowledge Dr.A.Kinbara, who always encouraged me in completing a series of studies on reactive sputtering process analysis.

CONTENTS

I INTRODUCTION
I.I REACTIVE SPUTTERING 1
I.II BACKGROUND OF RESEARCH
A. HISTORICAL REVIEW OF RESEARCH ON MECHANISMS OF REACTIVE SPUTTERING 2
B. DEFICIENCIES IN CURRENT UNDERSTANDINGS 9
I.III OBJECTIVE OF RESEARCH 11
I.IV REFERENCES 13

II APPARATUS
II.I APPARATUS 15
II.II DETERMINATION OF O_2 PARTIAL PRESSURE 15

III INVESTIGATION OF TIME-DEPENDENT TARGET CONDITION CHANGE
III.I INTRODUCTION 19
III.II EXPERIMENTAL METHOD 20
III.III RESULTS 21
A. TIME-DEPENDENT CONDITION CHANGES 21
B. EFFECTS OF PUMPING SPEED AND Ar/O2 PRESSURE RATIO 23
III.IV DISCUSSION
A. TIME-DEPENDENT CONDITION CHANGES 23
B. EFFECTS OF PUMPING SPEED AND Ar/O2 PRESSURE RATIO 26
III.V CONCLUSIONS 27
III.VI REFERENCES 28

IV QUANTITATIVE ESTIMATION OF GETTERING
IV.I INTRODUCTION 29
IV.II EXPERIMENTAL METHOD 29
V.III RESULTS 30

IV.IV DISCUSSION
A. GETTERING BEHAVIOR 35
B. QUANTITATIVE ANALYSIS OF PROCESS TRANSITION 37
IV.V CONCLUSIONS 39
IV.VI REFERENCES 40

V INVESTIGATION OF HYSTERESIS EFFECTS AS A FUNCTION OF PUMPING SPEED, SPUTTERING CURRENT, AND O_2/Ar PRESSURE RATIO
V.I INTRODUCTION 41
V.II EXPERIMENTAL METHOD 42
V.III RESULTS
A. HYSTERESIS INVESTIGATION 42
B. EFFECTS OF PUMPING SPEED 47
C. EFFECTS OF SPUTTERING CURRENT 47
D. EFFECTS OF O_2/Ar PRESSURE RATIO 49
V.IV DISCUSSION
A. HYSTERESIS 49
B. EFFECTS OF PUMPING SPEED, SPUTTERING CURRENT, AND O_2/Ar PRESSURE RATIO ON HYSTERESIS 51
V.V CONCLUSIONS 54
V.VI REFERENCES 56

VI MODELING OF TIME-DEPENDENT PROCESS CHANGE AND HYSTERESIS
VI.I INTRODUCTION 57
VI.II THEORETICAL BASIS 58
VI.III PROGRAM 62
VI.IV CALCULATION RESULTS
A. TIME-DEPENDENT PROCESS CHANGES 63
B. HYSTERESIS 70
VI.V DISCUSSION
A. APPROPRIATENESS OF SIMULATION MODEL 70
B. MASS BALANCE CHANGE DURING COMPOUND-LAYER FORMATION, AND SPUTTERING-ETCHING 75
C. MECHANISMS OF HYSTERESIS 76
VI.VI CONCLUSIONS 77
VI.VII REFERENCES 79

VII CONCLUSIONS 81

VIII APPENDIX
VIII.I HYSTERESIS SIMULATION PROGRAM 85

LIST OF TABLES AND FIGURES

Table 1. The magnitude of changes in process condition parameters at the mode transition.

Fig.2.1 A schematic drawing of the experimental apparatus.

Fig.3.1 Typical results of time-dependent process condition changes.

Fig.3.2 Changes in plasma emission spectra with elapsed time after glow discharge ignition.

Fig.3.3 Time to reach a steady state as a function of S_p ;the time is defined as a time to reach a sharp bend point of I_{Ti} changes in time-dependent process changes.

Fig.3.4 Time constant of compound layer formation at target surface as a function of S_p.

Fig.3.5 Time to reach a steady state as a function of Ar/O_2 ratio;the time is defined as a time to reach a sharp bend point of I_{Ti} changes in time-dependent process changes.

Fig.3.6 Time constant of compound layer formation at target surface as a function of Ar/O_2 ratio.

Fig.4.1 O_2 partial pressure change on discharge ignition as a function of O_2 partial pressure prior to discharge ignition.

Fig.4.2 The amount of gettered O_2 and ratio of gettered/introduced O_2 amount as a function of O_2 partial pressure prior to discharge ignition.

Fig.4.3 Calculated getter pumping speed for O_2 as a function of O_2 partial pressure prior to discharge ignition.

Fig.4.4 Sputtering yield and mass deposition rate obtained from film composition analysis as a function of O_2 partial pressure prior to discharge ignition.

Fig.4.5 O/Ti atomic ratio in deposited films as a function of O_2 partial pressure prior to discharge ignition.

Fig.4.6 Relationship between the gettered amounts of O_2 obtained from pressure change and film composition analysis.

Fig.4.7 Oxygen flux and Ti flux onto the deposition area on the wall surface and their ratio as a function of O_2 partial pressure prior to discharge ignition.

Fig.4.8 Adsorbed/incident O_2 flux ratio calculated from the amount of gettered oxygen and oxygen flux intensity as a function of O_2 partial pressure prior to discharge ignition.

Fig.5.1 Typical hysteresis curves observed at a pumping speed of $0.20X10^{-1}$ m^3/s and with a sputtering current of 2.0 A :(a)Ti emission intensity (b)Mass deposition rate (c)cathode voltage (d)O_2 partial pressure.

Fig.5.2 Emission spectra with increasing and decreasing Q_{O2} at I_{sp}=2A and S_p=$2.0X10^{-1}$ m^3/s.

Fig.5.3 The effect of pumping speed on the transition points as a function of O_2 flow rate :o increasing O_2 flow rate :• decreasing O_2 flow rate.

Fig.5.4 Oxygen partial pressure at the transition onsets versus pumping speed at a sputtering current of 2.0A:o increasing O_2 flow rate :• decreasing O_2 flow rate.

Fig.5.5 Titanium emission intensity at the transition onsets at a sputtering current of 2.0A:o increasing O_2 flow rate :• decreasing O_2 flow rate.

Fig.5.6 Mass deposition rate at the transition onsets at a sputtering current of 2.0A: o increasing O_2 flow rate :• decreasing O_2 flow rate.

Fig.5.7 The effect of sputtering current on the transition points as a function of O_2 flow rate at a pumping speed of $4.0X10^{-1}$ m^3/s :o increasing O_2 flow rate :• decreasing O_2 flow rate.

Fig.5.8 Hysteresis curves of Ti emission intensity at various sputtering current : (a)I_{sp}=3.0A (b)I_{sp}=2.0A (c)I_{sp}=1.0A (d)I_{sp}=0.5A.

Fig.5.9 The effect of Ar partial pressure on the transition points as a function of O_2 flow rate at a pumping speed of $1.9X10^{-1}$ m^3/s and at a sputtering current of 2A : o increasing O_2 flow rate :• decreasing O_2 flow rate.

Fig.6.1 Schematic of reactive gas flow in reactive sputtering system.

Fig.6.2 Typical compound-layer formation calculation results for S_p=$1.5X10^{-1}$ m^3/s, Q_{in}=5.0 std.cm^3/min, and I_{sp}=2.0 A.

Fig.6.3 Typical compound-layer formation calculation results for S_p=$1.5X10^{-1}$ m^3/s, Q_{in}=8.0 std.cm^3/min, and I_{sp}=2.0 A.

Fig.6.4 Typical sputter etching calculation results for S_p=$1.5X10^{-1}$ m^3/s, Q_{in}=7.0 std.cm^3/min, and I_{sp}=2.0 A.

Fig.6.5 Typical sputter etching calculation results for S_p=$1.5X10^{-1}$ m^3/s, Q_{in}=3.0 std.cm^3/min, and I_{sp}=2.0 A.

Fig.6.6 Results of compound-layer formation calculation for various Q_{in} at I_{sp}=2.0 A and S_p=$1.5x10^{-1}$ m^3/s.

Fig.6.7 Results of sputter etching calculation for various Q_{in} at I_{sp}=2.0 A and S_p=$1.5x10^{-1}$ m^3/s.

Fig.6.8 Results of compound-layer formation calculation for various S_p at Q_{in}=8.0 std.cm^3/min and I_{sp}=2.0 A.

Fig.6.9 Results of sputter etching calculation for various S_p at Q_{in}=6.0 std.cm^3/min and I_{sp}=2.0 A.

Fig.6.10 Results of compound-layer formation calculation for various I_{sp} at Q_{in}=4.0 std.cm^3/min and S_p=$1.5x10^{-1}$ m^3/s.

Fig.6.11 Results of sputter etching calculation for various I_{sp} at Q_{in}=4.0 std.cm^3/min and S_p=1.5x10^{-1} m^3/s.

Fig.6.12 A typical hysteresis result at S_p=2.0X10^{-1}m^3/s, S_g=6.0X10^{-1}m^3/s, I_{sp}=2.0A, Y_m=0.32, and Y_c=0.015.

Fig.6.13 Results of hysteresis calculation for various S_p at I_{sp}=2.0A, S_g=3.0X10^{-1}m^3/s, Y_m=0.32, and Y_c=0.015.

Fig.6.14 Shift of mode transition points as a function of pumping speed, S_p.

Fig.6.15 Results of hysteresis calculation for various I_{sp} at S_p=3.0X10^{-1}m^3/s, S_g=3.0X10^{-1} m^3/s, Y_m=0.32, and Y_c=0.015.

Fig.6.16 Shift of transition points as a function of sputtering current, I_{sp}.

Fig.6.17 Results of hysteresis calculation for various Y_c at S_p=3.0X10^{-1}m^3/s, S_g=3.0X10^{-1} m^3/s, I_{sp}=2.0 A, and Y_m=0.32.

I. INTRODUCTION

I.I. REACTIVE SPUTTERING

Initially, the term "sputtering" referred to the phenomena that target material was ejected as a result of the interaction between impinging ion and target atoms, and the subsequent interaction amongst the latter[1]. However, nowadays especially in the field of thin film technologies, it refers to deposition of sputtered target materials onto substrate that locates typically on the opposite side of the target. The deposition process has currently been the main application of sputtering in industrial fields. This process has an advantage to deposit films with high adhesion to the substrate and with a high density without heating substrates. Furthermore, it is possible to obtain uniform coatings onto substrates with a large surface area by using planar magnetron method.

Recently as demand for thin films has been increased, the importance of sputtering deposition has been greatly increased, especially in the fields of electronics, optics, and hard coatings. Progresses in vacuum apparatus including pressure gauges, gas flow control systems, *etc*., have also supported for this method to be applied for industrial purposes.

Reactive sputtering is one technique involved in sputtering. In this process target that is nominally pure metal or alloy is sputtered in an atmosphere of reactive and inert gas mixtures. Sputtered target material reacts with reactive gas(*e.g.*, O_2, N_2, *etc*.) on the substrate, resulting in formation of compound films. A variety of compounds such as oxide, nitride, carbide, *etc*., have been deposited by this method. Today, applications of reactive sputtering have been widened to fields of electronics, optics, hard coatings, decorative coatings, *etc*. Still importance of reactive sputtering is drastically increasing.

In reactive sputtering it is known that there are two operation modes:metal mode and compound mode. In metal mode, the target surface is kept metallic, and metallic films are deposited. On the other hand, in compound mode the target surface is covered by compound layers, and compound films are deposited. The condition of target covered by compound layers is sometimes referred as "poisoned." The transition between two operation modes is generally exhibited in the relation between total pressure or mass deposition rate and reactive gas flow rate. The transition is avalanche-like and nonlinear. The point where the mode transition occurs when the reactive gas flow rate is increased is different from the point where the transition of the reverse direction occurred when the reactive gas flow rate is decreased. This behavior is well known as a hysteresis behavior.

Since mode transition and hysteresis affect process operation conditions strongly, understanding of their mechanisms is though to be crucial to deposit films with sufficient properties. Although many efforts have been made to understand mechanisms of mode transition and hysteresis in reactive sputtering, they have not been well understood. The reason may

be due to the complexity of phenomena involved in reactive sputtering. Therefore, a systematic study to reveal mechanisms involved in mode transition and hysteresis effects is indispensable to improve reactive sputtering process and widen its applications.

I.II. BACKGROUND

A. HISTORICAL REVIEW OF RESEARCH ON MECHANISMS IN REACTIVE SPUTTERING

In early years of the research on reactive sputtering, only compound formation (oxidation, nitridation, *etc.*) on target surface was in interests due to its effects on the decrease in etching or sputtering rates.

The first report relating with mechanisms of reactive sputtering was given by Greiner on rf sputter etching in O_2[2]. He assumed that the sputter and oxidation rates were independent and concurrent and indicated that the rate of change in target oxide thickness was given by:

$$dx/dt=R_{ox}-R_{sp} \quad (1.1)$$

where R_{ox} is the oxidation rate and R_{sp} is the sputter rate of the target. At the equilibrium, dx/dt reaches 0 and no further changes occur in target oxide thickness.

Then in 1973 the report focusing on mechanisms involved in reactive sputtering was given by J.Heller[3]. He reported a model for the reactive sputtering of a metal in an oxygen containing glow discharge. In the model spontaneous oxide formation on the target surface and a sharp decrease of the sputtering rate were explained to occur at a definite oxygen partial pressure. The O_2 definite pressure was given as a function of the oxidation rate of the target relative to the sputtering rate.

In the middle 1970's, several authors reported target oxidation models and compared the results obtained by proposed models to experimental results. Goranchev *et al.* proposed in 1976 a qualitative physical model explaining the influence of the oxygen content in the gas flow on the discharge current for reactive cathode sputtering in a dc diode system[4]. They concluded that the increase in the oxygen content affected the discharge current density in two main ways:(i)by the sharp change in secondary ion-electron emission coefficient from the target surface as a result of its oxidation: and (ii)by the influence of the oxygen content on the elementary ionization processes in the discharge region near the cathode as a result of the transition from a glow discharge in a noble gas to a glow discharge in oxygen. It was also shown that the experimental results with targets of different materials under different sputtering conditions were in good agreement with the conclusions from the proposed physical model.

A model that explained deposition rate changes in reactive sputtering of metals in oxygen and nitrogen atmosphere in an argon plasma was proposed by Abe and Yamashina, in

1975[5]. The model is based on the difference between sputtering rate of the metal and its chemical compound, the surface coverage, the sticking probability, and incident flux of reactive gas atoms. The basic equation is:

$$dN/dt=\alpha(P/P_0)^n G(P)(1-N/N_T)-B(N/N_T) \quad (1.2)$$

where P is the partial pressure of the reactive gas, P_0 is a constant related to the limiting pressure, N_T is the total number of active sites on the target surface that can be occupied by reactive gas atoms, N is the number of active sites that are occupied by reactive gas atoms under certain conditions, α is a constant, $\alpha(P/P_0)^n$ is the specific coefficient related to the sticking probability, B is the re-emission rate of reactive gas atoms when the target surface is completely covered with a monolayer of reactive gas atoms, G(P) is the incident flux of reactive gas given by the kinetic theory of gases, and n is the order of the reaction. By giving the value of (α/B), P_0, and n, they calculated normalized sputtering rate for various systems such as Mo-O_2, Ti-O_2, and Ti-N_2. They also investigated Mo-O_2, Mo-N_2, Ti-O_2, and Ti-O_2, and found that was an abrupt decrease in the sputtering rate in each experimental observation. They concluded that they successfully explained reactive sputtering of various metals.

Donaghey *et al.* reported the effect of target oxidation on reactive sputtering rate of Ti in Ar-O_2 plasmas[6]. In their report it was concluded that the threshold of target oxidation was independent of the total plasma pressure and that it was specified uniquely by a critical mole fraction of oxidant in the plasma.

They also reported that the sputter etch rate of the titanium target reached a maximum before the critical oxygen pressure and that the sputter deposition rate decreased sharply at a critical oxygen partial pressure[7]. Furthermore, it was found that the time dependence of the target oxidation process was found to be in qualitative agreement with a target oxidation model.

In 1980, Maniv *et al.* reported that the oxidation was not so sensitive to whether a simple exponential,

$$(dx/dt)_{OX}=K\exp(-x/x_o) \quad (1.3)$$

or a parabolic,

$$(dx/dt)_{OX}=K_1/2x \quad (1.4)$$

rate was assumed[8]. They also reported that the oxygen flow rate where an avalanche-like transition of the target surface condition occurred when O_2 flow rate was increased was different from that observed when O_2 flow rate was decreased after the target oxidation was completed. They further mentioned that, for O_2 flow rate less than the transition point, sputtered metal efficiently getters O_2. However, they did not discuss an origin of this behavior thoroughly. This behavior was later recognized as hysteresis effects in reactive sputtering.

As the existence of the abrupt transition of reactive sputtering process became recognized in late 1970's, some interests became to be taken in to obtain a better process control in reactive sputtering processes. R.McMahon *et al.* first reported a control method by using constant cathode voltage control to obtain an AlN film with stoichiometry and reported mechanisms of the control[9,10]. In their reports, it was revealed that controlled cathode voltage at constant flow rate provided means for stable operation for any degree of target coverage whereas controlled gas flow rates at constant power and controlled power at constant flow rates were found to exhibit runaway transitions associated with target coverage. They developed the model that allowed two distinct mechanisms of target coverage:chemisorption, and ion plating of reactive gas species to the target surface. By the model it was shown that, with the voltage control method, there was a one-to-one relationship between cathode voltage and film stoichiometry and that there was a method for calculating the film composition from the glow discharge characteristics alone.

In 1983 Reith *et al.* reported detailed results of the reactive sputtering of tantalum oxide for various target surfaces and O_2 flow rate conditions by observing partial pressure of O_2 during both reactive and non-reactive depositions[11]. They described the reactive sputtering of Ta in O_2 atmosphere in terms of two inverse reactions at two reactive surfaces: a dissociative reaction proceeded at the target while its inverse proceeded at the substrate. They concluded that a generalized process in which a metal oxide dissociated to a less-stable suboxide at the target, transferred to the substrate as the suboxide, and recombined to form the original target compound was applied for the reactive sputtering of any metal oxide that exhibited preferential sputtering effects.

In middle 1980's more efforts were performed to investigate reactive sputtering process, particularly hysteresis behavior, quantitatively and to reveal mechanisms of hysteresis behavior. More attention was paid to the roll of the gettering at the deposition area to reveal the correlation between target poisoning and gettering.

Hohnke *et al.* developed the model that described the reactive sputtering process in terms of three parameters:the reactive gas flow rate, the sputtering power, and the sputtering yield of the target[12]. The developed model established that the ratio of the sputtering power to the reactive gas flow rate was found to be as a fundamental parameter of reactive sputtering and predicted accurately the magnitude of the ratio for the deposition of such divers films as TiN and Cd_2SnO_4. Further, they first mentioned about the origin of the hysteresis behavior;the usual hysteresis effects mainly depended on intrinsic material properties, i.e., the difference in sputtering yield of the bare and nitrided or oxidized target surface and were weakly modified by varying process conditions. Although they gave a very clear explanation for the hysteresis behavior, their calculation was restricted only for the conditions where stoichio-

metric films were deposited. In addition to this, they did not mention about effects of wall gettering.

At almost the same time, Serikawa and Okamoto gave the report on the effects of N_2 flow rate on Si rf reactive sputtering[13]. They investigated changes in the deposition rate, the sputtering pressure, and the nitrogen concentration in the film. Most important was that they first mentioned the effects of the pumping speed of the vacuum pump system on hysteresis behavior. It was shown that at a high Ar flow rate(high pumping speed) the hysteresis was distinguished. They also showed that the nitrogen partial pressure where the onset of the abrupt process change occurred increased as the sputtering power was increased or the pumping speed was increased. However, they did not consider a role of gettering of reactive gas by sputtered metal.

Later they gave the explanation for the hysteresis formation by obtaining the relationship between the amount of consumed N_2 gas versus N_2 partial pressure[14]. Following their report, some authors mentioned that the hysteresis could be suppressed by increasing pumping speed of the vacuum pump system.

Until Serikawa and Okamoto first mentioned about consumption of reactive gas at chamber wall or substrate, no researcher had mentioned about the role of reactive gas consumption in mass balance changes in reactive sputtering.

Changes in sputtering yields during reactive sputtering have been also reported by several researches. Most of results have been examined in ion-beam sputtering. In 1980, Steinbruchel *et al.* reported the results of sputtering yield measurements of metals and oxides of both Ti and Zr for neutrals and ions by collecting the sputtered species in a noble gas matrix and determining their amounts from optical adsorption spectroscopy[15]. They concluded that the atomic ion fractions for Ti and Zr bombarded by O_2^+ at 2keV are 0.8 and 0.4, respectively, whereas TiO and ZrO are sputtered largely as neutrals. They further reported that ratios of sputtering yields by bombarding 1keV O^+ ion to those by bombarding 1keV Ar^+ ion were about a half for Ti metal target and about one tenth for Zr metal target respectively.

In 1985, Gruen *et al.* examined effects of monolayer coverages on sputtering yield in ion beam sputtering by using laser fluorescence measurement[16]. In their report, it was revealed that Ti sputtering yield decreases as oxygen coverage on target surface was increased. The factor of decrease reported was 6 in the case of three-monolayer oxygen coverage compared to a clean Ti metal surface. Although the primary ion energy(about 3keV) used in their measurements ranged much higher than those of diode sputtering system, the reported results were useful to discuss effects of surface coverage change on sputtering yields in reactive sputtering.

In 1986, Betz and Husinsky also reported the results of investigation of sputtering yield changes under increased O_2 partial pressure conditions by using laser fluorescence

spectroscopy and microbalance weight measurement method[17]. They summarized that sputtering yield decreased when $1X10^{-3}$ Pa of O_2 was introduced by a factor of about 5.1 for Cr, 1.8 for Ta, 2.7 for Ti, and 1.7 for Cu.

In 1984, Lemperiere *et al.* examined Ti−N_2 sputtering and reported that there was the abrupt decrease in deposition rate accompanied with film structure changes[18]. They also proposed a reactive sputtering model that took into account the gettering effects of the deposited material. The model allowed the calculation of the surface coverage of the target by the reactive gas or the metallic compound and the determination of the deposition rate as a function of the reactive gas partial pressure. They obtained good agreement between experimental and theoretical values for the fractional surface coverage. This model is believed to be the first model that dealt with the gettering effects.

In relation with the hysteresis effects, Hmiel discussed the method to develop stable operation in the region where abrupt transition occurred in Ti−N_2 system[19]. He mentioned that there was a negative slope region of the equilibrium mass flow rate versus nitrogen partial pressure curve and that the existence of the negative slope was a phenomenon that could be observed with partial pressure control. It was also reported that the shape of the equilibrium flow versus partial pressure curve and the time response of the system were affected by the configuration of the sensor sampling port, the target, and the nitrogen gas inlet. He concluded that partial pressure control allowed access to pressure region that appeared to make superior TiN films, without hysteresis.

In 1987, Kadlec *et al.* reported results of investigation of effects of pumping speed and cathode power on hysteresis in Ti−N_2 reactive sputtering[20-22]. In their experiments, total pressure was kept constant, so that if N_2 was consumed by gettering, Ar gas flow rates were increased.

They assumed the existence of critical pumping speed to avoid hysteresis effects and gave the critical pumping speed from the calculation. In their calculation, they first gave the relation among masses of reactive gas introduced in the chamber, gettered, and pumped out and the relation between total pressure and N_2 partial pressure by the following equations:

$$\phi_r = p_r S_r + {}^s\phi_r \tag{1.5}$$

$$p_t = k_r p_r + k_i p_i \tag{1.6}$$

where ϕ_r is the mass of reactive gas introduced in the chamber, p_{rp} is reactive gas partial pressure, S_r is pumping speed for reactive gas, ${}^s\phi_r$ is reactive gas gettered by deposited metal atoms, p_T is pressure inside the chamber, p_r is reactive gas partial pressure, p_i is inert gas partial pressure, k_r is gauge sensitivity for reactive gas, k_i is gauge sensitivity for inert gas.

From the equations, the following equation was derived:

$$\frac{dp_r}{d\phi} = \frac{1}{S_r + (d^s\phi/dp_r)} \tag{1.7}$$

This equation meant that under the following conditions, the hysteresis effect could be avoided.

$$S_r + \frac{d^s\phi_r}{dp_r} < 0 \tag{1.8}$$

Therefore, the critical pumping speed to avoid the hysteresis effects was defined by the following equation:

$$S_c = (-d^s\phi/dp_r)\mathrm{max} \tag{1.9}$$

From the experimental results, they concluded;

i)The hysteresis effect can be avoided if the pumping speed of the pumping system is greater than the critical pumping speed.

ii)Under the conditions that the ratio of N_2 flow rate to Ar flow rate and total pressure are constant, it is possible to avoid the hysteresis effect even if the pumping speed is smaller than the critical pumping speed.

iii)Experimentally it was shown that the critical pumping speed does not depend on cathode power, substrate bias, and target−substrate distance although it is strongly depends on substrate temperature and total pressure;the critical pumping speed decreases with increasing substrate temperature and total pressure.

iv)A smooth transition from the metal to the nitride mode in the relation between Ar flow rate and N_2 flow rate arises only in the absence of the hysteresis and at pumping speeds sufficiently higher than critical pumping speed.

More currently Berg *et al.* reported a model of hysteresis in a series of reports, by using a similar way to the model proposed by Abe and Yamashina[23-24]. The proposed model can evaluate effects of process conditions such as pumping speed, sputtering power on hysteresis effects and predict the composition of sputtered materials as a result of calculation of transition curves. In their model they treated compound formation on the target surface and gettering at the deposition area by assuming coverage both for target and getter wall. By combining these two effects on target surface and on getter wall surface, they succeeded to show the abrupt transition in relationship between deposition rate and reactive gas (N_2) flow.

The basic equations in their model are the mass balance equation between the reaction and sputter removal at the target and that between deposited metal atoms and adsorbing nitrogen atoms at getter wall surface during deposition; the former one is as follows:

$$dN/dt = 2\alpha_1 F(1-\theta_1) - (J/e)S_N\theta_1 \tag{1.10}$$

where N is the number of nitrogen atoms reacted with metal atoms per unit area at the target surface, F is the flux of neutral reactive molecules onto a unit area at a partial pressure of P_N,

J is the current density of Ar ions causing sputtering from the target surface, θ_1 is fractional coverage of the target surface by reactively formed compound(TiN), S_N is sputtering yield of the compound by the incoming argon ions, and α_t is the sticking coefficient of the nitrogen molecule to the titanium target.

The mass balance equation at the getter wall surface is given by:

$$dN/dt=2\alpha_c F(1-\theta_2)+(J/e)S_N\theta_1(A_t/A_c)(1-\theta_2)-(J/e)S_M(1-\theta_1)(A_t/A_c)\theta_2 \quad (1.11)$$

where S_M is sputtering yield of the elemental metal by incoming argon ions, θ_2 is relative coverage of the getter wall surface of the reactively formed compound(TiN), and α_c is the sticking coefficient for the nitrogen molecules to the titanium covered part$(1-\theta_2)$ of the getter wall surface. The first term

$$2\alpha_c F(1-\theta_2) \quad (1.12)$$

in the equation denotes the spontaneous nitriding by neutral nitrogen molecules of the free Ti at the getter wall surface. The coefficient

$$(J/e)S_N\theta_1 \quad (1.13)$$

in the second term in the equation is the sputtering rate of TiN from the target. They assumed that the all the material sputtered from the target area A_t will arrive at the getter wall surface. This area is donated A_c. Thus, the deposition rate of sputtered nitride from the target that arrives to the getter wall A_c will be:

$$(J/e)S_N\theta_1(A_t/A_c) \quad (1.14)$$

due to the difference in the area of the target and the getter wall surface. A fraction $(1-\theta_2)$ will be deposited onto non-reacted(bear) Ti on the getter surface. Thus, the change in population of nitride on the surface increases with the amount given by:

$$(J/e)S_N\theta_1(A_t/A_c) \quad (1.15)$$

The nitride that is deposited onto the already nitride covered fraction θ_2 does not change the population of the nitrogen at the getter wall surface.

The factor $(J/e)S_M(1-\theta_1)$ denotes the sputtering of elemental Ti from the target. In the same way, the deposition rate onto the getter wall surface will be then given by:

$$(J/e)S_M(1-\theta_1)(A_t/A_c) \quad (1.16)$$

due to the difference in the surface areas. A fraction of θ_2 of the sputtered Ti will be deposited onto the surface part of the getter wall covered by formed nitride. Thus the population of nitride on the getter wall surface decreases with the amount given by:

$$(J/e)S_M(1-\theta_1)(A_t/A_c)\theta_2 \quad (1.17)$$

The part of sputtered Ti that is deposited onto the $(1-\theta_2)$ covered fraction of the getter wall will not change the population of nitride on the getter wall.

Under the steady state conditions, dN/dt=0 for both target surface and getter wall surfaces, from Eq.1.10, the relationship is given by:

$$2\alpha_t F(1-\theta_1)-(J/e)S_N\theta_1=0 \quad (1.18)$$

and from Eq.1.11,

$$2\alpha_c F(1-\theta_2)+(J/e)S_N\theta_1(A_t/A_c)(1-\theta_2)-(J/e)S_M(1-\theta_1)(A_t/A_c)\theta_2=0 \quad (1.19)$$

They obtained consumption of nitrogen in the process chamber:

$$q_t=\alpha_t F(1-\theta_1)A_t \quad (1.20)$$

$$q_c=\alpha_c F(1-\theta_2)A_c \quad (1.21)$$

The flux intensity of neutral nitrogen can be calculated from the kinetic theory:

$$F=P_N/(2\pi kTM)^{1/2} \quad (1.22)$$

where M is the mass of the nitrogen molecule. The total sputtering rate can be obtained by

$$R=(J/e)(S_N\theta_1+S_M(1-\theta_2)) \quad (1.23)$$

From these equation systems, they can find analytical expression for θ_1, θ_2, P_{N2}, and R as a function of incoming nitrogen mass flow q_0.

As a result of the calculation, they obtained transition curve of deposition rate versus reactive gas mass flow rate. The curve indicated a negative slope in transition region, and they concluded that the calculated curve agreed well with curves experimentally observed in the system with a feed back system. They also indicated that with the model it was possible to predict the effect of the pumping speed on the hysteresis behavior and to calculate a critical size of pumping speed to suppress hysteresis. In a later literature, it was showed that hysteresis width was increased in portion to the rf power fed to the cathode, and they concluded that it was thus impossible to eliminate the hysteresis effect by any kinds of variation of the sputtering intensity[25)].

They also reported that if the pumping speed was high enough, there was a smooth transition between the reactive and non-reactive sputtering mode in a more current literature[26)]. They also propose an optimum design of reactive sputtering system based on the discussion of results obtained by their model calculation[27)].

In 1988, A.G.Spencer *et al.* and, in 1989, R.P.Howson *et al.* reported about pressure stability in reactive sputtering by considering reactive gas consumption[28-29)]. They investigated that when the depositing film was substoichiometric, the film's consumption of reactive gas was limited by the arrival rate of that gas and, thus, consumption increased with reactive gas partial pressure and when the film was saturated with reactive gas, the reactive gas consumption was limited by the metal arrival rate. In conclusion, they mentioned that the way to avoid a runaway reactive gas pressure behavior was to ensure that most of reactive gas was removed by the vacuum pumps but not by consumption by the growing film.

B. DEFICIENCIES IN CURRENT UNDERSTANDING

From reported experimental results to date, the followings are generally recognized

about mode transition and hysteresis in reactive sputtering;

i)there is nonlinear behavior in relationship between deposition rate or reactive gas partial pressure after glow discharge ignition and reactive gas flow rate.

ii)this nonlinear behavior is thought to be resulted from strong correlation between target poisoning or cleaning and reactive gas gettering on the chamber wall.

iii)as a result of strong correlation, whole process condition drastically changes. This resultant process change is well known as an avalanche-like mode transition from metal to compound mode or from compound to metal mode.

iv)the point where the mode transition occurs when reactive gas is increased is different from the point where the inverse mode transition occurs when reactive gas is decreased after the target poisoning is completed. This is known as hysteresis.

v)the shape of hysteresis depends on pumping speed and cathode power or current.

vi)higher pumping speeds reduce hysteresis width.

vii)higher cathode power or current increases hysteresis width.

Although much knowledge has been accumulated especially in the last decade, there are still gaps in understanding of mechanisms of mode transition and hysteresis. In particular, mechanisms of mode transition and hysteresis have not been well understood, though they have been investigated by several authors. Furthermore, it is sometimes suggested that pumping speed affects mode transition and hysteresis and that there is a critical pumping speed at which hysteresis can be distinguished. However, no physical explanation has been given since effects of pumping speed on hysteresis has not been investigated for a range of pumping speed and sputtering current. Further, although gettering is believed to be a key to discuss mass balance changes in reactive sputtering, it has not been examined from the view point of quantitative relation to other parameter changes, as a function of reactive gas mass flow rate change. Therefore, it is thought to be crucial to investigate gettering quantitatively. Effects of pumping speed and other parameters on mode transition and hysteresis should be also investigated systematically to reveal mechanisms of mode transition and hysteresis.

Moreover, some models have been proposed on the basis of knowledge obtained empirically. However, since they are not based on physical mechanisms of target and wall phenomena, they cannot explain mechanisms of hysteresis and mode transition. Further, although time-dependent target condition changes have been investigated and reported by several researchers, most of models deal with a steady-state condition, but no model has been reported that deals with time-dependent condition changes.

In addition, a model more currently proposed by Berg *et al.* explains hysteresis effects by obtaining an S-shape curve; *i.e.*, they mentioned that hysteresis is formed as a result of a runaway process that occurred at a bend point of the S-shape curve[23-24]. However, the purpose of the modeling is to exhibit this runaway process by model calculation and explain

mechanisms of avalanche-like process. In this respect, their model does not explain hysteresis effects that observed in an actual reactive sputtering process. They also mentioned that an S-shape curve was obtained in a system with a feed back system of reactive gas mass flow rate. However, the S-shape curve observed in an actual process is a consequence of the delay of the response time, and the shape of the curve, therefore, mainly depends on a response time of the feed back system[19]. Consequently, the approach used in Berg *et al.*'s model to explain hysteresis does not seem to be appropriate since an S-shape obtained in an actual process is not based on physical mechanisms of hysteresis behavior. Thus, it is also necessary to develop a model that involves physical mechanisms in mode transition and hysteresis. If the model is appropriate, it should exhibit time-dependent target condition changes and hysteresis without assuming how the process reaches a steady-state.

In conclusion, even though understanding of mechanism of reactive sputtering is a classical issue and there is much knowledge obtained both by experimental investigation and by modeling of the process, still there exist deficiencies in understanding of the process. Furthermore, a model that is based on the physical mechanisms involved in reactive sputtering and that deals with time-dependent target condition changes should be developed to examine mode transition and hysteresis effects.

I.III. OBJECTIVE

The objective of this study is to reveal mechanisms of mode transition and hysteresis behavior in reactive sputtering. In particular, effects of pumping speed and sputtering current on mode transition and hysteresis will be discussed since these parameters mainly affect reactive gas mass balance in the chamber. Gettering of reactive gas will be also investigated quantitatively, and its role in mass balance change will be discussed in comparison with the evacuation of reactive gas by vacuum pump system. It is believed that, by discussing mass balance changes systematically, deficiencies in current understanding would be filled.

First, in Chapter III, the time-dependent changes in process conditions such as deposition rate, partial pressure, and cathode voltage will be investigated, and effects of pumping speed and reactive/inert gas ratio on these condition changes will be discussed. This purpose of these experiments is to indicate time-dependent process condition change and to discuss mechanisms of time-dependent process change by revealing effects of pumping speed and reactive/inert gas ratio on time-dependent process change.

In Chapter IV, gettering of reactive gas will be investigated quantitatively as a function of reactive gas flow rate. The purpose of the experiment reported in this chapter is to discuss effects of gettering on avalanche-like mode transition and to demonstrate strong depend-

ence of mode transition on the reactive gas gettering.

In Chapter V, hysteresis curves and effects of pumping speed, sputtering current, and reactive/inert gas ratio will be investigated. In this chapter, hysteresis curves of reactive gas partial pressure, cathode voltage, plasma emission intensity of sputtered metal atoms, and mass deposition rate versus reactive gas mass flow rate will be demonstrated. Furthermore, mechanisms of hysteresis will be revealed by discussing effects of pumping speed and sputtering current on hysteresis curves. This discussion is most important in this thesis.

In addition to the experimental investigation, in Chapter VI, a model will be proposed on the basis of physical mechanisms obtained from discussion concerning results obtained experimentally.

The purpose of modeling is to examine mode transition and hysteresis and to prove the hypothesis used to model the process mass balance; *i.e.*, to exhibit time-dependent target condition changes and hysteresis curves as a consequence of time-dependent target condition change calculations. By discussing effects of pumping speed and sputtering current, the appropriateness of hypothesis used to develop the simulation model will be discussed. If an appropriate model is developed on the basis of physical mechanisms involved in reactive sputtering, it must clearly indicate mode transition and hysteresis behavior observed in an actual process.

As the conclusions of the study, mechanisms of mode transition and hysteresis behavior will be discussed on the basis of experimentally obtained results and model calculation results.

In this study $Ti-O_2$ dc reactive sputtering is examined. The reasons are as follows;

i)TiO_2 is a typical oxide as high index materials, and thus its deposition process is widely used and studied.

ii)Ti is highly reactive to O_2, resulting in a drastic process change in reactive deposition processes.

iii)$Ti-O_2$ system is known to be stable and reproducible empirically.

Furthermore, to lower the difficulty to investigate the complicated reactive sputtering process and to enhance the reliability of measured data a computer-controlled measurement system will be used. This system is especially helpful to investigate time-dependent target condition changes and hysteresis behavior.

Kinetics of reaction between reactive gas and target material at the target surface, as well as kinetics of thin film growth, will not be discussed in this study since the principal objective is to investigate mass balance change.

I.V. REFERENCES

1) B.Chapman, *Glow Discharge Processes*(JOHN WILEY & SONS, New York, 1980), Chapter 6, pp.177-184

2) J.H.Greiner, J.Appl.Phys.42, 5151(1971)

3) J.Heller, Thin Solid Films 17, 163(1973)

4) B.Goranchev, V.Ornov, and V.Popov, Thin Solid Films 33, 173(1976)

5) T.Abe and T.Yamashina, Thin Solid Films 35, 19(1976)

6) L.F.Donaghey and K.G.Geraghty, Thin Solid Films 38, 271(1976)

7) L.F.Donaghey and K.G.Geraghty, J.Electrochem.Soc.123, 1201(1976)

8) S.Maniv and W.D. Westwood, Surf.Sci.100, 108(1980)

9) R.McMahon, J.Affinito, and R.R.Parsons, J.Vac.Sci.Technol. 20(3), 376(1982)

10) J.Affinito, and R.R.Parsons, J.Vac.Sci.Technol.A2(3), 1275(1984)

11) T.M.Reith and P.J.Ficalora, J.Vac.Sci.Technol.A1(3), 1362(1983)

12) D.K.Hohnke, D.J.Scmatz, and M.D.Hurley, Thin Solid Films 118, 301(1984)

13) T.Serikawa and A.Okamoto, Thin Solid Films 101, 1(1983)

14) A.Okamoto and T.Serikawa, Thin Solid Films 137, 143(1986)

15) Ch.Steinbruhel and D.M.Gruen, Surf.Sci.93, 299(1980)

16) D.M.Gruen, A.R.Krauss, and M.J.Pellin, Radiation Effects 89,113(1985)

17) G.Betz and W.Husinsky, Nuclear Instruments and Methods in Physics Research B13, 343(1986)

18) G.Lemperiere and J.M.Poitevin, Thin Solid Films 111, 339(1984)

19) A.F.Hmiel, J.Vac.Sci.Technol.A3(3),592(1985)

20) S.Kadlec, J.Musil, and J.Vyskocil, J.Phys.D 19, L187(1986)

21) S.Kadlec, J.Musil, and J.Vyskocil, Vacuum 37, 729(1987)

22) J.Musil, S.Kadlec, J.Vyskocil, and V.Valvoda, Thin Solid Films 167, 107(1988)

23) S.Berg, H-O.Blom, T.Larsson, and C.Nender, J.Vac.Sci.Technol. A5(2), 202(1987)

24) S.Berg, H-O.Blom, M.Moradi, and C.Nender, J.Vac.Sci.Technol. A7(3), 1225(1989)

25) S.Berg, T.Larsson, C.Nender, and H-O.Blom J.Appl.Phys.63(3), 887(1988)

26) T.Larsson, H-O.Blom, C.Nender, and S.Berg, J.Vac.Sci.Technol. A6(3),1832(1988)

27) S.Berg, M.Moradi, C.Nender, and H-O.Blom Surf.Coat.Technol 39/40, 465(1989)

28) A.G.Spencer, R.P.Howson, and R.W.Lewin, Thin Solid Films 158, 141(1988)

29) R.P.Howson, A.G.Spencer, K.Oka, and R.W.Lewin, J.Vac.Sci.Technol. A7, 1230(1989)

II. APPARATUS

II.I. APPARATUS

Figure 2.1 shows a schematic drawing of the experimental apparatus. The sputtering machine used in the experiments was a load-lock type sputtering machine. The process chamber was about 76 X 66 X 30 cm^3, *i.e.*, the chamber volume was about $1.5X10^{-1}$ m^3. The chamber was evacuated by two throttled oil diffusion pumps, one of which was capable of pumping the load-lock chamber. The pumping speed for O_2 could be varied from about $5.0X10^{-2}$ to $4.0X10^{-1}$ m^3/s by throttling the two pumps. The process chamber was equipped with three circular planar magnetron sputtering sources, one of which with 15cm diam. Ti target(99.9%) was used in the experiment.

The working gases were Ar(99.99%) and O_2(99.99%), whose flow rates were separately controlled with Tylan FC-260 mass flow controllers. The accuracy of the flow rates was 0.02 standard cm^3/min. The total pressure was measured with an MKS type 128 capacitive manometer. Deposition rates were monitored with a quartz crystal rate detector. The sputtered titanium flux was monitored by measuring the emission from the Ti emission lines(in 398-400nm) in the plasma region over the sputtering target. Emission spectra were observed with a plasma monitor with a diode array type detector.

Cathode voltage, V_{sp}, total pressure, P, Ti emission intensity, I_{Ti}, and deposition rate, R_{dep}, were acquired by using a computer data acquisition system. The computer used in this experiment is one of the HP 300series(Hewlett Packard) with A/D and D/A converters. The obtained pressure data were averaged by the computer. The accuracy of the pressure measurement was estimated to be $5.3x10^{-3}$ Pa after averaging, including a possible zero point shift of $2.7x10^{-3}$ Pa. Oxygen partial pressure was calculated using the relationship between total pressure and O_2 partial pressure, which was obtained for a range of O_2 mass flow rates(details are described in Chapter II.II). Argon partial pressure was set to $2.7x10^{-1}$ Pa throughout the experiment except those for Ar/O_2 ratio investigation. To obtain O_2 partial pressure, it was assumed that Ar partial pressure remained constant during deposition. The pumping speed of O_2 was calculated from the relationship between O_2 flow rates and O_2 pressures. The cathode power supply was operated in a constant current mode.

Mass flow rates and sputtering current were automatically set to a required value by the same computer system as used for the data acquisition.

II.II. DETERMINATION OF O_2 PARTIAL PRESSURE

Oxygen partial pressure was calculated using a relationship between total pressure and O_2

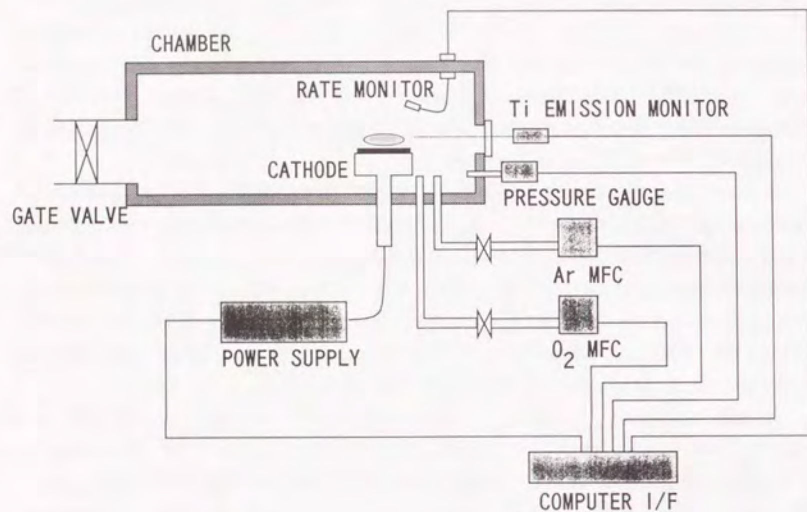

Fig.2.1 A schematic drawing of the experimental apparatus.

partial pressure. The relationship was obtained by measuring pressure for a range of O_2 flow rates with and without Ar introduction to the chamber; *i.e.*, two equations were obtained by the measurement:

$$P_{O2}=k_1Q_{O2}+P_{Base} \quad \text{(without Ar introduction)} \quad (2.1)$$

and

$$P=k_2Q_{O2}+P_{Ar} \quad \text{(with Ar introduction)} \quad (2.2)$$

where P_{O2} is pressure measured without Ar introduction, Q_{O2} is O_2 flow rate, P_{Base} is base pressure(usually negligible), P is pressure measured with Ar introduction, P_{Ar} is Ar partial pressure, and $k_{1,2}$ are constants. By eliminating the term of Q_{O2}, the relationship between P and P_{O2} was obtained;

$$P_{O2}=k_1(P-P_{Ar})/k_2+P_{Base} \quad (2.3)$$

As clearly shown in the equations, if $k_1=k_2$, P_{O2} is obtained simply subtracting P_{Ar} from the total pressure. However, in the measurement, usually k_2 is about 4/5 of k_1. Therefore, P_{O2} was not determined by subtracting. The reason for the difference in k_1 and k_2 has been unknown. During experiments, O_2 partial pressure was calculated by the computer from the total pressure measured.

III. INVESTIGATION OF TIME-DEPENDENT TARGET CONDITION CHANGES

III.I. INTRODUCTION

It is generally accepted that target surface condition changes result in the whole process changes in reactive sputtering. At the target surface two competitive phenomena occur simultaneously: formation of compound layers as a result of adsorption of reactive gas atoms to metal sites and sputtering of the formed compound layers[1-2]. Until these two phenomena balance under given conditions, the process changes continuously with elapsed time. For example, when a glow discharge is ignited in an Ar-O_2 mixture with a metallic target, the formation of oxide layers dominate the whole process change until adsorption and sputtering rates of O_2 on the target surface balance. When these two phenomena balance, the process reaches a steady-state. In stable regions(metal or compound mode), the time to reach a steady-state after process condition changes is thought to be very short and generally not observed. However, at the transition region where the process is unstable, it takes a longer time to reach a steady-state after a glow discharge is ignited since compound formation rate and sputtering rate are competitive in this region. Although the reason for the difference of the time to reach a steady-state is thought to be the difference of reactive gas mass balance among three process regions, no physical explanation has been obtained.

This time-dependent target behavior is thought to strongly correlate to wall gettering behavior. Once the compound layer formation starts on the target surface, the number of metal atoms sputtered from the target surface decreases as a result of the decrease in sputtering yield. This causes the decrease in the wall gettering capacity, resulting in the increase in reactive gas partial pressure. The increase in reactive gas partial pressure accelerates the formation of compound layer on the target surface. Thus, the wall gettering behavior is thought to strongly relate to the formation of the compounds on the target surface.

The time to reach a steady-state is thought to be determined by the correlation above mentioned. If this hypothesis is correct, the time to reach a steady state should be affected by pumping speed of the vacuum pump system since the wall gettering that consumes reactive gas is competing to the evacuation of reactive gas by the vacuum pump system.

In addition, the target surface phenomena are thought to be affected by the inert/reactive gas ratio in arriving flux since, as mentioned above, the formation of compound layers and the sputtering are competitive phenomena. Thus, the ratio of inert/reactive gas should also affect the time to reach the steady state. Therefore, to discuss mechanisms of time-dependent target surface behavior, it is meaningful and unavoidable to examine the effects of the inert/reactive gas ratio and pumping speed.

There have been some reports that investigated time-sependent condition changes[3-7].

Although in the reports time–dependent target condition changes, associated with other condition changes, were investigated, no explanations were given on mechanisms of the condition change and on effects of operation parameters such as pumping speed or sputtering current or power.

In this respect, the purpose of the research is to observe time–dependent process changes after glow discharge is ignited under given conditions and discuss effects of pumping speed and of Ar/O_2 ratio on the time to reach a steady–state. Furthermore, since the mode transition and hysteresis occur as a result of a target condition change, it is necessary to investigate and discuss the time–dependent target surface condition change to reveal their mechanisms.

In the experiment, changes in O_2 partial pressure, deposition rate, cathode voltage, and Ti emission intensity after glow discharge is ignited are observed. Oxygen flow rate is set to the value where the mode transition from metal to compound mode occurs.

III.II. EXPERIMENTAL METHOD

Before observing time–dependent parameter changes, onset flow rate of O_2 for mode transition was determined by observing a process as a function of O_2 mass flow rate; after pre–sputtering of the target in a pure Ar atmosphere, O_2 flow rate was increased in step of 0.5 std. cm^3/min until the avalanche–like mode transition occurred. An onset flow rate for a given condition was defined as the critical flow rate at which an avalanche–like mode transition occurred. After an onset flow rate was determined, the target was again pre–sputtered in a pure Ar atmosphere until the cathode voltage and Ti emission intensity values returned to those values before the mode transition occurred. Then, after glow discharge was turned off, O_2 was again injected into the chamber with the flow rate of the onset point. After glow discharge was again ignited, changes in O_2 partial pressure, deposition rate, cathode voltage, and Ti emission intensity were measured. Interval time to measure the parameters was 2 second for the first 2 minute, 10 second for 2–6 minute, and 20 second for 6–10 minute of elapsed time.

For an investigation of effects of pumping speed, pumping speed was varied under the condition where Ar/O_2 ratio was kept constant at 5, whereas, for an investigation of effects of Ar/O_2 ratio, Ar partial pressure was varied under the condition where O_2 flow rate and pumping speed were kept constant.

III.III. RESULTS
A. TIME–DEPENDENT CONDITION CHANGES

In Fig.3.1 typical results is shown. After the glow discharge is ignited, O_2 partial pressure increases gradually. Prior to glow discharge ignition, O_2 partial pressure was 5.2×10^{-2} Pa, and when the glow discharge was ignited, the pressure decreased drastically. Titanium emission intensity I_{Ti} decreases until 30s after it reaches a maximum value at 2s. After 40s, it is almost constant. Mass deposition rate R_{dep} increases until 8s. After the maximum at 8s, it decreases to about 1/5 of its maximum value. Cathode voltage decreases slightly after the glow discharge was ignited, and then reaches a maximum value at 30s. After reaching the maximum, it decreases gradually.

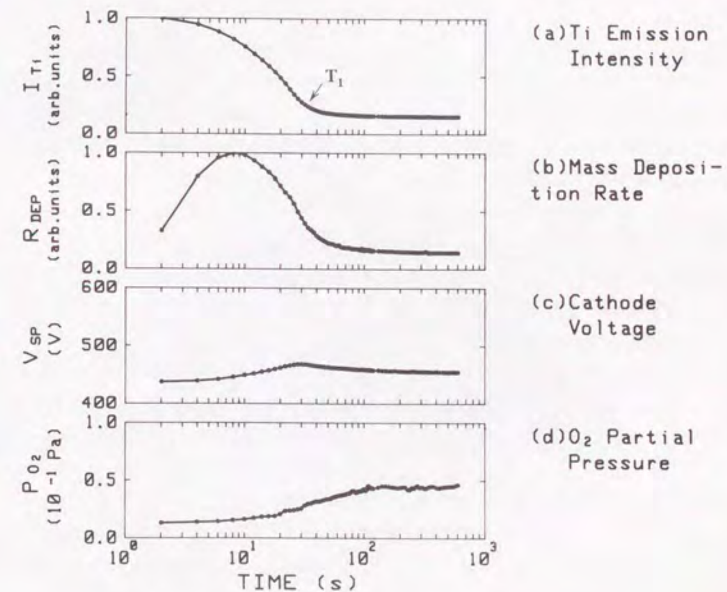

Fig.3.1 Typical results of time–dependent process condition changes.

There is a sharp bend both in I_{Ti} and R_{dep} curves. The bend point of I_{Ti} is nearly equal to the point where cathode voltage shows its maximum. The bend point of R_{dep} is different from the maximum of V_{sp}. The increase in P_{O2} continues after I_{Ti}, R_{dep} , and V_{sp} become stable.

In addition, changes in emission spectra are shown in Fig.3.2. Spectrum lines observed at 364–365, 399–400, 498–499, and 550–551 nm are identified as emission lines from Ti[8], and they drastically decrease with elapsed time. Emission spectra lines observed at 420 and 430nm are from Ar[9] and do not show much change in intensity. Weak emission observed at about 560nm is an emission line from O_2^{+} [10], and it increase gradually with elapsed time. The result of emission spectroscopy clearly show changes in plasma conditions.

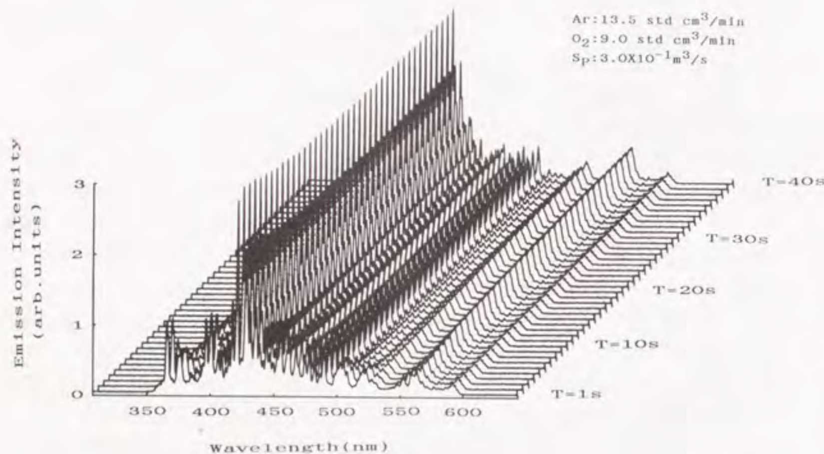

Fig.3.2 Changes in plasma emission spectra with elapsed time after glow discharge ignition.

B. EFFECTS OF PUMPING SPEED AND Ar/O_2 RATIO

In Fig.3.3 bend points of I_{Ti} curves are shown as a function of pumping speed, S_p. In Fig.3.4 time constant τ is shown as a function of pumping speed. A bend point, T_1, was defined as the crossing point of the extrapolation lines of two parts of an obtained curve of I_{Ti} and , as shown in Fig.3.1. Time constant τ was obtained from the gradient of a I_{Ti} curve in negative slope region. The bend point, T_1, increases as pumping speed increases, whereas, τ decreases as S_p increases.

In Figs.3.5 and 3.6, T_1 and τ are shown as a function of Ar/O_2 ratio. During the experiment S_p was kept 0.30m^3/s. As Ar/O_2 ratio increases, T_1 increases and τ decreases.

III.IV. DISCUSSION

A. TIME DEPENDENT CONDITION CHANGES

Changes in the target surface condition are reflected to changes in I_{Ti}, R_{dep}, V_{sp}, and P_{O2}. In particular, I_{Ti} is thought to reflect condition changes of target surface since I_{Ti} is directly related with a change in the amount of Ti in the plasma region that is sputtered off from the target surface. Thus, of course, if the sputtering yield of Ti decreases as a consequence of the formation of oxide layers on the target surface, I_{Ti} decreases. Although mass deposition rate is thought to decreases when oxide layers are formed on the target surface, it increases in the case that the mass of gettered O_2 is larger than the decrease in mass of Ti deposited. Cathode voltage reflects changes in the target surface condition and plasma conditions(change in gas contents in the plasma). Generally secondary electron emission coefficient increases when oxide layers are formed on the target surface. As a consequence, cathode voltage decreases when the power supply is operated at a constant current mode. On the other hand, O_2 content in the plasma is increased, cathode voltage increases due to a low ionization coefficient of O_2 compared to that of Ar. Oxygen partial pressure increases if the amount of gettered O_2 decreases.

The decrease in I_{Ti} in the first 40s can be explained simply by assuming the target surface oxidation. The increase in R_{dep} until 8s may relate with a slight increase in P_{O2}. Since R_{dep} is given as the sum of deposited Ti and gettered O_2, the amount of gettered O_2 is increased when P_{O2} is increased. This increase in P_{O2} is indicated in the curve of P_{O2};i.e., P_{O2} increases gradually from 6s after the discharge ignition, inducing an increase in flux to the gettering surface and target. Therefore, the mass deposition rate shows the maximum at 8s. The reason why the change in P_{O2} lasts for a longer time than those in other three parameters is

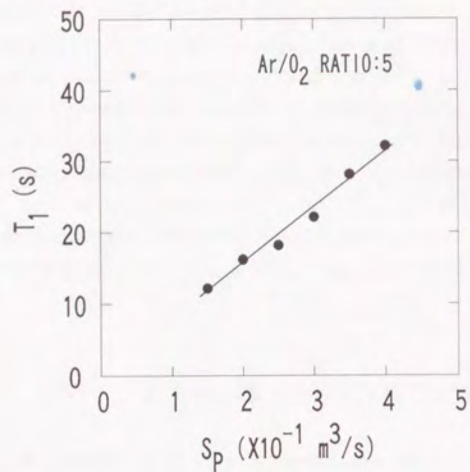

Fig.3.3 Time to reach a steady state as a function of S_p ;the time is defined as a time to reach a sharp bend point of I_{Ti} changes in time-dependent process changes.

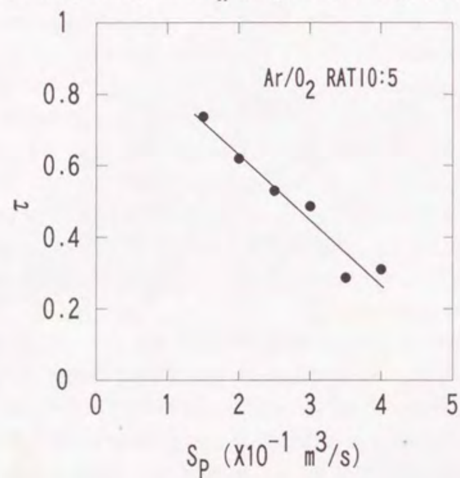

Fig.3.4 Time constant of compound layer formation at target surface as a function of S_p.

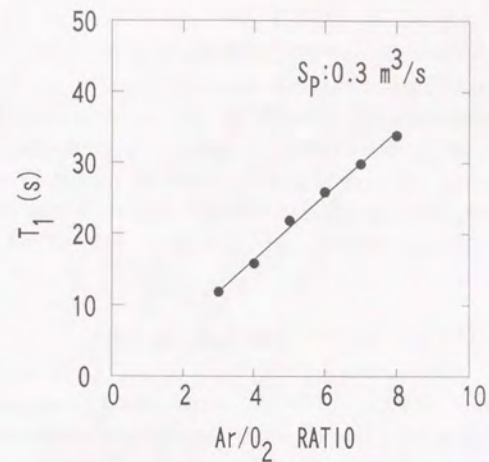

Fig.3.5 Time to reach a steady state as a function of Ar/O_2 ratio;the time is defined as a time to reach a sharp bend point of I_{Ti} changes in time-dependent process changes.

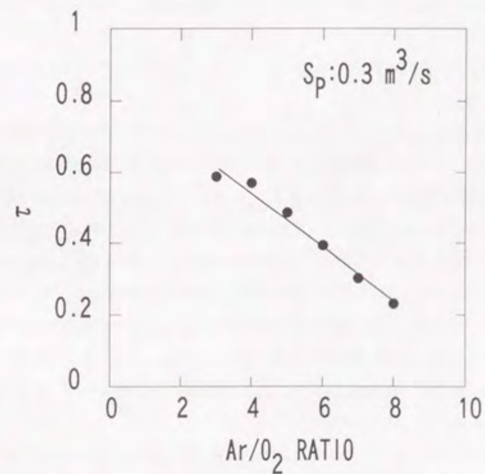

Fig.3.6 Time constant of compound layer formation at target surface as a function of Ar/O_2 ratio.

unknown. The cathode voltage change seems to be affected by the O_2 content change in the plasma region until about 30s since, as described above, an increase in V_{sp} is resulted from the increase in O_2 content in the plasma region. This hypothesis is also supported by the fact that the change in V_{sp} is very similar to that in P_{O2}. However, this is inconsistent with the behavior of I_{Ti}. The decrease in V_{sp} from about 30s is thought to be due to the change in the target surface condition. In this region, the target surface is oxidized, resulting in an increase in secondary electron emission coefficient.

B. EFFECTS OF PUMPING SPEED AND Ar/O_2 RATIO

The phenomena occurred on the target surface are two competing phenomena:formation of compound layers as a result of reactive gas adsorption to active metal sites and sputtering of formed compound layers. The following simple model is recognized to discuss phenomena on the target surface;

i)If O_2 flux attacks a metal site on the target surface, an oxide is formed.

ii)If O_2 flux attacks an already oxidized site, oxide may be sputtered, but there is no change in the target surface condition.

iii)If Ar flux attacks a metal site, a metal atom will be sputtered; a surface site remains as a metal site.

iv)If Ar flux attacks an already oxidized site, an oxide is sputtered and the site becomes a metal site.

Although events actually occur on the target surface are more complicated, it is possible and meaningful to discuss mass balance changes on the basis of the model described above.

The reason for the shift of T_1 due to changes in Ar/O_2 ratio is understood on the basis of the model. The condition changes shown in Fig.3.1 result from target surface oxidation. Therefore, if the ratio of O_2 in the incident flux to the target is increased, the probability for the formation of oxide on the target surface is increased, shortening the time to reach a steady-state. On the other hand, if the ratio of Ar is increased, formation of oxide layers on the target surface is delayed since the probability for sputtering of formed oxide layers increases. It should be noted that in both cases absolute values of O_2 flux were not changed;only the ratio of Ar/O_2 was changed.

Effects of S_p are not directly introduced in the model described above;in the model only effect of the flux is described. Since the flux is defined by partial pressure, pumping speed or mass flow rate is not taken into account. However, by taking effects of gettering into account, it becomes possible to discuss effects of S_p with a model. Since oxygen is consumed by gettering as well as it is pumped out by the vacuum pump system, an increase in S_p

implies that the probability that O_2 is consumed by gettering decreases. Mass balance of O_2 in the chamber is affected by changes in gettering surface condition as well as it is affected by changes in target surface condition. Therefore, in the case that less O_2 is consumed by gettering due to larger S_p, the formation of oxide on the target surface is delayed, resulting in the longer time to reach a steady state.

The results indicate that to obtain a fast response to the change in reactive gas mass flow rate it is better to operate the process under the conditions with a low Ar/O_2 ratio and a low vacuum pumping speed.

III.V. CONCLUSIONS

Changes in O_2 partial pressure, deposition rate, cathode voltage, and Ti emission intensity after glow discharge is ignited and effects of pumping speed and Ar/O_2 flow rate ratio have been investigated. It is shown that O_2 partial pressure, deposition rate, cathode voltage, and Ti emission intensity change continuously after glow discharge is ignited until the process reaches a steady-state. Both pumping speed and Ar/O_2 ratio affect the time to reach a steady-state. The results suggested that a low pumping speed or low Ar/O_2 ratio shortens response time for process condition change such as reactive gas flow rate.

III.VI. REFERENCES

1) S.Maniv and W.D.Westwood, J.Appl.Phys., 51, 718(1980)
2) S.Maniv and W.D.Westwood, Surface Science 100, 108(1980)
3) J.Heller, Thin Solid Films, 17, 163(1973)
4) L.F.Donaghey and K.G.Geraghty, Thin Solid Films, 38, 271(1976)
5) B.Goranchev, V.Orlinov, and V.Popova, Thin Solid Films, 33, 173(1976)
6) T.M.Reith and P.J.Ficalora, J.Vac.Sci.Technol.A1, 1362(1983)
7) A.G.Spencer, R.P.Howson, and R.W.Lewin, Thin Solid Films, 158, 141(1988)
8) A.N.Zaidel' et.al., *Tables of Spectra Lines*(IFI/PLENUM, New York, 1970),pp.695-702
9) A.N.Zaidel' et.al., *Tables of Spectra Lines*(IFI/PLENUM, New York, 1970), pp.362-370
10) P.W.B.Pearse and A.G.Gaydon, *The Identification of Molecular Spectra*(CHAPMAN AND HALL, London, 1976), pp.255-262

IV. QUANTITATIVE ESTIMATION OF GETTERING OF REACTIVE GAS

IV.I. INTRODUCTION

It has been recognized that the nonlinearity is due to an avalanche-like change in a reactive gas mass balance in the chamber that takes place as a result of strongly correlated gas consumption at the target and chamber wall. The consumption of the reactive gas at the chamber wall is referred as gettering. Gettering affects mass balance changes in the chamber, consequently whole process changes in the chamber. Recently several authors have reported that reactive gas mass balance is strongly affected by pumping speed of vacuum pump system[1-7]. The reason why the pumping speed affects process mass balance is thought to be that the vacuum pump system evacuates reactive gas in competition with gettering;changes in the pumping speed affect the balance of reactive gas consumption between evacuation and gettering. However, quantitative estimation of gettering as a function of reactive gas flow rate or partial pressure prior to glow discharge ignition has not been performed. Therefore, gettering should be analyzed from the view point of the quantitative relationship to vacuum pump evacuation. Further, it should be discussed in relation to other condition changes, especially to sputtering yield changes, since they clearly relate to gettering.

In addition to investigation of gettering, by measuring changes in mass balance as a function of reactive gas partial pressure prior to discharge ignition, drastic mode transition at a critical reactive gas partial pressure will be exhibited.

In this Chapter reactive gas partial pressure change(reactive gas gettering), deposition rate, and sputtering yield have been measured as a function of O_2 partial pressure prior to discharge ignition to examine reactive gas mass balance and sputtering yield changes and to discuss process condition changes in relation to pumping capacity change of gettering. Gettering of reactive gas is estimated by observing pressure change on glow discharge ignition and composition analysis of films deposited. Sputtering yield is also calculated from the results of film composition analysis. The results will show a clear change in gettering capacity as a function of O_2 partial pressure. In addition, other condition changes such as sputtering yield, mass deposition rate at mode transition will be shown.

IV.II. EXPERIMENTAL METHOD

Estimation of gettering was performed by measuring pressure change on glow discharge ignition. Mass deposition rate, sputtering voltage, and Ti emission intensity were also measured. The target was pre-sputtered in pure Ar prior to each film deposition run.

Sputtering yield and film composition for a range of O_2 partial pressure were determined by analyzing films deposited onto two pieces of aluminum foil. Each of the Al pieces covered 1/8 of the hemisphere surface over the target. The total amount of deposit material was the measured deposited material on the two pieces of Al foil times 4. Aluminum foil pieces were weighed before they were set into the chamber. Deposition time was 10min (P_i=0 to $4.0X10^{-2}$ Pa) to 20min (P_i=$4.8X10^{-2}$ to $8.0X10^{-2}$ Pa). After a deposition run, they were first weighed to obtain the mass of the deposited film, and then dissolved into a boiling solution of hydrochloric and sulfuric acid to measure the amount of deposited Ti. The amount of Ti contained in the solution was analyzed with an inductively-coupled plasma atomic emission spectrometer (Seiko Instruments Inc., TYPE SPS1200A). The oxygen content of the film was obtained by subtracting the mass of Ti from the total weight of the deposited film on an Al piece. The accuracy of the measurement of dissolved Ti was assured to be $\pm$1% by examining test solution that contained almost the same amount of Al and Ti. The accuracy of the analytical balance used in the experiment was 0.01mg.

IV.III. RESULTS

The O_2 partial pressure change ΔP obtained from the total pressure change on glow discharge ignition is shown in Fig.4.1 as a function of O_2 partial pressure prior to discharge ignition, P_i. There is a drastic change in ΔP between P_i=$4.0X10^{-2}$ and $4.8X10^{-2}$ Pa. This is due to avalanche-like target oxidation and generally called mode transition. Until this transition, ΔP increases linearly to its maximum value of $3.6X10^{-2}$ Pa as P_i increases. After the transition, ΔP is about $4.0X10^{-3}$ Pa and remains almost constant.

The amount of gettered O_2 on the chamber wall Q_g is calculated from the values of ΔP by the following equation:

$$Q_g=\Delta P S_p \quad \text{(Pa m}^3\text{/s)} \quad (4.1)$$

where S_p is physical pumping speed for O_2. In Fig.4.2, the calculated Q_g and ratio of Q_g to Q_{in} are shown. The gettered O_2 amount reaches a maximum of $7.5X10^{-3}$Pa m^3/s(4.4 std.cm^3/min) just before the mode transition(at P_i=$4.0X10^{-2}$Pa). At P_i=$1.5X10^{-2}$Pa, P_f was less than the experimental measurement limit of $6.5X10^{-4}$ Pa. This implies more than 96% of O_2 was consumed by the gettering. Just before the transition, still more than 90 % of Q_{in} is gettered at the chamber wall. After the transition, Q_g drops to 15% of the value before the transition. The ratio of Q_g/Q_{in} ranges from about 5% to 10% after the transition.

The getter pumping speed S_g is calculated from the values of Q_g and P_f by the following equation:

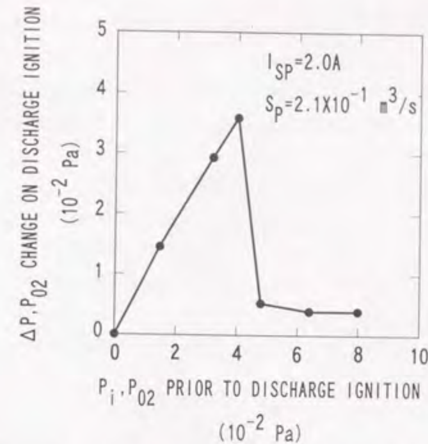

Fig.4.1 O_2 partial pressure change on discharge ignition as a function of O_2 partial pressure prior to discharge ignition.

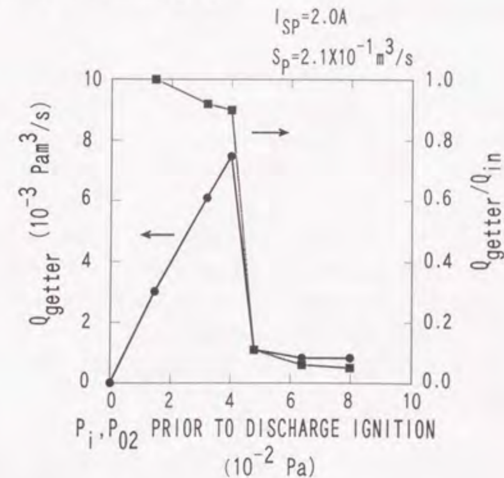

Fig.4.2 The amount of gettered O_2 and ratio of gettered/introduced O_2 amount as a function of O_2 partial pressure prior to discharge ignition.

$$S_g = Q_g / P_f \quad (m^3/s) \tag{4.2}$$

At $P_i = 1.5 \times 10^{-2}$ Pa, S_g of >4.7 m^3/s was estimated from the measurement limit of P_f. As shown in Fig.4.3, until the transition, S_g decreases linearly to 1.9 m^3/s, and at the transition it drops to 2.6×10^{-2} m^3/s or by a factor of about 100 relative to that before the transition. After the drop, it decreases gradually as P_i increases since P_f increases gradually while Q_g remains almost constant. The maximum values of Q_g and S_g are attained at different P_i values.

In Fig.4.4, the sputtering yield of Ti Y and normalized mass deposition rate R_{dep} determined from film composition analysis are shown. In the determination of Y, sticking probability of Ti on the Al foil pieces was assumed to be unity. The sputtering yield shows a drastic change at the mode transitions. Until the transition Y decreases gradually from 0.33 to 0.31 as P_i increases. After the transition, Y drops to 0.018. The value after the transition is about 17 times smaller than that before the transition. The value of the sputtering yield from the clean Ti target agrees with reported values[8].

As well as Y, R_{dep} decreases abruptly at the transition. Until the transition R_{dep} increases, and it reaches a maximum just before the transition. Since Y decreases gradually as P_i increases in this region, the increase of R_{dep} is due to the increase in Q_g. At the transition, R_{dep} decreases by a factor of 10. After the transition, the value of R_{dep} is almost 1/20 of the value before the transition and is constant since sputtering yield and gettering are stable in this region.

In Fig.4.5, O/Ti atomic ratio in deposited films is shown. The ratio before the transition is 0.54. After the transition, the ratio ranges from 2.0 to about 2.2. For $P_i > 4.8 \times 10^{-2}$ Pa, O/Ti atomic ratios may be overestimated. Since the analysis of dissolved Ti has a small error, the most possible reason for this is an error of the weight measurement or surface oxidation of aluminum foil pieces.

In Fig.4.6, the relationship between the gettered amounts of O_2 obtained from pressure change and film composition analysis is shown. The correlation factor of the relationship is 0.97, which implies the amount of gettering obtained from in-situ pressure measurement is in accord with that obtained from film composition analysis.

From the P_f and Y, the Ti and O_2 fluxes to the deposition area can be calculated;the Ti flux Γ_{Ti} was calculated by:

$$\Gamma_{Ti} = Q_{Ti} / A \quad (atom/(s\ cm^2)) \tag{4.3}$$

where A is the area of the deposition surface. In the Ti flux calculation, the deposition area value used was 1.3×10^3 cm^2, which was the area of the hemisphere surface where aluminum foil pieces were set. Thus, the obtained value refers to the flux which is incident on a unit area on an imaginary hemisphere surface over the target. The flux value is an average value that is obtained from the total amount deposited on the deposition area. O_2 flux Γ_{O2} was

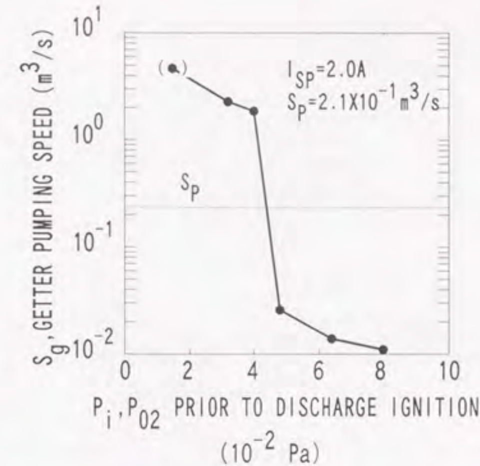

Fig.4.3 Calculated getter pumping speed for O_2 as a function of O_2 partial pressure prior to discharge ignition.

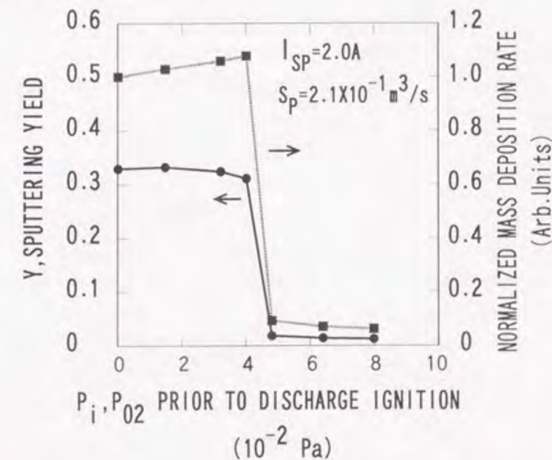

Fig.4.4 Sputtering yield and mass deposition rate obtained from film composition analysis as a function of O_2 partial pressure prior to discharge ignition.

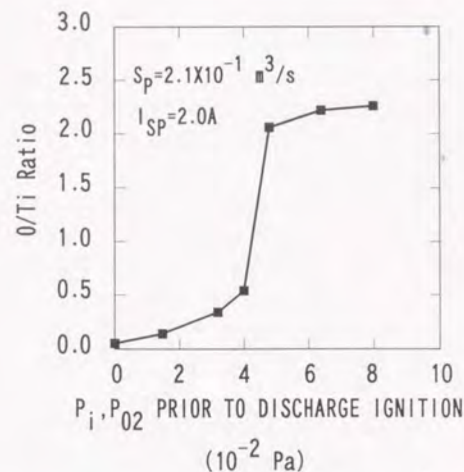

Fig.4.5 O/Ti atomic ratio in deposited films as a function of O_2 partial pressure prior to discharge ignition.

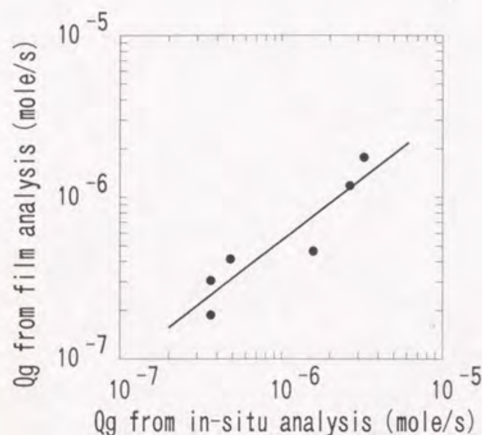

Fig.4.6 Relationship between the gettered amounts of O_2 obtained from pressure change and film composition analysis.

calculated by:

$$\Gamma_{O2}=P_f/(2\pi kTM)^{1/2} \quad \text{(molecule/(s cm}^2\text{))} \tag{4.4}$$

where k is the Boltzmann constant, T is the gas temperature in the chamber(assumed to be equal to room temperature), M is the O_2 molecule mass. Calculated results, as well as ratio Γ_{O2}/Γ_{Ti}, are shown in Fig.4.7. At P_i=1.49X10^{-2} Pa, Γ_{O2} is nearly equal to Γ_{Ti}; Γ_{O2}=1.8X10^{15} molecule/(s cm^2) and Γ_{Ti}=3.3X10^{15} atom/(s cm^2). Until the transition, Γ_{O2}/Γ_{Ti} increases linearly, because Γ_{O2} increases as P_i increases while Γ_{Ti} remains almost constant. At the transition, Γ_{O2} increases drastically from 1.1X10^{16} to 1.2X10^{17} molecule/(s cm^2), while Γ_{Ti} decreases from 3.1X10^{15} to 2.0X10^{14} (atom/(s cm^2)). Consequently, Γ_{O2}/Γ_{Ti} increases by a factor of about 170. After the transition, Γ_{O2} increases as P_i increase, while Γ_{Ti} decreases slightly. In this region, Γ_{O2} is almost 10^3 times larger than Γ_{Ti}.

Adsorbed/incident O_2 flux ratio on the deposition area α can be estimated by calculating the ratio of Γ_{O2} that is incident on the deposition area and the amount of gettered O_2 that is determined from film analysis;i.e., this ratio is defined as

$$\alpha=Q'_g/\Gamma_{O2} \tag{4.5}$$

where Q'_g is the amount of gettered O_2 per unit area and unit time. The calculated results show the existence of a drastic change in α at the transition(Fig.4.8). Before the transition, α decreases from 0.36 to 0.15 as P_i increases. At the transition it decreases to 2X10^{-3} by a factor of about 75. After the transition, it decreases linearly, and at P_{O2}=8X10^{-2} Pa, it reaches a value of 8.6X10^{-4}. This result implies that 1/1000 of the O_2 arriving at wall react with Ti. After the transition, the amount of O_2 that can be gettered at the chamber wall is limited by the amount of Ti arrived to the chamber wall. As a result, α decreases.

IV.IV. DISCUSSION
A. GETTERING BEHAVIOR

It is clearly shown in the obtained results that the getter pumping speed changes drastically at the mode transition. As reported by several authors, before the transition, the gettering dominates process conditions[3-4];most of introduced reactive gas is consumed by gettering, and thus reactive gas partial pressure remains very small, in some cases less than measurement limits. Therefore, as shown in the results, a value of the getter pumping speed becomes much higher than that of the physical pumping speed.

At the transition, getter pumping speed decreases drastically as a result of a target surface condition change; *i.e.*, as target surface is oxidized, sputtering yield drops, resulting in the decrease in gettering capacity and the increase in reactive gas partial pressure. Thus, calculated getter pumping speed decreases, on the obtained result by a factor of about 70. This

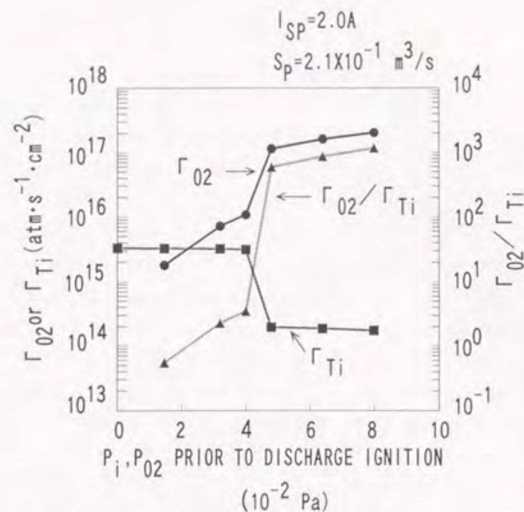

Fig.4.7 Oxygen flux and Ti flux onto the deposition area on the wall surface and their ratio as a function of O_2 partial pressure prior to discharge ignition.

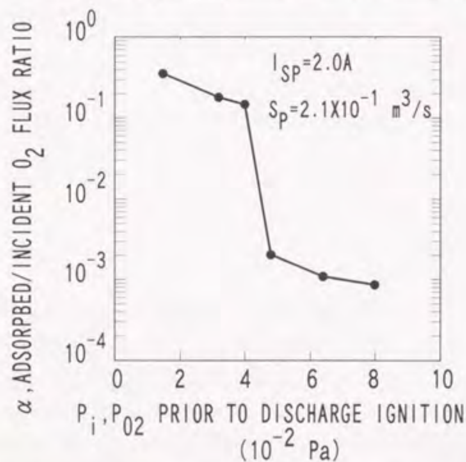

Fig.4.8 Adsorbed/incident O_2 flux ratio calculated from the amount of gettered oxygen and oxygen flux intensity as a function of O_2 partial pressure prior to discharge ignition.

drastic change makes process unstable and uncontrollable in the transition region. The fact that S_g reaches more than 10 times larger than S_p at the point just before the transition suggests the difficulty to suppress nonlinear behavior in an actual sputtering system.

After the transition, the getter pumping speed is lower than the physical pumping speed. In this region Y is stable, and thus Q_g are constant although S_g changes as P_f changes. The gettering does not dominate process conditions in this region.

B. QUANTITATIVE ANALYSIS OF PROCESS TRANSITION

As clearly shown in the obtained results, process operation conditions can be divided into three regions. The first region is P_i=0 to 3.99X10^{-2} Pa;in this region, sputtering is in so-called metal mode with target surface not oxidized. In the second region, the transition region, between P_i=3.99 and 4.79X10^{-2}Pa, a drastic change in process operation conditions occurs. In the third region where P_i is >4.79X10^{-2} Pa sputtering is in compound mode. In this region, the target surface is fully oxidized. The process is stable;it is not affected by Q_{in}.

In the first region(metal region), target surface remains metallic. Thus, the decreases in sputtering yield are less than 10%. Since the supply of sputtered Ti is large enough to getter most of O_2 introduced into the chamber until the transition, Q_g increases with increasing Q_{in}. As a consequence, P_f remains very low in this region. This implies that the most of O_2 reached the wall surface covered with active Ti is gettered, resulting in a large value of α. As a consequence, this yields a large value of S_g. The mass deposition rate increases as P_i increases in this region because the increase in Q_g surpasses the decrease in Q_{Ti}. In this region, the target surface condition is almost constant, and wall gettering dominates the process condition change. The small decrease in this region may be due to a slight change in target surface condition.

In the transition region, Y decreases drastically:from 0.31 to less than 0.02. This drastic drop in Y is due to target oxidation. Although change in sputtering yield is thought to be influenced by changes in surface binding energy[9], secondary electron emission coefficient[10], etc., theoretical explanation has not been obtained in diode sputtering systems. However, Gruen *et al.* reported that the Ti sputtering yield for 3keV Ar^+ ion beam under a pressure of O_2 decreased by a factor of six when target is covered by 3 monolayer of oxygen and that the decrease was mainly resulted from changes in binding energy due to oxygen adsorption and topography[11]. The oxide layer may be thicker in our case, resulting in a larger sputtering yield drop.

At the transition all process operation conditions change drastically as a result of the change in Y. The magnitude of the changes in the process condition is tabulated in Table 1.

Table 1 The magnitude of changes in process condition parameters at the mode transition.

Parameters	Q_g Pa m^3/s	S_g m^3/s	Y	Γ_{O2}/Γ_{Ti}	O/Ti	α
Before Transition	7.5×10^{-3}	1.9	0.31	6.96	0.54	1.5×10^{-1}
After Transition	1.1×10^{-3}	2.6×10^{-2}	0.020	1.18×10^{3}	2.2	2.0×10^{-3}
Magnitude	6.8	73	15.2	170	4.1	75

Most remarkable change is shown in the change in Γ_{O2}/Γ_{Ti} ratio because this parameter is affected by both Ti yield and P_f changes; at the transition, the sputtering yield decreases Γ_{Ti} by a factor of 15.8 and the P_f increases Γ_{O2} by a factor of 9.4, resulting in the change in Γ_{O2}/Γ_{Ti} of about 170. In addition, S_g and α show the large transition because they are also affected both by the yield and P_f changes. On the other hand, the magnitude of Q_g is not as large as that of Y, since in the change in Q_g, the change in *Y* is canceled by the change in the O/Ti ratio.

The obtained magnitude is thought to be affected by cathode operation power, target surface, pumping speed, system configurations etc. However, as discussed above, the change at the transition is originally due to sputtering yield changes introduced by target oxidation. In Ti-O_2 reactive sputtering, the decrease in *Y* by target oxidation is rather large compared to other Ti-reactive gas systems such as Ti-N_2[1,12-14], Ti-CH_4[15]. Other than Ti systems, Al-O_2 system has been reported to show a large change in deposition rate at the transition[16-17].

It is also interesting that the transition occurs at a low O/Ti ratio in the deposited films. This is due to a dynamic process change, which is described in Chapter III;i.e., once the O_2 consumption balance among target surface oxidation, wall surface gettering, and physical pumping is broken, the increasing P_{O2} during the dynamic change accelerates target oxidation. The composition of deposited film is thought to be changing during this dynamic transition. This dynamic transition cannot be controlled without a feedback control system. Thus, substoichiometric films cannot be obtained. If the change could be made more gradual, it would be easy to obtain substoichiometric films.

In the compound region, the sputtering yield remains constant. The value of P_f has already reached a high value enough to oxidize target surface completely at the transition. At the target surface, formation and sputtering of a compound layer are balanced. Thus, there is only a slight decrease in Y with increasing P_f.

The O_2 flux to the wall surface reached 2.3×10^{17} atoms/cm^{2}s, about 10^3 times larger than the Ti flux to the wall. This result suggests that 1/1000 of the O_2 arriving at wall can react with Ti. Thus, α decreases to 2.0×10^{-2}. The existence of excess O_2 flux makes deposited Ti oxidized. Therefore, the O/Ti ratio reaches stoichiometry and is also constant in this region. The amount of O_2 that can be gettered at the chamber wall is limited by the amount of Ti arrived to the chamber wall. As a result, only P_f changes as Q_{in} increases.

The adsorbed/incident O_2 flux ratio obtained in this paper is smaller than previously reported sticking coefficient values for evaporated Ti films(about 0.80)[18]. Since before the transition arriving Ti is thought to be active, the value obtained in this experiment may be underestimated. One possible reason would be the error of flux calculation of O_2, including the pressure measurement error. However, the relative change in α to the O_2 partial pressure change clearly explains that the adsorption probability decreases as O/Ti ratios of deposits on deposition area increase.

The results obtained in this chapter quantitatively show an important role of gettering effects in reactive sputtering. It has also been reported by a few authors that there is a critical pumping speed to eliminate hysteresis effect in reactive sputtering[4]. The critical pumping speed is generally thought to be at least equal or several times larger than the gettering speed. However, the results shown in this paper suggest that it is difficult to eliminate hysteresis effect by increasing pumping speed in an actual deposition system.

IV.V. CONCLUSIONS

Reactive gas mass balance change and sputtering yield change have been analyzed by pressure change observation and by composition analysis of the deposited films. The obtained results show the drastic change in gettering effects at the mode transition that takes place at a critical O_2 partial pressure. Until this transition, more than 90% of the introduced O_2 is consumed by gettering. The amount of gettered O_2 displays a maximum just before target oxidation occurs. At that point the calculated getter pumping speed reaches 2.3 m^3/s, which is 10 times larger than the physical pumping speed. Furthermore, the adsorbed/incident O_2 flux ratio is found to decrease from 0.36 to 0.0010 with increasing O_2 partial pressure. The obtained results show impotant roles of gettering effects in mass balance changes in reactive sputtering.

IV.VI. REFERENCES

1) G.Lemperiere and J.M.Poitevin, Thin Solid Films 111, 339(1984)
2) A.Okamoto and T.Serikawa, Thin Solid Films 137, 143(1986)
3) A.G.Spencer, R.P.Howson, and R.W.Lewin, Thin Solid Films 158, 141(1988)
4) S.Kadlec, J.Musil, and J.Vyscocil, Vacuum 37(10), 729(1987)
5) S.Berg, H-O.Blom, T.Larsson, and C.Nender,J.Vac.Sci.Technol. A5(2), 202(1987)
6) J.Danroc, A.Aubert, and R.Gillet, Sur.Coat.Technol.33, 83(1987)
7) S.Berg, H-O.Blom, M.Moradi, and C.Nender, J.Vac.Sci.Technol. A7(3), 1225(1989)
8) B.Chapman, *Glow Discharge Processes*(JOHN WILEY & SONS, New York, 1980), Appendix 5, pp.374-382
10) M.A.Lewis and D.A.Glocker, J.Vac.Sci.Technol.A7(3), 1019(1989)
11) D.M.Gruen, A.R.Krauss, and M.J.Pellin, Radiation Effects 89, 113(1985)
12) A.F.Hmiel, J.Vac.Sci.Technol.A3(3), 592(1985)
13) S.Shiller, U.Heisig, Chr.Korndoerfer, G.Beister, J.Reschke, K.Steinfelder, and J.Strumpfel, Surf.Coatings Technol.33, 405(1987)
14) W.D.Sproul, P.J.Rudnic, and C.A.Gogol, Thin Solid Films 171,171(1989)
15) G.Georgiev, N.Feschiev, D.Popov, and Z.Uzunov, Vacuum 36(10), 595(1986)
16) S.Maniv and W.D.Westwood, J.Vac.Sci.Technol.17(3), 743(1980)
17) M.Scherer and P.Wirz, Thin Solid Films 119, 203(1984)
18) N.E.Biryukova and M.I.Vinogradov, Russ.J.Phys.Chem.45, 1441(1971)

V. AN INVESTIGATION OF HYSTERESIS EFFECTS AS A FUNCTION OF PUMPING SPEED, SPUTTERING CURRENT, AND O_2/Ar RATIO

V.I. INTRODUCTION

The hysteresis of deposition rate or total pressure in relation to reactive gas flow rate is a well-known behavior in reactive sputtering[1]. This hysteresis is a consequence of the fact that the points where a change in the process condition occurs when the reactive gas flow rate is increased are different from the points where a change in the process condition occurs when the reactive gas flow rate is decreased.

The change in the process is drastic and avalanche-like, and is caused by the target surface condition change from a metallic condition to a compound-covered condition or from a compound-covered condition to a metallic condition, as a function of reactive gas flow rate[2]. The target surface condition change is believed to correlate to gettering on the chamber wall. The resultant process change is generally called mode transition: *i.e.*, metal-compound(nonreactive-reactive) mode transition and compound-metal(reactive-nonreactive) mode transition.

The target surface condition change is a result of two competitive phenomena:formation of compound layers by chemisorption of reactive gas to active metal sites and sputtering of formed compound layers. This resulting change is affected by mass balance between the reactive gas and metal atoms or ions sputtered from target and by the arrival inert/reactive gas flux ratio. On the other hand, reactive gas gettering is considered to be a result of interaction between arrival reactive gas flux and sputtered metal flux to the chamber wall where gettering takes place. The interaction depends on reactive gas mass flow rate and the cathode power that determines the sputtered metal flux. Consequently, hysteresis is thought to be affected by reactive gas flow rate, cathode power, and the ratio between reactive (*e.g.*, O_2, N_2) and inert gases (*e.g.*, Ar).

In addition to these factors, since the gettering is thought to be in competition with evacuation of reactive gas by the vacuum pumping system, hysteresis is considered to be affected by the physical pumping speed of the pumping system.

In fact, some researchers have reported that pumping speed and cathode power affect mode transitions and hysteresis[3-9]. Although these results may be explained by the hypothesis described above, to date the effects of these factors on hysteresis have not been clearly and systematically explained. Furthermore, the mechanisms of hysteresis have not been discussed.

In this respect, effects of physical pumping speed, sputtering current, and reactive/inert gas ratio on mode transitions and hysteresis will be discussed in this chapter. First hysteresis

and associated process changes due to mode transitions will be discussed. Secondary effects of pumping speed, sputtering current, and Ar partial pressure will also be investigated and discussed. By discussing the effect of pumping speed and sputtering current on hysteresis, the mechanisms of hysteresis will be revealed.

V.II. EXPERIMENTAL METHOD

To investigate transition point behavior, O_2 flow rate, Q_{O2}, was increased in steps of 0.5 std.cm^3/min from 0 std.cm^3/min until a mode transition was observed, after which Q_{O2} was again decreased to 0 std.cm^3/min. Titanium emission intensity, I_{Ti}, total pressure, P, sputtering voltage, V_{sp}, and mass deposition rate, R_{dep} were acquired every 15 s after Q_{O2} was set to a desired value until the process was balanced;*i.e.*,the change in P and I_{Ti} was less than $\pm 1\%$ compared to previous values. After the process was balanced, Q_{O2} was set to the next value. The data for certain Q_{O2} values were the data obtained after the process became balanced. Oxygen partial pressure, P_{O2}, was calculated from measured total pressure.

V.III. RESULTS

A. HYSTERESIS INVESTIGATION

Figure 5.1 shows typical hysteresis curves observed under S_p=2.0X10^{-1} m^3/s and I_{sp}=2.0A. When Q_{O2} is increased, the first transition occurs at Q_{O2}=7.5 std. cm^3/min, and when it is decreased, the other, reverse transition occurs at Q_{O2}=4.5 std.cm^3/min. The first transition is the mode transition from metalto compound mode, T_{M-C}, and the second one is from compound to metal, T_{C-M}. The width of the hysteresis is 3.5 std.cm^3/min. Before T_{M-C} occurs I_{Ti} decreases gradually, and R_{dep} reaches its maximum value when Q_{O2}=7.0 std.cm^3/min. Discharge voltage, V_{sp}, which reflects the target surface condition and plasma condition, increases gradually until T_{M-C} takes place. Before the transition T_{M-C}, P_{O2}<6.7X10^{-3} Pa. After the transition T_{M-C}, I_{Ti} and R_{dep} are reduced to 1/10 of their values before the transition. At the transition T_{M-C}, V_{sp} increases and P_{O2} increases drastically. After the transition T_{M-C}, V_{sp} decreases gradually, and P_{O2} increases linearly. Above Q_{O2}=8 std.cm^3/min, I_{Ti} and R_{dep} are constant.

After the target surface has become fully oxidized, when Q_{O2} is decreased until the transition T_{C-M} occurs, P_{O2} decreases linearly while V_{sp} increases only gradually. Before the transition T_{C-M}, R_{dep} increases slightly and I_{Ti} remains almost constant. After the transition T_{C-M} occurs, those values trace curves obtained before the target surface oxidation.

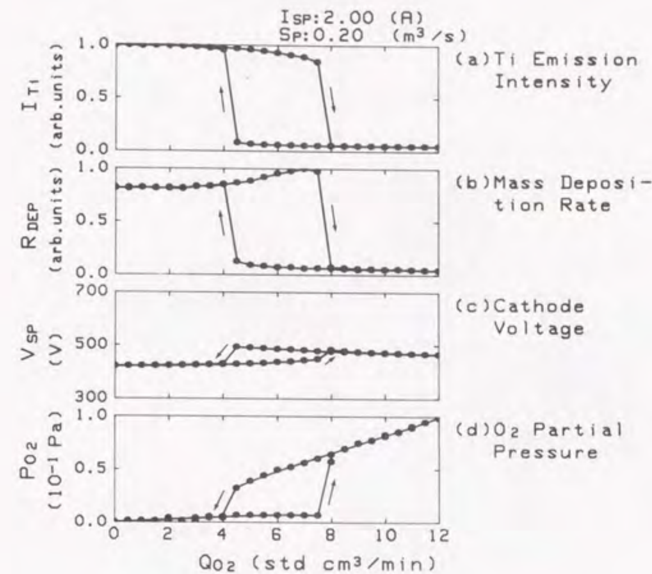

Fig.5.1 Typical hysteresis curves observed at a pumping speed of 0.20X10^{-1} m^3/s and with a sputtering current of 2.0 A :(a)Ti emission intensity (b)Mass deposition rate (c)cathode voltage (d)O_2 partial pressure.

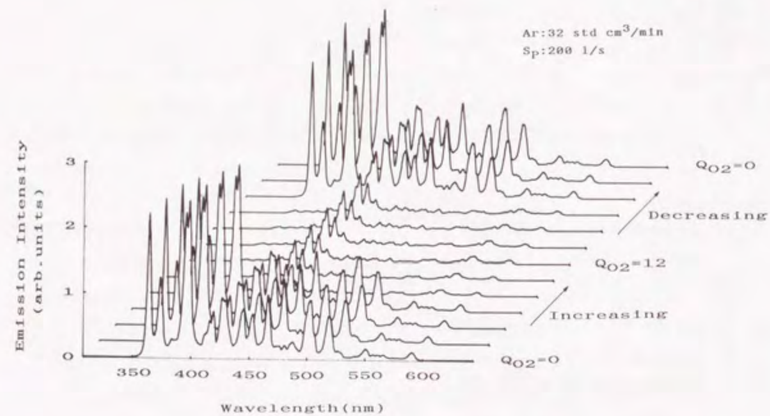

Fig.5.2 Emission spectra with increasing and decreasing Q_{O2} at I_{sp}=2A and S_p=2.0X10^{-1} m^3/s.

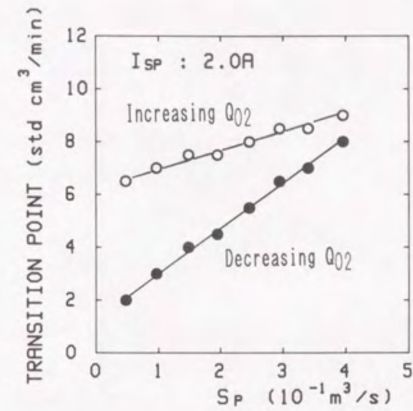

Fig.5.3 The effect of pumping speed on the transition points as a function of O_2 flow rate :o increasing O_2 flow rate :● decreasing O_2 flow rate.

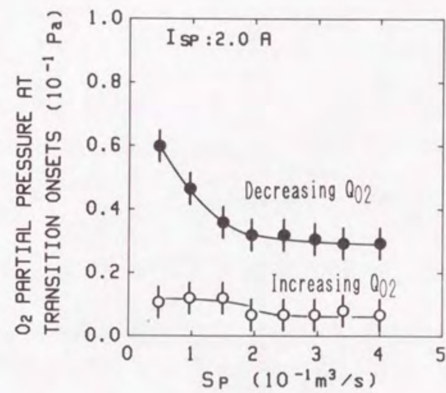

Fig.5.4 Oxygen partial pressure at the transition onsets versus pumping speed at a sputtering current of 2.0A:o increasing O_2 flow rate :● decreasing O_2 flow rate.

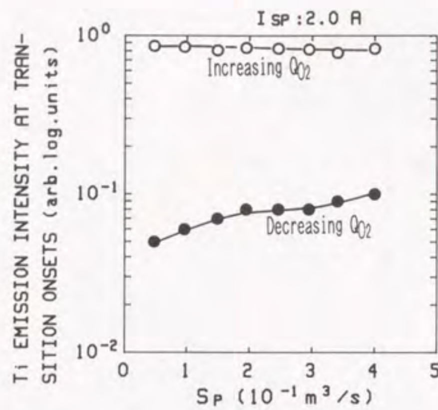

Fig.5.5 Titanium emission intensity at the transition onsets at a sputtering current of 2.0A:o increasing O_2 flow rate :• decreasing O_2 flow rate.

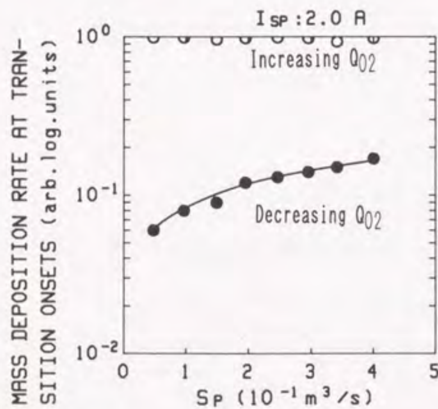

Fig.5.6 Mass deposition rate at the transition onsets at a sputtering current of 2.0A: o increasing O_2 flow rate :• decreasing O_2 flow rate.

Figure 5.2 shows results of plasma emission spectroscopy for various Q_{O2} values at I_{sp}=2.0A and S_p=2.0X10^{-1} m^3/s. Drastic changes in emission spectra are observed between Q_{O2}=6 and 8 std.cm^3/min for increasing Q_{O2} and between Q_{O2}=6 and 4 std.cm^3/min for decreasing Q_{O2}. Spectra lines investigated at 364–365, 399–400, 498–499, and 550–551 nm before the transition T_{M-C} and after the transition T_{C-M} were identified as emission lines from Ti[10]. Emission spectra lines observed at 420 and 430nm are from Ar[11] and do not show much change in intensity. Weak emission is observed at about 560nm between the two transitions. This is an emission line from O_2^+[12].

B. EFFECTS OF PUMPING SPEED

Variation in transition points as a function of O_2 flow rate for various pumping speeds, S_p, was observed. Figure 5.3 shows the results obtained at I_{sp}=2.0 A. Although both onset points for the increase and decrease of Q_{O2} increase linearly as S_p increases, the second transition onset(for T_{C-M}) increases with a larger slope. The width of the hysteresis, which is defined by difference in onsets for T_{M-C} and T_{C-M}, therefore, decreases with increasing S_p. The width at the maximum S_p of 4.0X10^{-1} m^3/s is 1.0 std.cm^3/min.

In Fig.5.4, P_{O2} at the transition onsets are shown. Since the O_2 partial pressure at the transition onsets for T_{M-C} did not change within experimental error(5.3X10^{-3} Pa), the results obtained are not reliable enough. On the other hand, change in the second transition T_{C-M} is clearer. Values of P_{O2} at the onsets for T_{C-M} decrease sharply until S_p=2.0X10^{-1} m^3/s and then are constant.

As shown in Figs.5.5 and 5.6, I_{Ti} and R_{dep} at transition onsets show a similar tendency versus variation of S_p; *i.e.*, while for T_{M-C}, S_p does not have much effect on I_{Ti} and R_{dep}, for T_{C-M} both I_{Ti} and R_{dep} increase as S_p increases.

C. EFFECTS OF SPUTTERING CURRENT

In addition to the effects of S_p, the effects of I_{sp} on hysteresis were investigated at S_p=4.0X10^{-1} m^3/s. Figure 5.7 shows hysteresis curves of I_{Ti} versus Q_{O2} for I_{sp}=0.5A, 1.0A, 2.0A, and 3.0A at S_p=4.0X10^{-1} m^3/s. In Fig.5.8 the mode transition values obtained are shown. Transition points shift to higher values of Q_{O2} with increasing I_{sp}. Moreover, the hysteresis width increases as I_{sp} increases. Although at I_{sp}=0.5A the two onset points over-lapped, hysteresis was still present and there were drastic changes in I_{Ti} for Q_{O2} between 1.0 and 2.0 std.cm^3/min.

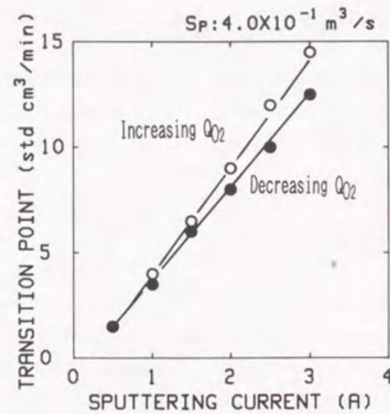

Fig.5.7 The effect of sputtering current on the transition points as a function of O_2 flow rate at a pumping speed of $4.0X10^{-1}$ m^3/s :o increasing O_2 flow rate :● decreasing O_2 flow rate.

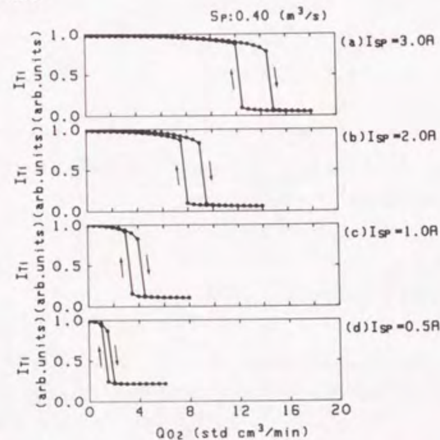

Fig.5.8 Hysteresis curves of Ti emission intensity at various sputtering current : (a)I_{sp}=3.0A (b)I_{sp}=2.0A (c)I_{sp}=1.0A (d)I_{sp}=0.5A.

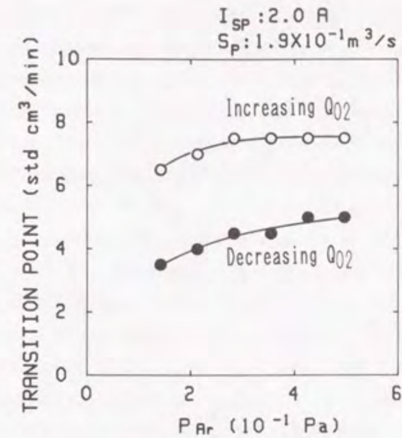

Fig.5.9 The effect of Ar partial pressure on the transition points as a function of O_2 flow rate at a pumping speed of $1.9X10^{-1}$ m^3/s and at a sputtering current of 2A : o increasing O_2 flow rate :● decreasing O_2 flow rate.

D. EFFECTS OF O_2/Ar RATIO

Figure 5.9 shows the effect of Ar partial pressure on the transition points at S_p=$1.9X10^{-1}$ m^3/s and at I_{sp}=2.0A. As P_{Ar} increases both onsets for T_{M-C} and T_{C-M} shift to slightly larger values of Q_{O2}. There is no significant change in hysteresis width. The influence is not so strong as that of pumping speed or sputtering current.

V.IV. DISCUSSION

A. HYSTERESIS

In the hysteresis curve in Fig.5.2 two avalanche-like changes are visible when Q_{O2} is increased or decreased. As a consequence of the target surface becoming oxidized several events occur. The most remarkable change is shown in the change in P_{O2}. Before the transi–

tion T_{M-C} almost all of O_2 introduced into the chamber was consumed by gettering. Once the target surface is oxidized, the amount of consumed gas decreases to about 1/4 compared to that before the transition. As a result P_{O2} increases drastically at the transition T_{M-C}.

This change in P_{O2} is also shown in the emission spectra measurement results. While the target surface is kept metallic, no emission line from oxygen was observed. However, when the target surface is oxidized, resulting in an increase in P_{O2}, an emission line from O_2^+ was observed. Emission lines from Ti are stronger in the metallic condition. There is no remarkable intensity change in Ar emission lines, indicating that there is no detectable change in P_{Ar}.

The decrease of the gettering amount is a result of the reduction in sputtering yield, $Y/(1+\gamma)$, where γ refers to secondary electron emission coefficient. The reduction in $Y/(1+\gamma)$ is well shown by the change in intensity of the Ti emission line. The reduction is believed to be due to an increase of γ, and change in binding energy as a result of surface oxidation of the Ti target surface. Although the change in γ, in the Ti–O_2 sputtering system, has not been reported, generally surfaces exposed to oxygen yield higher values of γ[13]. This is further supported by results reported on a change in γ in the case of Ti–N_2 reactive sputtering[14]. In this experiment it is concluded that when a Ti target is bombarded by N_2 with an energy of 500 eV, γ increases to 0.12 from 0.08, the value obtained when the target is bombarded by Ar^+. Form this discussion, it can be sdetermined that there is an increase in γ when the target surface is oxidized by O_2. This increase enhances e^- current, reducing effective O^+, O_2^+, or Ar^+ flux to the target surface in diode systems. The influence of the change in binding energy has not been experimentally investigated. However, from the basic theory of sputtering it is suggested that the formation of the Ti–O bond reduces the sputtering yield[15].

In addition to changes in γ, when the reactive gas is O_2, an effect of O^- ion reflection should be involved in discussion. As reported and discussed by Tominaga *et al.*[16], when O_2 is used as a reactive gas, energetic O^- ions are reflected from the target. This also reduces the sputtering yield by decreasing positive ion current. Therefore, such factors as γ, O^- reflection, and surface binding energy acts to reduce the sputtering yield from a target covered by oxide layers. This is also supported by results reported by Gruen *et al*[17]. It is further found in our experiment that the decrease in the sputtering yield result a drastic decrease in mass deposition rate and Ti emission intensity.

The increase of R_{dep} until the transition T_{M-C} is due to weight gain by gettering. Since R_{dep} is the summed mass of arriving Ti and gettered O_2, it increases when the increase in O_2 flux overcomes the reduction in arriving Ti flux. Thus R_{dep} shows the maximum at Q_{O2}=4.0 std.cm^3/min.

The operating cathode voltage (when the cathode power supply is operated at a constant current mode) reflects the change in the target surface condition and plasma condition. As

discussed above, changes in γ and negative ion reflection occur at the transitions. This change can vary plasma impedance. In addition to the target surface condition change, gas concentration in the plasma can affect the cathode voltage[18]. The ionization cross section for O_2 by electron impact in the energy range up to 500eV is 1/3 to 1/4 less than that for Ar[19]. Therefore, electron and ion densities in the plasma decrease when the O_2 content in the plasma region increases, resulting in an increase in the plasma impedance.

The increase or decrease in V_{sp} at the transition is considered to be induced by a gas concentration change. The gradual decrease in V_{sp} after the transition T_{M-C} results from the difference in relative $Ar^+/(O^+$ or $O_2^+)$ ion ratio of flux bombarding the target surface because variation in this ratio can induce a plasma impedance change by influencing γ and O^- reflection. However, it is dangerous to discuss this slight change in plasma condition further because a complicated interaction between plasma and cathode or anode can result in a subtle change in the plasma condition.

Once the target surface is fully oxidized, no clear change occurs in the process. In this region the surface condition is at a steady state; *i.e.*, sputtered and adsorbed O_2 are balanced. As a result, there is no obvious change in the sputtering yield. Thus, values of R_{dep} and I_{Ti} are constant for increases or decrease of Q_{O2}. In the steady state, the mass of consumed O_2 by gettering, Q_G, remains constant. Therefore, O_2 partial pressure increases linearly with Q_{O2}. The relationship between P_{O2} and Q_{O2} in this region is shown by following equation:

$$P_{O2}=Q_{O2}/S_p-C \qquad (5.1)$$

where C is equal to Q_G/S_p and constant.

Opposite changes in P_{O2}, R_{dep}, V_{sp}, and I_{Ti} occur when compound layers on the target surface are removed by sputtering. These changes can also be explained by a change in target surface and plasma conditions;*i.e.*, when Q_{O2} reaches a critical point, the compound layers on the target surface are removed, resulting in an increase in Ti sputtering yield and the following changes in P_{O2} and R_{dep}. Once avalanche-like cleaning takes place, the target surface condition returns to the condition present for the same Q_{O2} before target surface oxidation. This suggests that, once the cleaning of the target surface takes place, the new steady state condition is not affected by the initial condition of the target surface.

B. EFFECTS OF PUMPING SPEED, SPUTTERING CURRENT, AND Ar PARTIAL PRESSURE ON TRANSITION POINTS

As shown in Fig.5.3, the effects of S_p on the transition from compound to metal condition are remarkable. This widens the hysteresis for smaller S_p. The reason why the transition point, T_{M-C}, is not much affected by S_p is explained as follows.

In the metallic condition, since almost all of O_2 is consumed by the gettering, gettering strongly influences mass balance in O_2, which consequently induces an avalanche-like mode transition. This means that getter pumping more strongly affects mode transition T_{M-C} than physical pumping does. To discuss the pumping speeds quantitatively, it is possible to estimate getter pumping speed for O_2 and S_G, by the following equation:

$$S_G=Q_{O2}/P_{O2}-S_p \qquad (5.2)$$

From the calculation, S_G at the onsets for T_{M-C} are estimated to range between $8.0X10^{-1}$ and 2.0 m^3/s, several times larger than S_p. Therefore variations in S_p have negligible effects on the mode transition T_{M-C}, less affecting the shift of mode transition points. In other words, before the transition T_{M-C}, getter pumping is the dominant pumping mechanisms for O_2.

In addition, this viewpoint is supported by the fact that I_{Ti} at the transition points remains almost constant when S_p is varied. Since I_{Ti} is thought to be related linearly to getter pumping capacity, it can be said that, when Q_{O2} exceeds a critical getter pumping capacity, O_2 that has not been consumed by the gettering strikes the target surface and poisons it. At this point the amount of consumed O_2 is almost constant against the variation of S_p. This suggests that relationship between introduced O_2 and the getter pumping capacity mainly dominates in determining the mode transition point for T_{M-C}. Mass deposition rates are also constant at the T_{M-C} onsets against the variation of S_p because at this point the process condition is independent of S_p.

On the other hand, S_p influences the T_{C-M} transition onset point. In contrast to the transition T_{M-C}, O_2 pumping speed dominates this transition. In the reactive operation mode, to break the O_2 mass balance among introduced, gettered, and pumped out and to advance target cleaning, it is required that the sputtered oxygen atoms or molecules be removed from the chamber;if the oxygen atoms or molecules removed from the target are simply gettered on the chamber wall, it does not change the mass balance of O or O_2 in the chamber. The probability for a given sputtered O or O_2 to be pumped out is given by the ratio S_p/S_G. The gettering pumping speed is estimated to range from $8X10^{-3}$ m^3/s(for $S_p=4.8X10^{-2}$ m^3/s) to $6.5X10^{-2}$ m^3/s(for $S_p=4.0X10^{-1}$ m^3/s) at the onset of T_{C-M}. These values are smaller than those of S_p. Thus, S_p has a greater influence on the T_{C-M} transition than on T_{M-C} transition and, therefore, at larger pumping speeds, where the amount of O removed from the chamber is larger, the transition occurs at a larger Q_{O2}.

This discussion on the getter pumping can explain pressure behavior at the transitions. Since the O_2 partial pressure, P_{O2}, is given by the following equation:

$$P_{O2}=Q_{O2}/(S_G+S_p) \qquad (5.3)$$

if S_G is much larger than S_p, P_{O2} is dependent mainly on S_G, whereas if S_p is comparable to

S_G, P_{O2} is dependent both on S_G and on S_p. Therefore, at the transition T_{M-C}, P_{O2} is almost constant versus S_p. On the other hand, at the transition T_{C-M}, P_{O2} depends predominantly on S_p especially for low S_p.

Variation of I_{sp} also influences getter pumping capacity, Q_G. As discussed above, since a change in Q_G affects T_{M-C} more than T_{C-M}, the variation in onsets for T_{M-C} is larger than that in onsets for T_{C-M} as shown in Fig.5.7, causing the hysteresis width to decrease at low I_{sp}.

Argon partial pressure also affects mode transitions by affecting the balance between target surface oxidation and sputtering;when an oxidized site is attacked by O or O_2, it remains oxidized;when an oxidized site is attacked by Ar, it is cleaned. In the same way, when a metallic site is attacked by O or O_2, it is oxidized;when a metallic site is attacked by Ar, it remains metallic. Therefore, when Ar pressure is increased, the probability that an oxidized site on the target surface is cleaned or that a metallic site is kept metallic increases. On the other hand, when the O_2 pressure is increased, the probability of surface oxidation increases. Thus, to advance surface oxidation more O_2 flux is required. Therefore, as P_{Ar} increases the transition points shifts to higher values. However, the arrival flux ratio does not dominate hysteresis behavior, thus, minimizing its effects on the transition point.

The origin of hysteresis is the difference in getter pumping capacity between the metallic condition and the oxidized condition; in the metallic condition getter pumping capacity is very large, and gettering dominates mass balance change;once the target surface is oxidized, the gettering pumping capacity is drastically decreased and consequently the total pumping speed is decreased. Thus, to trigger target cleaning, less Q_{O2} is required. This results in the onsets of T_{C-M} occurring at smaller Q_{O2} compared to the value where the onsets of T_{M-C} occur.

It is sometimes reported that at a critical S_p the hysteresis can be eliminated[5]. However, in this experiment the elimination of the hysteresis has not been investigated. As revealed in above discussion, the difference in gettering pumping capacity between the metallic condition and the oxidized condition is the origin of hysteresis. Since the difference is introduced by the difference between two sputtering yields:from a metallic target and from an oxidized target, as far as there is a difference in the two sputtering yields, the hysteresis cannot be eliminated completely and nonlinearity will remain. In particular, in the $Ti-O_2$ case, the difference in the yields is relatively large (the sputtering yield ratio between that of an oxidized target and that of a metallic target is estimated to be about 1/20 in this experiment. Thus hysteresis is significant in the $Ti-O_2$ reactive sputtering compared to other systems. Of course, if the ratio of the two sputtering yields is smaller, the mode transition would be more subtle and variation of S_p would be more effective in minimizing hysteresis.

Generally hysteresis and mode transition depend on apparatus dimensional factors, e.g,

chamber volume, positions of the pumping port, the gas inlet, and the cathode, *etc*[6]. The results shown in this paper will also be affected by those apparatus factors. However, as revealed in the above discussion, the key phenomena influencing mode transition and hysteresis are the phenomena that occur at the target or chamber wall surfaces where sputtered metal films are deposited. Therefore, it is possible to narrow these dimensional factors by focusing the issues on the phenomena at target surface and chamber wall surfaces. For example, relationship between chamber volume and physical pumping speed can be parametrized using reactive gas residual time,τ, in the chamber:

$$\tau=V/S_p \tag{5.4}$$

where V is chamber volume and S_p is pumping speed. By multiplying σ by incident flux, the possible incidence that reactive gas atoms or molecules which are incident on the target surface or chamber wall before being pumped out can be calculated. The equation is as follows:

$$N_I=\Gamma\tau \tag{5.5}$$

where N_I is the number of incident O_2 molecules times per unit area and Γ is O_2 flux calculated from P_{O2} and temperature. Consequently, if the chamber is very small or if the pumping speed is very large, the residence time would be small and the reactive gas would be pumped out before having time to interact with active sites on the target surface or chamber wall. In contrast, if the chamber is very large or pumping speed is very small, possible incidence times to the surface would be large and the reactive gas would have a much greater probability of reciting with active sites on the target surface or chamber wall before being pumped out. In the former case the reactive gas partial pressure would dominate the mode transition not the amount of reactive gas introduced.

In addition to these two factors, the effects of chamber configuration (positions of the reactive gas inlet, the cathode, *etc*.) should be analyzed in terms of the probability for the introduced gas to be pumped out by the vacuum pump or to reach the active target surface or wall surface. For example if the gas inlet is set near the pumping port, the probability that an introduced O_2 molecule is pumped out before reaching and interacting with an active target surface site or an active wall surface site would be higher. On the other hand if the inlet is set near the cathode the probability would be lower. It would be helpful to examine the effects of those configurational factors to generalize understandings of the reactive sputtering process.

V. CONCLUSIONS

Hysteresis behavior and the effects on it of physical pumping speed, sputtering current,

and Ar partial pressure have been investigated, and mechanisms of the hysteresis process have been discussed. It is shown that many events happen as a consequence of the target surface oxidation or cleaning. The results obtained explain the important roles of pumping speed and sputtering current on hysteresis. As pumping speed increases hysteresis width decreases since the transition point from compound to metal mode shifts to higher values of Q_{O2} while the transition point from metal to compound mode remains constant against variation of pumping speed. In addition, for smaller sputtering currents and constant pumping speed, hysteresis width decreases. The change in transition points as a function of pumping speed and sputtering current have successfully been explained by considering getter pumping capacity or getter pumping speed. Elimination of hysteresis has not been investigated in this experiment. From the discussion it is suggested that hysteresis is a result of the difference in sputtering yields from an oxidized target and from a metallic target, which provides the difference in gettering capacities.

V.VI. REFERENCES

1) W.D.Westwood, Physics of Thin Films 14, 1(1989)
2) S.Maniv and W.D.Westwood, J.Vac.Sci.Technol.17(3), 743(1980)
3) G.Lemperiere, Le Vide, les Counches Minces 235, 3(1987)
4) G.Lemperiere and J.M.Poitevin, Thin Solid Films 111, 339(1984)
5) T.Serikawa and A.Okamoto, Thin Solid Films 101, 1(1983)
6) J.Danroc, A.Aubert, and R.Gillet, Surf.Coating.Technol.33, 83(1987)
7) S.Kadlec, J.Musil, and J.Vyscocil, Vacuum 37(10), 729(1987)
8) J.Musil,S.Kadlec,J.Vyskocil, and V.Valvoda, Thin Solid Films 167, 107(1988)
9) T.M.Pang, M.Scherer, B.Heinz, C.Williams, and G.N.Chaupt, J.Vac.Sci.Technol.A7(3), 1254(1989)
10) A.N.Zaidel' et.al., *Tables of Spectra Lines*(IFI/PLENUM, New York, 1970),pp.695-702
11) A.N.Zaidel' et.al., *Tables of Spectra Lines*(IFI/PLENUM, New York, 1970), pp.362-370
12) P.W.B.Pearse and A.G.Gaydon, *The Identification of Molecular Spectra*(CHAPMAN AND HALL, London, 1976), pp.255-262
13) B.Chapman, *Glow Discharge Processes*(WILEY INTERNATIONAL, New York, 1980), Chapter 4, pp.84-91
14) M.A.Lewis, D.A.Glocker, and J.Jorne, J.Vac.Sci.Technol.A7(3), 1019(1989)
15) G.Betz and G.K.Wehner, *Sputtering by Particle Bombardment II*(Springer-Verlag, Berlin 1983), Chapter 2, pp.48-60.
16) K.Tominaga, S.Iwamura, Y.Shintani, and O,Tada, Jpn.J.Appl.Phys, 21, 688(1982)
17) D.M.Gruen, A.R.Krauss, and M.J.Pellin, Radiation Effects 89, 113(1985)
18) B.Gorvanchev, V.Orlinov, and V.Popova, Thin Solid Films 33, 173(1976)
19) S.C.Brown, *Basic Data of Plasma Physics*(M.I.T.PRESS, Cambridge, MA, 1966), Chapter 5, pp.141-143

VI. MODELING OF TIME-DEPENDENT PROCESS CHANGE AND HYSTERESIS

VI.I. INTRODUCTION

Modelling is sometimes useful to examine process conditions. There have been some models to examine reactive gas mass balance in reactive sputtering processes[1-3]. However, most of them are empricaly obtained models, and therefore they cannot explain physical mechanisms of mode transition or hysteresis behavior. Further, although, in an actual situation, hysteresis is obtained at a steady-state after a dynamic target surface condition change reaches a steady-state, no models have provided hystersis curves as a result of time-dependent target surface condition changes. Thus it is thought to be crucial to develop a model based on physiscal mechanisms involved in reactive sputtering, and this model should exhibit hysteresis as a result of time-dependent target surface condition calculations.

Most genarally accepted is a model currently proposed by Berg *et al.*[4-7] and Larsson *et al*[8]. However, in their model, hysteresis effects have been explained as a runaway at a bend point in S-shape curves. The purpose of the modeling of hysteresis effects is to obtain this runaway process by the model. In this respect, their model does not explain hysteresis effects that observed in an actual reactive sputtering process. In addition, they also mentioned that in an actual situation an S-shape curve is obtained with a feed back control system of a reactive gas mass flow rate. However, the S-shape curve observed in an actual process is a result of the delay of the response of the feed back system and therefore depends mainly on a response time of the feed back system[9]. The S-shape curve observed in an actual process is not a result of physical mechanisms of hysteresis effects.

In this chapter a model of reactive sputtering that calculated target compound-layer formation and sputter-etching as a function of elapsed time will be proposed. The model will provide hysteresis curves as a result of the calculations of target coverage changes(compound-layer formation or sputter-etching) as a function of reactive gas mass flow rate. The simulation will be performed by dealing with mass balance among the amount of gas gettered at the chamber wall, the amount of gas adsorbed at the target surface, the amount of gas sputtered from the target surface, and the amount of gas pumped out. It will be emphasized that modeling of reactive sputtering should involve simulation of compound-layer formation and sputter-etching as a function of elapsed time since nonlinear behavior and hysteresis in reactive sputtering are principally resulted from the balance between compound-layer formation and sputter-etching.

The goal of the simulation model is to exhibit changes in reactive gas partial pressure and target coverage as a function of elapsed time and their hysteresis curves as a function of reactive gas flow rate. We will report results of time-dependent compound-layer formation

and sputter–etching on the target surface, calculated by using the simulation program. The results will reveal effects of reactive gas flow rate, physical pumping speed, and sputtering current on compound–layer formation and sputter–etching. Hysteresis curves provided as a consequence of time–dependent compound–layer formation and sputter–etching calculations will be also reported. The appropriateness of the simulation model will be discussed. Mechanisms of reactive sputtering process changes will be also discussed.

VI.II. THEORETICAL BASIS

The fundamental idea for modeling is given by considering reactive gas flow in reactive sputtering process. Flow of reactive gas is schematically shown in Fig.6.1. Introduced gas molecules react with active metal atoms at the target surface and form compound layers, and are gettered at the wall surface by sputtered metal flux. Simultaneously they are pumped out by the vacuum pump. Gas adsorbed on the target surface is sputtered as well as the metal target material is. Desorption of the gas gettered at the chamber wall is usually negligible. This relationship is given by:

$$Q_{in}=Q_a-Q_s+Q_g+Q_p \qquad (6.1)$$

where Q_{in} is the amount of introduced reactive gas, Q_a is the amount of reactive gas adsorbed at the target, Q_s is the amount of reactive gas sputtered from the target, Q_g is the amount of reactive gas gettered at the chamber wall, and Q_p is the amount of reactive gas pumped out. This equation is also expressed by the following equation:

$$Q_{in}+Q_s=P(S_a+S_g+S_p) \qquad (6.2)$$

where P is reactive gas partial pressure, S_a is target adsorbing speed, S_g is gettering speed, and S_p is pumping speed of the vacuum pump system. Then, reactive gas partial pressure P can be given by:

$$P=(Q_{in}+Q_s)/(S_a+S_g+S_p) \qquad (6.3)$$

This equation must be satisfied during moment–by–moment mass balance changes. S_P and Q_{in} are treated as constant values within the pressure range to be considered. Other terms depend on elapsed time; *i.e.*, P, Q_s, S_a, and S_g change as a function of elapsed time until the process reaches a steady–state.

There may be some approaches to display the change in P as a function of elapsed time. To understand and simulate mechanisms of reactive sputtering it is better to express Q_s, S_a, and S_g as a function of target coverage θ first and then deal with θ as a function of elapsed time. As shown below, this is possible by a simple treatment of Q_s, S_a, and S_g.

Adsorption of reactive gas at the target surface is shown as a function of target coverage by the following equation:

$$Q_a=\Gamma_{O2}\alpha_T(1-\theta)A_T \qquad (6.4)$$

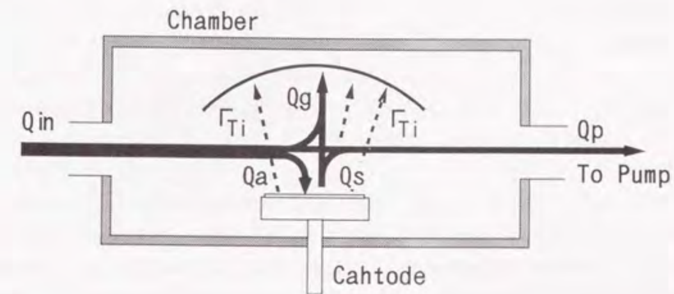

Fig.6.1 Schematic of reactive gas flow in reactive sputtering system.

where Γ_{O2} is O_2 flux, α_T is adsorption coefficient at the target wall, and A_T is target surface area. By introducing reactive gas partial pressure P, Eq.6.4 can be written by:

$$Q_a=PC_1\alpha_T(1-\theta)A_T \qquad (6.5)$$

where C_1 is a constant.

Since $S_a=Q_a/P$, the following equation is obtained:

$$S_a=C_1\alpha_T A_T(1-\theta) \qquad (6.6)$$

By this equation, S_a can be expressed as a function of θ by determining C_1, α_T, and A_T. A constant C_1 can be given from a kinetic theory, whereas α_T and A_T in an actual situation vary as a function of P and θ. Although theoretically it is possible to provide α with a change in P, this makes the model much more complicated and actually makes it disable to solve. In other words, it is very difficult to give an accurate value for α in a moment-by-moment model calculation. In addition, it is also thought to be meaningless to use a value of an appeared surface area as A_T.

As a consequence of this discussion, a constant that is equal to $C_1\alpha_T A_T$ is introduced. This covers the problem described above, and further simplifies the calculations. Thus Eq.6.6 can be written as the following equation:

$$S_a=C_1'(1-\theta) \qquad (6.7)$$

In the computer program, C' is given as an initial target adsorption speed, S_t^0.

The gettering at the chamber wall surface can be also provided as a function of θ. The gettering amount is determined from the amount of incident reactive gas and the number of metal sites that can adsorb reactive gas atoms or molecules. The relationship will be given by the following equation:

$$Q_g=\Gamma_{O2}\alpha_W Q_m A_W/N_s \qquad (6.8)$$

where α_W is adsorption coefficient of reactive gas at chamber wall, Q_m is the number of active metal site at the chamber wall, A_W is the area of the gettering surface, and N_s is the number of sites on the gettering surface. By introducing P, Eq.6.8 can be rewritten by the following equation:

$$Q_g=PC_2\alpha_W Q_m A_W/N_s \qquad (6.9)$$

By the same way used in the case of dealing with target behavior, S_g is given by:

$$S_g=C_2\alpha_W Q_m A_W/N_s \qquad (6.10)$$

Since active metal atoms that can adsorb reactive gas are provided by sputtering, the number of active metal site, Q_m is given by the following equation:

$$Q_m=Q_i(Y_c\theta+Y_m(1-\theta)) \qquad (6.11)$$

where Q_i is the number of incident positive ions(e.g. Ar^+) on the whole target area, Y_c is sputtering yield for the compound-covered surface of the target, and Y_m is sputtering yield for the metallic surface of the target. In this treatment the wall surface area is not considered;*i.e.*, it is assumed that sputtered metal atoms can adsorb reactive gas anywhere

the metal atoms deposit. In addition, it is assumed that the metal atoms covered with newly arriving metal atoms cannot adsorb reactive gas atoms.

From Eqs.6.10 and 6.11, the following equation is obtained:

$$S_g=C\alpha_W Q_i(Y_c\theta+Y_m(1-\theta))A_W/N_s \qquad (6.12)$$

By a similar approach to dealing with target behavior, the equation is simplified as follows:

$$S_g=C_2'Q_i(Y_c\theta+Y_m(1-\theta)) \qquad (6.13)$$

Thus, S_g is determined by Q_i, Y_c, Y_m, and θ. In the computer program, C_2' is given as an initial gettering speed, S_g^0. In the simulation calculation, S_g^0 is estimated to be 2-3 times larger than pumping speed of the vacuum pump.

The remaining term, Q_s, is given by the following equation:

$$Q_s=Q_iY_c\theta \qquad (6.14)$$

For this equation, Q_i is determined from sputtering current;Y_c is determined from an experimental result.

As a consequence, P can be expressed as a function of θ:

$$P=(Q_{in}+Q_iY_c\theta)/(C_1'(1-\theta)(C_2'Q_i(Y_c\theta+Y_m(1-\theta))+S_p) \qquad (6.15)$$

The change in θ is given as a function of elapsed time from the results of the calculation of the amount of reactive gas adsorbed on the target surface and sputtered off from the target. The equations to calculate these amounts are derived from Eqs. 11 and 14.

There are two ways to obtain changes in P and θ as a function of elapsed time; one is to induce the differentiation of Eq.6.3 for elapsed time, and the other is a time-incremental method. The differentiation seems to require considerably complicated equations to solve. Compared to the differentiation, the time-incremental method is simpler and easier since it is unnecessary to use a complicated differentiation,*i.e.*, since elapsed time is used as a calculation step of the simulation program, it is unnecessary to use the differentiation. Thus the time-incremental method is thought to be better for the purpose of modeling, and preferred as the method to solve the problem. Furthermore, in this method, since a computer is used as it were an actual process chamber, it becomes easier for us to understand what obtained results mean. The use of the time-incremental method is a feature of this simulation.

In addition to this, in the program, the calculation is divided into three parts: wall gettering of reactive gas, adsorption of reactive gas on to the target, and sputtering of the target. This simplifies programming and calculation, and makes equations understandable. The outline of the program will be explained in the next section.

There are some assumptions with the simulation model:

(i)At the target one O_2 molecule can be adsorbed by one Ti atom on the surface. The formation of the compound is not considered. Possible physisorption on the target is neglected. The reactive gas cannot adsorb onto already compound-covered target sites. Incorporation of inert gas is neglected.

(ii)At the chamber wall, similar to phenomena at the target surface, one arriving Ti atom can adsorb one O_2 molecule. Gettered gas cannot desorb spontaneously. The gettering is regarded as a monolayer phenomenon.

(iii)The physical pumping speed S_p is assumed to be constant for the simulated pressure range.

(iv)Reactive gas partial pressure is uniform in the chamber.

VI.III. PROGRAM

In the program, $Ti-O_2$ reactive sputtering is modeled. First the constants are given: S_g^0, S_t^0, N_s, Y_m, and Y_c. Typical values of the constants are: $S_g^0=3.0X10^{-1}$ m^3/s, $S_t^0=2.0X10^{-2}$ m^3/s, $N_s=10^{18}$, $Y_m=2.3X10^{-1}$, and $Y_c=1.5X10^{-2}$. For calculation of target compound-layer formation the initial θ is given as 0, whereas for that of target sputter-etching it is given as unity.

Then the calculation is progressed with an increase of time increment. At time step, T=t, first, reactive gas partial pressure P is calculated from Q_{in}, S_p, S_t at T=t−1, and S_g at T=t−1:

$$P(t)=Q_{in}/(S_p+S_t(t-1)+S_g(t-1)) \quad (6.16)$$

Then $Q_t(t)$ and $Q_g(t)$ are calculated:

$$Q_t(t)=P(t)S_t(t-1) \quad (6.17)$$

$$Q_g(t)=P(t)S_g(t-1) \quad (6.18)$$

Then target coverage θ(t) is calculated:

$$\theta(t)=\theta(t-1)+Q_t(t)/((1-\theta(t-1))N_s) \quad (6.19)$$

If calculated θ(t) exceeds 1, $Q_t(t)$ is recalculated from the number of target surface sites so that θ becomes unity. In this case, P(t) is also recalculated from the newly determined $Q_t(t)$ to satisfy Eq.6.16.

If there are no sufficient numbers of wall sites to getter reactive gas, an excess amount of reactive gas is treated as an over flow. This over-flowed amount of reactive gas is added to the amount of introduced gas at the next time step, T=t+1.

Next, sputtering of target is dealt with. The amount of sputtered Ti is given by the following equation:

$$Q_m(t)=((1-\theta(t))Y_m+\theta(t)Y_c)Q_i \quad (6.20)$$

Here, N_s is not considered since Q_i is smaller than N_s in the program. The amount of Q_m determines the capacity of the gettering pump at T=t+1. Then a part of O_2 is gettered if there are active metal sites on the wall to getter sputtered gas. Not-gettered gas is also treated as an additional over flow.

A new value of θ(t), θ'(t), is calculated from the following equation:

$$\theta'(t)=\theta(t)-\theta(t)Y_cQ_i/N_s \quad (6.21)$$

Then the amount of sputtered reactive gas is calculated from the change in θ:

$$Q_s(t)=(\theta(t)-\theta'(t))N_s \quad (6.22)$$

Then if there is enough numbers of active metal site on the wall to getter sputtered gas, sputtered gas is gettered. Not-gettered gas is also treated as another over flow.

Finally, new pumping speeds, $S_t(t)$ and $S_g(t)$ are calculated from θ'(t):

$$S_t(t)=(1-\theta'(t))S_t^0 \quad (6.23)$$

$$S_g(t)=(1-\theta'(t)+Y_c/Y_m\theta'(t))S_g^0 \quad (6.24)$$

After determining $S_t(t)$ and $S_g(t)$, the calculation of next time step,T=t+1, starts. The calculation is repeated until variations in P and θ between T=t−1 and t become less than 1/1000.

Hysteresis curves are obtained by calculating steady-state values of target compound-layer formation and sputter-etching for a range of Q_{in}. The calculation is started from $Q_{in}=0$ std.cm³/min with the initial θ, $\theta_i=0$. Then, until the transition is observed, Q_{in} is increased in step of 0.5 std.cm³/min. After the transition is observed, it is decreased by the same step, starting the calculation with $\theta_i=1$. In the hysteresis calculations, S_p, I_{sp}, and Y_p are varied.

VI.IV. CALCULATION RESULTS

A. TIME-DEPENDENT PROCESS CHANGE

Figure 6.2 shows typical compound-layer formation calculation results for $S_p=1.5X10^{-1}$ m^3/s, $Q_{in}=5.0$ std.cm³/min, and $I_{sp}=2.0$ A. It is clearly shown that θ increases with elapsed time. As a consequence, O_2 partial pressure P_{O2} increases, and sputtered Ti flux Γ_{Ti} decreases. The target condition reaches a steady-state at about 30 s, and after that, there are no changes in θ, Γ_{Ti}, and P_{O2}. The final value of θ is about 0.3, displaying that the target has not been fully covered with compound layers. In Fig.6.3 compound-layer formation calculation results for a larger Q_{in} are shown under the condition of $S_p=1.5X10^{-1}$ m^3/s, $Q_{in}=8.0$ std. cm³/min, and $I_{sp}=2.0$ A. In this case at 40 s, the target is fully covered with compound layers(θ reaches 1). At this point Γ_{Ti} drops to less than 1/10 of the initial value. Until about 10 s, compound-layer formation is drastic, and then until 30 s, there is a plateau. After this point, compound-layer formation is again accelerated, and finally θ reaches 1.

In Figs.6.4 and 6.5 results of target sputter-etching calculation are shown. At $Q_{in}=7.0$ std. cm³/min, target is once sputter-etched, but again covered with compound layers after 8s. At the very first stage of the calculation, sputtered Ti getter O_2 in the chamber, resulting in reduction in P_{O2}. However, since Γ_{Ti} is too small to getter all of introduced O_2 and therefore to progress target sputter-etching, target is again covered with compound layers. Final-

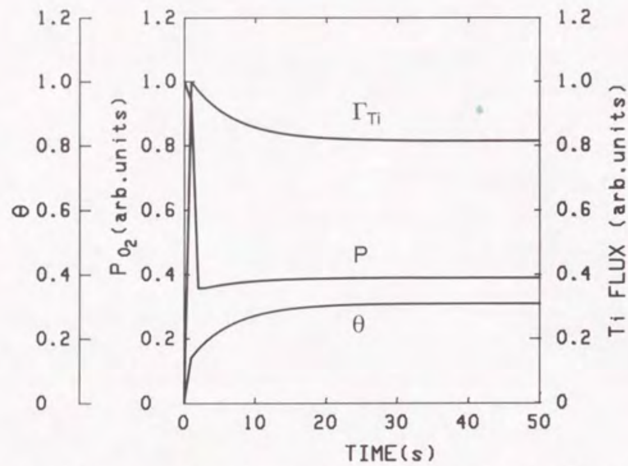

Fig.6.2 Typical compound-layer formation calculation results for S_p=1.5X10^{-1} m^3/s, Q_{in}=5.0 std.cm^3/min, and I_{sp}=2.0 A.

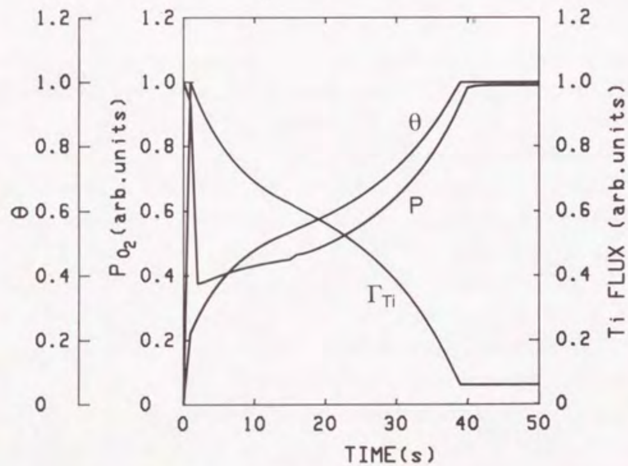

Fig.6.3 Typical compound-layer formation calculation results for S_p=1.5X10^{-1} m^3/s, Q_{in}=8.0 std.cm^3/min, and I_{sp}=2.0 A.

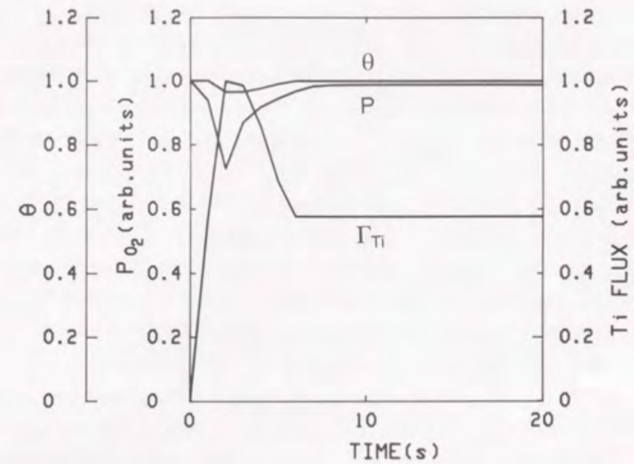

Fig.6.4 Typical sputter etching calculation results for S_p=1.5X10^{-1} m^3/s, Q_{in}=7.0 std.cm^3/min, and I_{sp}=2.0 A.

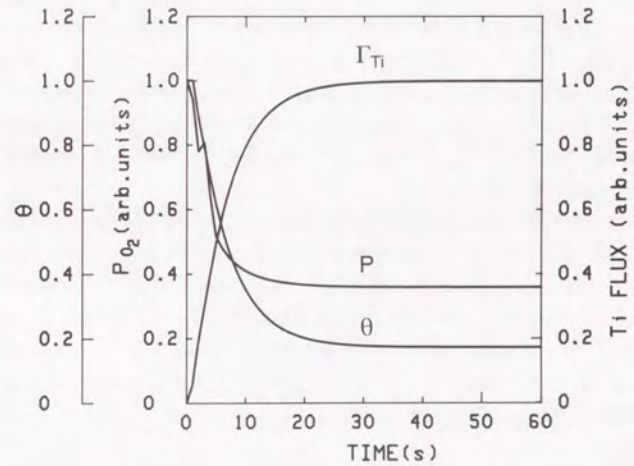

Fig.6.5 Typical sputter etching calculation results for S_p=1.5X10^{-1} m^3/s, Q_{in}=3.0 std.cm^3/min, and I_{sp}=2.0 A.

ly at 8s the target is fully covered again. In comparison to these results, at Q_{in}=3.0 std. cm^3/min the compound on the target is removed, and at 40s θ decreases to 0.18. In this case, θ decreases with elapsed time. As expected from these results, in the calculation results for Q_{in}=0 std. cm^3/min, compound layers are completely sputter-etched, and θ reaches 0.

Figures 6.6 and 6.7 respectively show results of compound-layer formation and sputter-etching calculation for various Q_{in} at I_{sp}=2.0 A and S_P=1.5x10^{-1} m^3/s. Up to Q_{in}=8.0 std. cm^3/min, the final θ increases as Q_{in} increases. At Q_{in}=2.0 std. cm^3/min, all of adsorbed reactive gas is sputtered, and then θ remains 0. At Q_{in}=10.0 std. cm^3/min, the final θ reaches 1, showing that the target surface is fully covered with compound layers. At Q_{in}=12.0 std. cm^3/min, the target surface is completed to be covered with compound layers faster. From the results it is shown that reactive gas flow rate of 8.0 std. cm^3/min is a critical flow rate for target compound-layer formation. At this point a jump of the process is observed.

On the other hand, the target sputter-etching does not take place until Q_{in} reaches 8.0 std. cm^3/min. At Q_{in}=8.0 std. cm^3/min, target sputter-etching starts, resulting in the final θ of about 0.4. For smaller Q_{in}, the final θ decreases as Q_{in} decreases. The critical gas flow rate for target sputter-etching is the same value to that for compound-layer formation:8 std. cm^3/min.

Pumping speed S_P, as well as Q_{in}, affects compound-layer formation and sputter-etching. In Figs.6.8 and 6.9, calculated results for various S_P are shown. As shown in Fig.6.8, for larger S_P the target is not covered with compound layers, whereas for S_P less than 1.5X10^{-1} m^3/s, target is fully covered with compound layers. In addition the compound-layer formation is completed earlier for lower S_P. On the other hand, sputter-etching takes place for S_P more than 1.5X10^{-1} m^3/s. Although there is a very little decrease in θ at the first time-increment for S_P=1.0X10^{-1} m^3/s, the target is covered with compound layers again at the next time step, providing θ=1.

Effects of sputtering current on target condition changes are shown in Figs.6.10 and 6.11 for Q_{in}=4.0std.cm^3/min and S_P=1.5X10^{-1} m^3/s. In the simulation model sputtering current relates to gettering ability. As shown in Fig.6.10, target is not completely covered with compound layers for higher I_{sp}, and the final θ increases as I_{sp} decreases. At I_{sp}=1.0 and 1.5 A, target surface is fully covered with compound layers. On the other hand, as shown in Fig.6.11, target is sputter-etched for I_{sp} higher than 2.0A. Being similar to the case of compound-layer formation, the final θ decreases as I_{sp} increases.

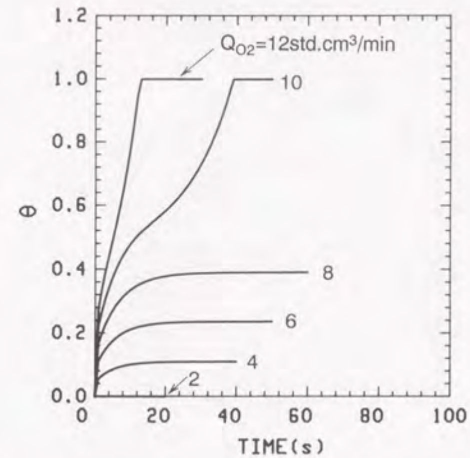

Fig.6.6 Results of compound-layer formation calculation for various Q_{in} at I_{sp}=2.0 A and S_P=1.5x10^{-1} m^3/s.

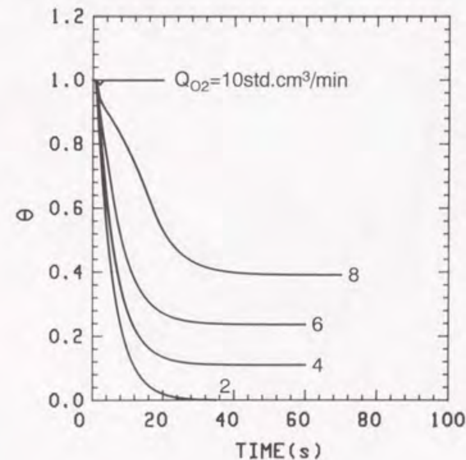

Fig.6.7 Results of sputter etching calculation for various Q_{in} at I_{sp}=2.0 A and S_P=1.5x10^{-1} m^3/s.

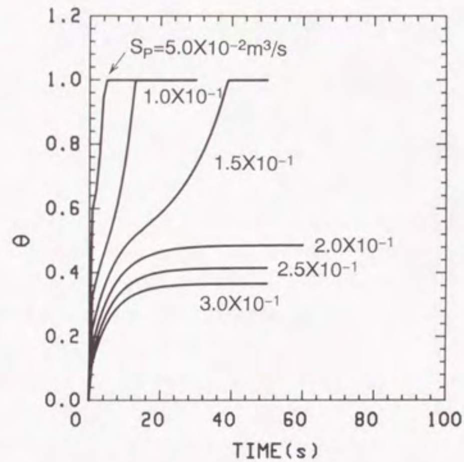

Fig.6.8 Results of compound–layer formation calculation for various S_P at Q_{in}=8.0 std.cm^3/min and I_{sp}=2.0 A.

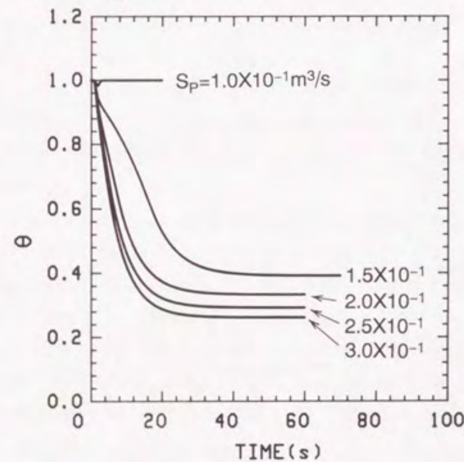

Fig.6.9 Results of sputter etching calculation for various S_p at Q_{in}=6.0 std.cm^3/min and I_{sp}=2.0 A.

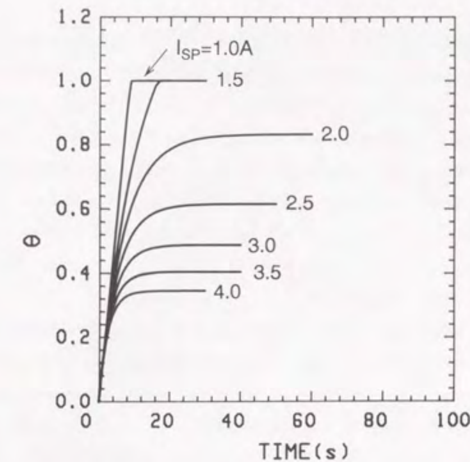

Fig.6.10 Results of compound–layer formation calculation for various I_{sp} at Q_{in}=4.0 std.cm^3/min and S_P=1.5x10^{-1} m^3/s.

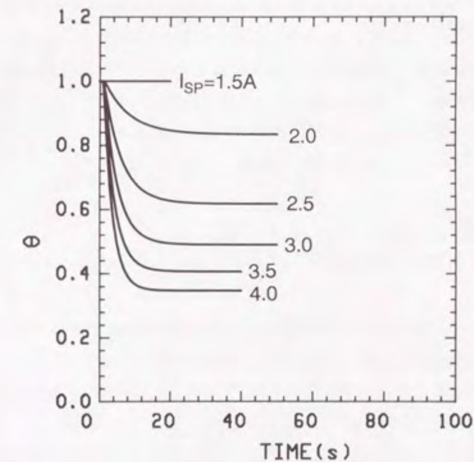

Fig.6.11 Results of sputter etching calculation for various I_{sp} at Q_{in}=4.0 std.cm^3/min and S_P=1.5x10^{-1} m^3/s.

B. HYSTERESIS

A hysteresis curve is obtained by calculating steady-state values of θ, Γ_{Ti}, and P_{O2} for a range of Q_{in}. A typical result is shown in Fig.6.12. Calculation conditions are S_p=2.0X10 $^{-1}$ m^3/s, S_g=6.0X10^{-1}m^3/s, I_{sp}=2.0A, Y_m=0.32, and Y_c=0.015. There are two drastic changes in θ, Γ_{Ti}, and P_{O2};the first transition occurs between Q_{in}=6.0 and 6.5 std.cm^3/min when Q_{in} is increased, and the second one occurs between Q_{in}=5.0 and 4.5 std.cm^3/min when Q_{in} is decreased. Until the first transition occurs, Γ_{Ti} decreases gradually and θ increases. As a result of these changes, P_O increases until the first transition. After the first transition Γ_{Ti} and θ are constant, and P_{O2} increases linearly. After the second transition, these values trace those obtained prior to the first transition.

In addition to obtaining hysteresis curves, effects of S_p, I_{sp}, and the difference between Y_c and Y_m on hysteresis are examined. In Fig.6.13, effects of S_p on hysteresis curves are shown for I_{sp}=2.0A and S_g=3.0X10^{-1}m^3/s. As S_p increases, the transition points shift to larger points of Q_{in} and the hysteresis width decreases. These shifts of transition points are also plotted in Fig.6.14 as a function of S_p. It is clearly indicated that, since the slope of shifts of the second transition is larger than that of the first transition, hysteresis width decreases as pumping speed increases.

In Fig.6.15, hysteresis curves are shown for various I_{sp} at S_p is 3.0X10^{-1}m^3/s and S_g=3.0X10^{-1}m^3/s, and in Fig.6.16, the shifts of transition points are shown as a function of I_{sp}. As I_{sp} increases, the transition points shift to larger points of Q_{in} and the hysteresis widens. At I_{sp}=1.0A, hysteresis disappears under the given calculation conditions.

Figure 17 shows calculated hysteresis curves for various Y_c at S_p is 3.0X10^{-1}m^3/s and S_g=3.0X10^{-1}m^3/s. As Y_c increases, hysteresis width decreases. At Y_c=0.045 hysteresis is disappeared, and transition becomes more smooth.

VI.V. DISCUSSION

A. APPROPRIATENESS OF SIMULATION MODEL

The general way to discuss appropriateness of the simulation model is to compare calculated results to experimental results. The time-dependent compound-layer formation and sputter-etching have been reported by several authors[10-12], though details of mechanisms of these behaviors have not been reported, and in Chapter III in this thesis.

Results calculated by the simulation model indicate a time delay in compound-layer formation and sputter-etching. These seem to be agree with reported result. Furthermore, the effects of pumping speed and sputtering current on target condition changes, which is discussed in Chaoter III, are clearly shown in the simulation results. However, since the

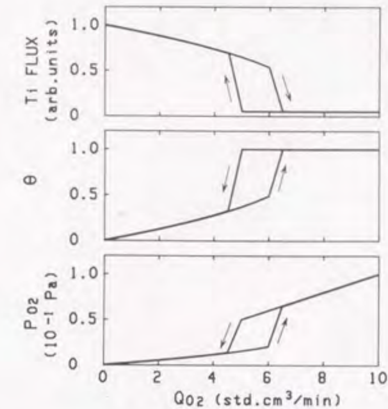

Fig.6.12 A typical hysteresis result at S_p=2.0X10^{-1}m^3/s, S_g=6.0X10^{-1}m^3/s, I_{sp}=2.0A, Y_m=0.32, and Y_c=0.015.

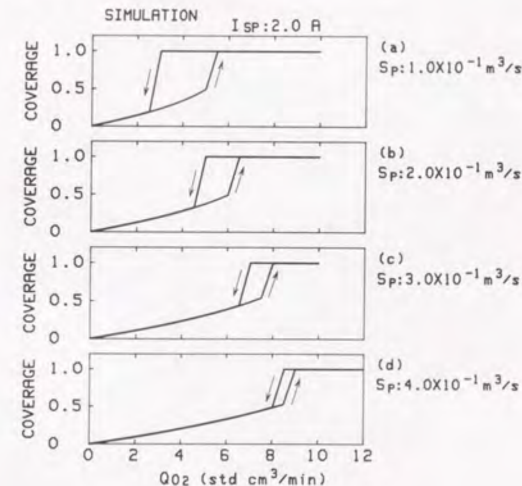

Fig.6.13 Results of hysteresis calculation for various S_p at I_{sp}=2.0A, S_g=3.0X10^{-1}m^3/s, Y_m=0.32, and Y_c=0.015.

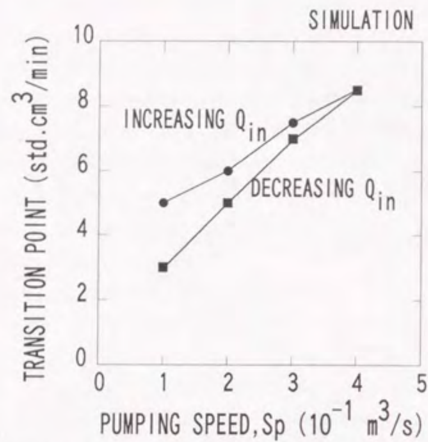

Fig.6.14 Shift of mode transition points as a function of pumping speed, S_p.

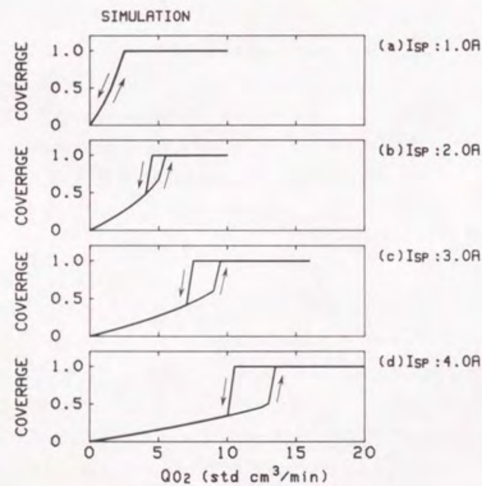

Fig.6.15 Results of hysteresis calculation for various I_{sp} at S_p=3.0X10^{-1}m^3/s, S_g=3.0X10^{-1} m^3/s, Y_m=0.32, and Y_c=0.015.

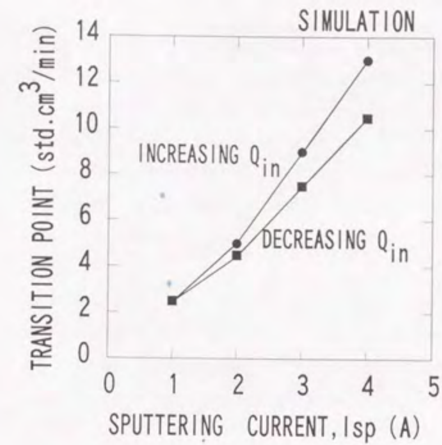

Fig.6.16 Shift of transition points as a function of sputtering current, I_{sp}.

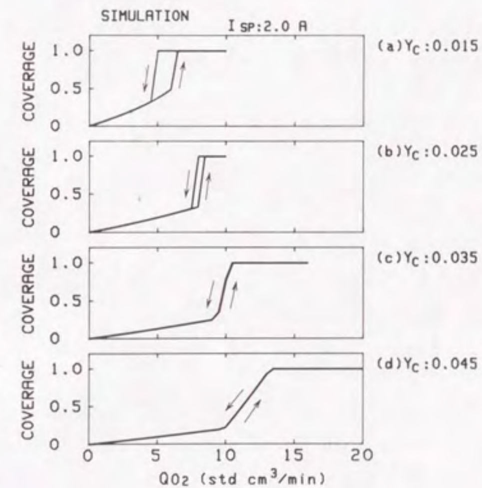

Fig.6.17 Results of hysteresis calculation for various Y_c at S_p=3.0X10^{-1}m^3/s, S_g=3.0X10^{-1} m^3/s, I_{sp}=2.0 A, and Y_m=0.32.

details of behavior have not been examined experiomentally, it is impossible to compare these results further.

Compared to time-dependent target surface condition change, hysteresis behavior has been well investigated, and the results have been reported by several authors[13-17] and in Chapter V in this thesis. Calculated hysteresis curves agree with these experimental results. Further, results obtained for the calculation of the dependence of transition points on S_p and I_{sp}, shown in Figs.14 and 16, are also in accord with experimental results shown in Chapter V;both in calculated and experimental results, as S_p increases, mode transition points shift to larger points in Q_{in} and hysteresis width decreases;as I_{sp} increases, hysteresis width increases.

In addition to the agreement between experimental and calculated results, the fact that the model provides a hysteresis curve as a result of time-dependent compound-layer formation and sputter-etching calculations also supports the appropriateness of the model.

The reason why the model can yield hysteresis curves is thought to be mainly that the program deals with an over-flow of reactive gas and correlation between target and wall behavior. This provides critical reactive gas flow rates for target compound-layer formation and sputter-etching. At a critical rate, the avalanche-like compound-layer formation or sputter-etching occurs as a consequence of the increase or decrease in surplus reactive gas.

Generally in modeling of reactive sputtering, the balance between compound-formation and sputter-etching is given by the following equation:

$$\Gamma_O (1-\theta)\, \alpha=\Gamma_{Ar}\, \theta\, Y \quad (6.25)$$

where Γ_O is O flux diffused to the target surface, θ is target coverage, α is adsorption coefficient of O atoms at metallic target surface, Γ_{Ar} is Ar ion flux to the target surface, and Y is sputtering yield of O from compound-covered target. This equation can be written as follows:

$$\theta=\Gamma_O\, \alpha/(\Gamma_{Ar}\, Y+\Gamma_O\, \alpha) \quad (6.26)$$

Thus, by this equation, θ is calculated as a function of Γ_O, and it approximates $\theta=1$ successively as Γ_O increases. From this treatment a critical reactive gas flow rate for changes in θ cannot be derived. This approach to obtain θ is the most different point from the model proposed in this study.

It should be also emphasized that the time-incremental simulation method enables us to simulate an actual reactive sputtering process without any assumptions about process behavior itself. Calculated values reach steady-state values without assuming how the process reaches a steady-state as an actual reactive sputtering process reaches a steady-state spontaneously. Moreover, a hysteresis curve, which is provided by calculating steady-state values for a series of Q_{in}, can be obtained also without assuming anything about process behavior.

The weakness of the simulation models is that correct values of gettering speed, adsorption speed, and sputtering speed should be given to perform quantitative simulation. In an actual process, although it is possible to measure the amount of reactive gas gettered at the wall at a steady-state, it is very difficult to measure the amounts of reactive gas adsorbed on the target, sputtered from the target, and gettered at the wall, during moment-by-moment process change. Estimating target behavior quantitatively is important to advance the simulation model. More sophisticated simulation will give us further knowledge on reactive sputtering process.

It is concluded that results obtained by the simulation model agree with reported results, and thus the model explains the mechanisms of process change in reactive sputtering resulted from the correlation between the target behavior and wall gettering.

B. MASS BALANCE CHANGE DURING COMPOUND-LAYER FORMATION AND SPUTTER ETCHING

Target behavior in reactive sputtering is thought to be given as a consequence of two competitive phenomena:the formation of compound layers and the sputtering of formed compound layers;*i.e.*, when the formation of compound layers overcomes the sputtering of formed compound layers, target is continuously covered with compound layers until two phenomena balances, and when the sputtering overcomes the formation, the target is continuously sputter-etched until two phenomena balances.

However, there are only few quantitative studies on compound-layer formation and sputter-etching as a function of time, including result reported in Chapter III. In Chapter III, it was found that it took 20-40s to reach a steady-state in the case of target oxidation, depending on pumping speed and O_2/Ar ratio of the discharge atomosphere. Donaghey *et al.* reported that there was 30-60 s delay to reach a steady-state after the introduction of O_2 gas is turned off or on[11]. Reith *et al.* also reported that there was a longer "incubation" time in target compound-layer formation when a fresh Ta target was sputtered in Ar-10%O_2 atmosphere[12]. They reported that the substrate conditions affected incubation time of target compound-layer formation and sputter-etching. The difficulty to measure unstable target condition changes seems to make detailed studies on the problems unachievable.

The calculated results shown in this chapter are thought to well explain these investigated results, and further provide suggestion to discuss unexamined changes in reactive sputtering process. For instance, as shown in Fig.6.2, until Q_{in} achieves a critical value, an increase in θ is gradual; once it passes a critical value, an increase in θ is accelerated and displays an inflection point in the curve. For a larger Q_{in} the acceleration of compound-layer

formation occurs at a shorter time. These results have not been observed experimentally.

In addition effects of pumping speed and sputtering current are well interpreted by calculated results. As shown in Fig.6.8, at a higher pumping speed, the compound-layer formation is suppressed since a larger amount of O_2 is pumped out. On the other hand, at a lower pumping speed, the compound-layer formation is accelerated and reaches a steady-state faster since a smaller amount of O_2 introduced and sputtered from the target surface is pumped out in this condition. Sputtering current also influences compound-layer formation and sputter-etching; at a higher current, the target is not covered with compound layers since sputter-etching overcomes compound formation, and sputtered metal getters more reactive gas, reducing the amount of reactive gas arriving target surface, thus target sputter-etching being accelerated.

The mechanisms of avalanche-like mode transition is explained as follows from the above discussion on the basic treatment in the model program;

i)when reactive gas flow rate excesses slightly a critical point where wall gettering cannot consume enough reactive gas, surplus reactive gas is generated and reactive gas partial pressure is increasing.

ii)this increase in reactive gas partial pressure further accelerates the formation of compound layers on the target surface

iii)as compound layers cover target surface, metal atom flux generated by sputtering decreases, resulting in the decrease in getting capacity at the chamber wall.

iv)this correlation between the compound-layer formation on target surface and wall gettering results in the decrease in wall gettering capacity, triggering an avalanche-like mode transition.

The inverse mode transition can be also explained in terms of the correlation between the target sputter-etching and the increase in wall gettering capacity. However, these discussions cannot explain the origin of hysteresis;they cannot explain the difference of two transition points, but only explain the origin of avalanche-like behavior.

C. MECHANISMS OF HYSTERESIS FORMATION

Mechanisms of hysteresis formation can be discussed by considering the role of getter pumping in the model. In the simulation program, since S_g is given as a function of θ, in the metallic condition(*i.e.*, θ is very small), the total pumping speed of getter pumping and pumping of the vacuum pump is so large that the transition occurs at a higher reactive gas mass flow rate;on the other hand, in the compound-covered condition, since getter pumping speed is decreased as the target is covered with compound layers, the total pumping speed is lower than that in the metallic condition, resulting in that the inverse transition occurs at a

lower reactive gas mass flow rate.

As shown in Chapters IV and V, getter pumping dominates the mode transition from metallic to compound-covered condition since getter pumping speed is higher than pumping speed of vacuum pump in the metal mode, whereas both getter pumping speed and pumping speed of vacuum pump affect the mode transition from compound-covered to metallic since S_g is decreased and becomes comparable to S_p as the target surface is covered with compound layers. Therefore, variation of S_p affects the transition from metallic to compound-covered condition more than the transition from compound-covered to metallic, resulting in the decrease in the hysteresis width at higher S_p, whereas variation of I_{sp} affects the transition from metallic to compound-covered condition more, resulting in the increase in the hysteresis width at higher I_{sp}.

These tendencies of effects of S_p and I_{sp} are in accord with the results obtained by the model calculation(shown in Figs.6.14 and 6.16). Therefore, it can be concluded that both by experimental investigation and model calculation effects of S_p and I_{sp} are clearly explained. This further implies that mechanisms of hysteresis obtained in this study explain the mechanisms of actual reactive sputtering process.

Since the decrease in metal flux is induced as a result of decrease in sputtering yield of compound-covered target, the difference in sputtering yield of compound-covered target is thought to influence hysteresis behavior. As shown in Fig.6.17, the variation in the sputtering yield obviously affects hysteresis. This can explain the difference of hysteresis phenomena observed among Ti-O_2(results in Chapter V), Ti-N_2[16-17], and Ti-B_2H_6[18] systems;as the difference in sputtering yields between compound-covered target and metallic target increases, the hysteresis width increases, and when the difference is smaller, hysteresis disappears.

VI.VI. CONCLUSIONS

A model simulating reactive sputtering mass balance changes has been proposed. The model is based on physical mechanisms involved in target and wall gettering behaviors. This enables us to calculate time-dependent condition changes until reaching a steady-state without assuming how the process reaches a steady-state. Another important feature of the model is that hysteresis curves are obtained as a result of the calculation of time-dependent target condition changes. This approach to obtain hysteresis curves is more similar to an actual reactive sputtering process.

Changes in target coverage, sputtered flux, and reactive gas partial pressure during compound-layer formation and sputter-etching processes are calculated as a function of

elapsed time by the proposed model. The investigation of influence of reactive gas flow rate indicates the followings;

i)as reactive gas flow rate is increased, target compound-layer formation is accelerated, and finally fully covered with compound layers.

ii)in the case of target surface sputter-etching simulation, the decrease in reactive gas flow rate accelerates target sputter-etching.

In addition, the dependence of compound-layer formation and sputter-etching on pumping speed and sputtering current has been shown. At a higher pumping speed, compound-layer formation is retarded, whereas at a lower pumping speed, target compound-layer formation is accelerated. The effects of the parameters have been discussed from the view point of reactive gas mass consumption by wall gettering and pumping.

Hysteresis curves are provided as a result of compound-layer formation and sputter-etching calculations. The curves obtained are in accord with experimental results. The effects of pumping speed and sputtering current on hysteresis curves are investigated. The investigation provided the following results;

i)as pumping speed increases, the width of hysteresis decreases.

ii)as sputtering current increases, the width of hysteresis increases.

iii)as the difference of sputtering yields between metallic and compound-covered targets decreases, the width of hysteresis decreases.

On the basis of the results obtained by the model calculation, mechanisms of hysteresis formation have been revealed; *i.e.*, the hysteresis is formed due to the difference between the gettering capacity for reactive gas before and after the compound-layer formation on the target surface. This difference is resulted from the difference of sputtering yield of compound-covered target to that of metallic target.

VI.VII. REFERENCES

1) T.Abe and T.Yamashina, Thin Solid Films 35, 19(1976)

2) D.K.Hohnke, D.J.Scmatz, and M.D.Hurley, Thin Solid Films 118, 301(1984)

3) A.Okamoto and T Serikawa, Thin Solid Films 137, 143(1986)

4) S.Berg, H-O.Blom, T.Larsson, and C.Nender, J.Vac.Sci.Technol. A5(2), 202(1987)

5) S.Berg, T.Larsson, C.Nender, and H-O.Blom J.Appl.Phys.63(3), 887(1988)

6) S.Berg, H-O.Blom, M.Moradi, and C.Nender, J.Vac.Sci.Technol. A7(3), 1225(1989)

7) S.Berg, M.Moradi, C.Nender, and H-O.Blom Surf.Coat.Technol 39/40, 465(1989)

8) T.Larsson, H-O.Blom, C.Nender, and S.Berg, J.Vac.Sci.Technol. A6(3),1832(1988)

9) A.F.Hmiel, J.Vac.Sci.Technol.,A3, 592(1985)

10) J.Heller, Thin Solid Films 17, 163(1973)

11) L.F.Donaghey and K.G.Geraghty, Thin Solid Films 38, 271(1976)

12) T.M.Reith and P.J.Ficalora, J.Vac.Sci.Technol.A1(3), 1362(1983)

13) S.Maniv and W.D.Westwood, J.Vac.Sci.Technol.17(3), 743(1980)

14) T.Serikawa and A.Okamoto, Thin Solid Films 101, 1(1983)

15) J.Danroc, A.Aubert, and R.Gillet, Sur.Coat.Technol.33, 83(1987)

16) S.Kadlec, J.Musil, and J.Vyskocil, Vacuum 37(10), 729(1987)

17) J.Musil,S.Kadlec,J.Vyskocil, and V.Valvoda, Thin Solid Films 167, 107(1988)

18) T.Larsson, S.Berg, and H.-O.Blom, Thin Solid Films, 172,241(1989)

VII. CONCLUSIONS

Mode transition and hysteresis effects in reactive sputtering have been investigated systematically, and their mechanisms have been discussed. On the basis of discussion of results obtained experimentally, a model simulating target surface condition change and hysteresis has been proposed.

In Chapter III, time-dependent changes in O_2 partial pressure, deposition rate, cathode voltage, and Ti emission intensity after glow discharge ignition and effects of pumping speed and O_2/Ar flow rate ratio were investigated. It was shown that O_2 partial pressure, deposition rate, cathode voltage, and Ti emission intensity changed drastically and continuously after glow discharge was ignited until the process reached a steady-state. Both pumping speed and O_2/Ar ratio affected the time to reach a steady-state. The results suggested that lower pumping speed or higher O_2/Ar ratio shortens response time for process condition change such as reactive gas flow rate.

To estimate the role of gettering in mass balance change, in Chapter IV, reactive gas mass balance change and sputtering yield change were examined by pressure change observation and by composition analysis of the deposited films. The obtained results displayed the drastic change in gettering effects at the mode transition that takes place at a critical O_2 partial pressure. Until this transition, more than 90% of the introduced O_2 was consumed by gettering. The amount of gettered O_2 displayed a maximum just before target poisoning occurred. At that point the calculated getter pumping speed reached 2.3 m^3/s, which was 10 times larger than the physical pumping speed. Furthermore, the adsorbed/incident O_2 flux ratio was found to decrease from 0.36 to 0.0010 with increasing O_2 partial pressure. The obtained results showed an important role of gettering effects in mass balance changes in reactive sputtering.

In Chapter V, hysteresis behavior and the effects on it of physical pumping speed, sputtering current, and Ar partial pressure were investigated, and mechanisms of the hysteresis process were discussed. It was shown that many events happen as a consequence of the target oxidation or sputtering of formed compound layers. The obtained results indicated strong dependence of hysteresis on pumping speed and sputtering current. As pumping speed increased hysteresis width decreased since the transition point from compound to metal mode shifted to higher values of Q_{O2} while the transition point from metal to compound mode remained constant against variation of pumping speed. In addition, for smaller sputtering currents and constant pumping speed, hysteresis width decreased. The changes in transition points as a function of pumping speed and sputtering current were successfully explained by considering getter pumping capacity or getter pumping speed for reactive gas. Elimination of hysteresis was not investigated in this experiment. From the discussion it was

suggested that hysteresis is a result of the difference in sputtering yields from a target covered by compound layers and from a metallic target, which provides a difference in gettering capacity.

A model simulating reactive sputtering mass balance changes was proposed on the basis of discussion in Chapters from III to V, in Chapter VI. The model was based on physical mechanisms involved in target and wall gettering behaviors. This enabled us to calculate time-dependent condition changes until reaching a steady state without assuming how the process reached a steady-state. Another important feature of the model was that hysteresis curves were obtained as a result of the calculation of time-dependent target condition changes. This approach to obtain hysteresis curves was more similar to an actual reactive sputtering process.

Changes in target coverage, sputtered flux, and reactive gas partial pressure during compound-layer formation and sputter-etching processes were calculated as a function of elapsed time by the proposed model. The investigation of the influence of reactive gas flow rate indicated the followings;

i)as reactive gas flow rate is increased, target compound-layer formation is accelerated, and the target surface is finally fully covered with compound layers.

ii)in the case of target surface sputter-etching simulation, the decrease in reactive gas flow rate accelerates target sputter-etching.

In addition, the dependence of compound-layer formation and sputter-etching on pumping speed and sputtering current was shown. At a higher pumping speed, compound-layer formation was retarded, whereas at a lower pumping speed, target compound-layer formation was accelerated. The effects of the parameters have been discussed from the view point of reactive gas consumption by wall gettering and pumping.

Hysteresis curves were also obtained as a result of compound-layer formation and sputter-etching calculations. The obtained curves were in accord with experimental results. The effects of pumping speed and sputtering current on hysteresis curves were investigated. The investigation provided the following results;

i)as pumping speed increases, the width of hysteresis decreases.

ii)as sputtering current increases, the width of hysteresis increases.

iii)as the difference of sputtering yields between metallic and compound-covered targets decreases, the width of the hysteresis decreases.

The results obtained from the model calculation revealed mechanisms of hysteresis formation ; *i.e.*, the hysteresis is formed as a consequence of the difference between the gettering capacity for reactive gas before and after the compound-layer formation on the target surface. This difference was resulted from the difference in sputtering yields of a compound-covered target to that of a metallic target.

This thesis presented a study of mechanisms involved in reactive sputtering process. It was shown that gettering of reactive gas by sputtered metal materials plays an important role in reactive sputtering. Mass balance changes in reactive sputtering were strongly related with gettering behavior, and therefore related with pumping speed and with sputtering current. The results obtained by experimental investigation and model calculation revealed that a difference in gettering capacity between metal and compound modes induces hysteresis. Therefore, it is concluded that as far as there is a difference in sputtering yields between metallic target and compound-covered target, hysteresis cannot be eliminated. Furthermore, it was proved that it is effective to increase pumping speed in order to obtain a more controllable system, though, in case that a difference in the two sputtering yields is very large like $Ti-O_2$ system, it is difficult to avoid instability in the near-transition region.

VIII. APPENDIX

VIII.I. HYSTERESIS SIMULATION PROGRAM

The program listed below is used to calculate hysteresis curves. The program used to calculate time-dependent compound-layer formation and sputter-etching is a part of hysteresis simulation program. The program is written in HP BASIC.

```
100    !*********************************************************************
101    !*          SPUTTERING SIMULATION PROGRAM (5 HYST)                   *
102    !*                    BY    KUSANO Eiji                              *
103    !*                                             2/7/90                *
105    !*********************************************************************
106    !
107    !This program calculates the hysteresys of the reactive sputtering by mean
s of assumed pumping speeds, Sgetter and Starget.
108    !Those pumping speeds are assumed to be a function of the target coverage.
109    !The pressuer would be caculated by the following equation.
110    !       P_o2=Q_o_in/(Spump+Sgetter+Star)
111    !The calculated perssure, however, does not affect to the target poisoning
        as well as gettering on the wall in the program.
112    !The important point is that how the function is determined.
113    !
114    !
115    CLEAR SCREEN
116    !
117    !SUB ROUTINES
118    !   TARGET: CALUCULATING TARGET PHENOMENA
119    !   PLOT  : PLOT CALCULATED RESULTS
120    !
121    ON ERROR GOTO Error_trap
122    !
123    !
124 Declaration:  !
125    REAL Th(800),Th_a(800),P(800),Qti(800),Qt(800),Qg(800),St(800),Sg(800),Ra(
800)
126    REAL Tm(200),Th_f(200),P_f(200),Sg_f(200),St_f(200),Ra_f(200),Qti_f(200)
127    REAL X_data(200),Y_data(5,200)
128    DIM Line$(10)[10],Graph_title$[25],Y_label_1$[30],Y_label_2$[30],Y_label_3
$[30],X_label$[30]
129 !
130 !*********************************************************************
131 !*                                                                   *
132 !*********************************************************************
133 Main_programm:!
134                  !
135    GOSUB Data_typein
136    GOSUB Set_const
137    N_case=(O2_flow_max-O2_flow_int)/O2_flow_step
138    !
139 Main_cal_loop:  !
140    FOR I_p=1 TO N_case*2+1
141      O2_flow=O2_flow_step*(N_case-ABS(I_p-N_case-1))+O2_flow_int
142      GOSUB Init_valiables
143      IF Print_freq>0 THEN
144        PRINTER IS PRT
145        GOSUB Print_condition
146        GOSUB Print_data_0
147        PRINTER IS CRT
149      END IF
150      !
151      FOR I=1 TO Max_run
154        GOSUB Calculation
171        !
173        IF I>=20 THEN
175          IF DROUND(Th_a(I),4)=DROUND(Th_a(I-20),4) OR Th_a(I)<=1.0E-4 THEN
176            GOSUB Data_transfer
```



```
177            IF Print_freq>0 THEN
178              PRINTER IS PRT
179              PRINT CHR$(12)
180              PRINTER IS CRT
181            END IF
182            GOTO 188
184          END IF
185        END IF
186      NEXT I
187      !
188    NEXT I_p
189    !
190    GOSUB Print_data_f
191    IF Print_final=1 THEN
192      PRINTER IS PRT
193      GOSUB Print_data_f
194      PRINT CHR$(12)
195      PRINTER IS CRT
196    END IF
197    !
198    IF Plot_flag1<>99 THEN
200      GOSUB Data_treat
201      GOSUB Plot_data
203    END IF
204 !
205    CLEAR SCREEN
206    KEY LABELS ON
208    STOP
209 !
210 !*********************************************************************
211 !*                                                                   *
212 !*********************************************************************
213 !
214 Calculation:   !
215    GOSUB Target
216    GOSUB Print_out
217    DISP O2_flow
218    IF Print_freq>0 THEN
219      IF I/Print_freq=INT(I/Print_freq) THEN
220        PRINTER IS PRT
221        GOSUB Print_out
222        PRINTER IS CRT
223      END IF
224    END IF
225        !
226    RETURN
227 !
228 !
229 !*********************************************************************
230 !*                                                                   *
231 !*********************************************************************
232 !
233 !
234 Data_typein:!
235    CLEAR SCREEN
236    INPUT "TYPE SPUTTERING CURRENT ? ",I_sp
237    PRINT TABXY(1,5)
238    PRINT USING "5X,20A,2A,3D.D,10A";"SPUTTERING CURRENT",":",I_sp,"(A)"
239    INPUT "TYPE PUMPING SPEED IN LITER/SEC ? ",Sp
240    PRINT TABXY(1,6)
```

```
241   PRINT USING "5X,20A,2A,3D.D,15A";"PUMPING SPEED       ",":",Sp,"(LITER/SEC)"
242   INPUT "TYPE TARGET GETTER SPEED IN LITER/SEC ? ",St_0
243   PRINT TABXY(1,7)
244   PRINT USING "5X,20A,2A,3D.D,15A";"GETTER SPEED       ",":",St_0,"(LITER/SEC)
"
245   INPUT "TYPE  INIT O2 FLOW RATE IN SCCM ? ",O2_flow_int
246   PRINT TABXY(1,8)
247   PRINT USING "5X,20A,2A,3D.2D,15A";"INT O2 FLOW RATE        ",":",O2_flow_int
,"(SCCM)"
248    !
249   INPUT "TYPE  MAX O2 FLOW RATE IN SCCM ? ",O2_flow_max
250   PRINT TABXY(1,9)
251   PRINT USING "5X,20A,2A,3D.2D,15A";"MAX O2 FLOW RATE        ",":",O2_flow_max
,"(SCCM)"
252    !
253   INPUT "TYPE O2 FLOW RATE STEP IN SCCM ? ",O2_flow_step
254   PRINT TABXY(1,10)
255   PRINT USING "5X,20A,2A,3D.2D,15A";"O2 FLOW RATE STEP ",":",O2_flow_step,"(
SCCM)"
256    !
257    !
258   INPUT "TYPE PRINT FREQUENCY  ? ",Print_freq
259   PRINT TABXY(1,12)
260   PRINT USING "5X,20A,2A,3D";"PRINT FREQUENCY   ",":",Print_freq
261    !
262   INPUT "TYPE FINAL RESULTS  0/1  ? ",Print_final
263   PRINT TABXY(1,13)
264   PRINT USING "5X,20A,2A,3D";"PRINT RESULTS  ",":",Print_final
265   INPUT "DRAW GRAPH  0/SELECT PLOTTER, 1/CRT, 2/705, 99/NO  ? ",Plot_flag1
266   PRINT TABXY(1,14)
267   PRINT USING "5X,20A,2A,3D";"DRAW GRAPH          ",":",Plot_flag1
268   WAIT 2
269   CLEAR SCREEN
270   RETURN
271    !
272 !**************************************************************************
273 !*                                                                        *
274 !**************************************************************************
275 !
276 Set_const:  !
277   Max_run=800
278   Sg_0=150*I_sp
279    !
280   E=1.6*10^(-19)
281   Kb=1.38*10^(-23)
282   Abo=6.02*10^23
283    !
284    !
285   Ym_m=.32
286   Ym_c=.015
287   Yg_c=.015
288    !
289   Temp=300
290    !
291   Site_t=1.E+18
292    !
293   RETURN
294    !
295 !**************************************************************************
296 !*                                                                        *
```



```
297 !**************************************************************************
298   !
299 Print_condition:   !
300   PRINT "**************************SPUTTERING SIMULATION  5****************"
301   PRINT "*****************CALCULATION BY ASSUMING THE PUMPING SPEED*******"
302   PRINT "-----------------------------------------------------------------"
303   PRINT TAB(5),DATE$(TIMEDATE),TIME$(TIMEDATE)
304   PRINT
305   PRINT USING "5X,20A,2A,3D.D,2X,10A";"SPUTTERING CURRENT",":",I_sp,"(A)"
306   PRINT USING "5X,20A,2A,3D.D,2X,20A";"PUMPING SPEED       ",":",Sp,"(LITER/SE
C)"
307   PRINT USING "5X,20A,2A,3D.D,2X,20A";"GETTER  SPEED       ",":",Sg_0,"(LITER/
SEC)"
308   PRINT USING "5X,20A,2A,3D.D,2X,20A";"TARGET  SPEED       ",":",St_0,"(LITER/
SEC)"
309   PRINT USING "5X,20A,2A,3D.2D,2X,10A";"O2 FLOW RATE        ",":",O2_flow,"(SC
CM)"
310   PRINT "-----------------------------------------------------------------"
311   PRINT USING "5X,20A,2A,D.DDE";"Ym_m",":",Ym_m
312   PRINT USING "5X,20A,2A,D.DDE";"YM_C",":",Ym_c
313   PRINT USING "5X,20A,2A,D.DDE";"YG_C",":",Yg_c
314   PRINT "-----------------------------------------------------------------"
315   !
316   PRINT USING "5X,20A,2A,D.DDE,2X,20A";"Q_o2_in       ",":",Q_in_0,"((Torr*lit
er)/SEC)"
317   PRINT USING "5X,20A,2A,D.DDE,2X,20A";"N_o_in       ",":",N_o_in,"(Atoms/SEC)
"
318   PRINT USING "5X,20A,2A,D.DDE,2X,20A";"Ar FLUX     ",":",Flux_ar,"(IONS/CM2)
"
319   PRINT
320   PRINT "-----------------------------------------------------------------"
321   RETURN
322   !
323 !**************************************************************************
324 !*                                                                        *
325 !**************************************************************************
326   !
327 Init_valiables:   !
328   I=0
329   !
330   Q_in_0=O2_flow*760/1000/60                 !(TORR*LITER)/SEC
331   Flux_ar=I_sp/E                             !IONS/SEC
332   N_o_in=2*O2_flow*Abo/(22.4*1000*60)        !(atm)
333   !
334   IF I_p<=N_case+1 THEN
335     Th(0)=0
336     Th_a(0)=0
337   ELSE
338     Th(0)=1
339     Th_a(0)=1
340   END IF
341   !
342   Q_in=Q_in_0
343   St(0)=St_0
344   Sg(0)=0
345   P(0)=Q_in/Sp                                        ! Torr
346   Qti(0)=0
347   !
348   RETURN
349   !
```

```
350 !********************************************************************
351 !*                                                                  *
352 !********************************************************************
353 !
354 Print_data_0:  !
355   PRINT USING "6A,2X,8A,X,8A,X,8A,X,8A,X,8A,X,8A";"NUMBER","PRESSURE","THEAT
A","S target","S getter","Q TI ","Q IN","RATIO"
356   !
357   PRINT
358   PRINT USING "3D,2X,MD.DDE,2X,MD.DDE,2X,MD.DDE,2X,MD.DDE,2X,MD.DDE,2X,MD.DD
E,2X,MD.DDE";I,P(I),Th_a(I),St(I),Sg(I),Qti(I),Q_in,Ra(I)
359   !
360   RETURN
361    !
362 !********************************************************************
363 !*                                                                  *
364 !********************************************************************
365    !
366 Data_transfer:!
367   Tm(I_p)=I
368   P_f(I_p)=P(I)
369   Th_f(I_p)=Th_a(I)
370   St_f(I_p)=St(I)
371   Sg_f(I_p)=Sg(I)
372   Ra_f(I_p)=Ra(I)
373   Qti_f(I_p)=Qti(I)
374    !
375   IF O2_flow_step=0 THEN STOP
376   !
377   RETURN
378   !
379 !********************************************************************
380 !*                                                                  *
381 !********************************************************************
382 !
383 Print_data_f:  !
384   PRINT "***************************SPUTTERING SIMULATION  5 HYST **********"
385   PRINT "******************CALCULATION BY ASSUMING THE PUMPING SPEED*******"
386   PRINT "-----------------------------------------------------------------"
387   PRINT TAB(5),DATE$(TIMEDATE),TIME$(TIMEDATE)
388   PRINT
389   PRINT USING "5X,20A,2A,3D.D,2X,10A";"SPUTTERING CURRENT",":",I_sp,"(A)"
390   PRINT USING "5X,20A,2A,3D.D,2X,20A";"PUMPING SPEED      ",":",Sp,"(LITER/SE
C)"
391   PRINT USING "5X,20A,2A,3D.D,2X,20A";"GETTER  SPEED      ",":",Sg_0,"(LITER/
SEC)"
392   PRINT USING "5X,20A,2A,3D.D,2X,20A";"TARGET  SPEED      ",":",St_0,"(LITER/
SEC)"
393   PRINT USING "5X,20A,2A,3D.2D,2X,10A";"O2 FLOW RATE       ",":",O2_flow,"(SC
CM)"
394   PRINT "-----------------------------------------------------------------"
395   PRINT USING "5X,20A,2A,D.DDE";"Ym_m",":",Ym_m
396   PRINT USING "5X,20A,2A,D.DDE";"YM_C",":",Ym_c
397   PRINT USING "5X,20A,2A,D.DDE";"YG_C",":",Yg_c
398   PRINT "-----------------------------------------------------------------"
399   !
400   PRINT USING "5X,20A,2A,D.DDE,2X,20A";"Q_o2_in      ",":",Q_in_0,"((Torr*lit
er)/SEC)"
401   PRINT USING "5X,20A,2A,D.DDE,2X,20A";"N_o_in      ",":",N_o_in,"(Atoms/SEC)
"
```



```
402   PRINT USING "5X,20A,2A,D.DDE,2X,20A";"Ar FLUX     ",":",Flux_ar,"(IONS/CM2)
"
403   PRINT
404   PRINT "--- -------------------------------------------------------------"
405   PRINT
406      !
407   PRINT USING "8A,2X,8A,2X,10A,2X,10A,2X,10A,2X,10A,2X,10A,2X,10A";"O2 FLOW"
,"TIMES","PRESS","THETA","S TARGET","S GETTER","RATIO"
408      !
409   FOR I_p=1 TO N_case*2+1
410     O2_flow=O2_flow_step*(N_case-ABS(I_p-N_case-1))+O2_flow_int
411     !
412     PRINT USING "#,X,DD.DD";O2_flow
413     PRINT USING "4X,3D,4X,MD.DDE,4X,MD.DDE,4X,MD.DDE,4X,MD.DDE,4X,MD.DDE";Tm
(I_p),P_f(I_p),Th_f(I_p),St_f(I_p),Sg_f(I_p),Ra_f(I_p)
414   NEXT I_p
415   RETURN
416    !
417    !
418    !
419   !
420   !******************************************************************
421   !*   SUBROUTINE  TARGET                                            *
422   !******************************************************************
423   !
424   !
425   !
426   !This subroutine calculates the target gettering behavior.
427   !
428   !
429   !
430   !
431   !
432 Target:  !
433   !
434 Press:  !
435   P(I)=Q_in/(Sp+St(I-1)+Sg(I-1))                     ! Torr
436   Qt(I)=P(I)*St(I-1)                                ! Torr-liter/sec
437   Qg(I)=P(I)*Sg(I-1)                                ! Torr-liter/sec
438   !
439   IF Th(I-1)=1 THEN
440     Th(I)=1
441   ELSE
442     Th(I)=Th(I-1)+Qt(I)*Abo/(760*22.4)/((1-Th(I-1))*Site_t)! No dimension
443   END IF
444   !
445   IF Th(I)>1 THEN
446     Qt_a=(1-Th(I-1))*Site_t                        ! Atoms/sec
447     Qt_a=Qt_a*760*22.4/Abo                         ! Torr-liter/sec
448     St(I-1)=St(I-1)*(1-Th(I-1))/(Th(I)-Th(I-1))     ! Liter/sec
449     GOTO Press
450   END IF
451   !
452   Q_in=Q_in_0
453   Qg_o=Qti(I-1)*(760*22.4)/Abo-Qg(I)
454   IF Qg_o<0 THEN
455     Q_in=Q_in-Qg_o
456    !Sg(I-1)=Sg(I-1)*Qti(I-1)/(Qg(I)*Abo/(760*22.4))
457    !Qg(I)=Qti(I-1)*(760*22.4)/Abo
458   END IF
```

```
459   !
460   IF Qti(I-1)=0 THEN
461     Ra(I)=0
462   ELSE
463     IF Qg_o<0 THEN
464       Ra(I)=(Qg(I)+Qg_o)*Abo/(760*22.4)/Qti(I-1)
465     ELSE
466       Ra(I)=Qg(I)*Abo/((760*22.4)*Qti(I-1))
467     END IF
468   END IF
469   !
470 Sputter:  !
471   !
472   Qti(I)=((1-Th(I))*Ym_m+Th(I)*Ym_c)*Flux_ar          ! Atoms/sec
473   Th_a(I)=Th(I)
474   Th(I)=Th(I)-Th(I)*Yg_c*Flux_ar/Site_t
475   Th(I)=MAX(Th(I),0)
476   Qgs=(Th_a(I)-Th(I))*Site_t*(760*22.4)/Abo
477   IF Qgs>Qg_o THEN
478     Q_in=Q_in+Qgs
479   END IF
480   !
481 Det_speed:  !
482   St(I)=(1-Th(I))*St_0
483   Sg(I)=((1-Th(I))+Ym_c/Ym_m*Th(I))*Sg_0
484   !
485   !
486   RETURN
487   !
488   !
489   !*******************************************************************
490   !*          SUBROUTINE PRINT_OUT                                  *
491   !*******************************************************************
492   !
493   ! In this subroutine calculated results are printed out.
494   !
495   !
496 Print_out:  !
497   !
498   !
499   PRINT USING "3D,2X,MD.DDE,2X,MD.DDE,2X,MD.DDE,2X,MD.DDE,2X,MD.DDE,2X,MD.DD
E,2X,MD.DDE";I,P(I),Th_a(I),St(I),Sg(I),Qti(I),Q_in,Ra(I)
500   !
501   RETURN
502   !
503   !
504   !*******************************************************************
505   !*          SUBROUTINE GRAPH                                      *
506   !*******************************************************************
507   !
508   !
509 Data_treat:!
510   !
511   Ymin=0
512   Ymax=1.2
513   Xmin=0
514   Xmax=O2_flow_max
515   !
516   X_label$="O2 FLOW (SCCM)"
517   Y_label_1$="THETA (a.u.)"
```



```
518   Y_label_2$="PRESSURE (a.u.)"
519   Y_label_3$="Ti FLUX (a.u.)"
520   Graph_title$="HYSTERESIS SIMULATION"
521   Data_num=3
522   Line_1$=" THETA"
523   Line_2$=" PRESSURE"
524   Line_3$=" Ti FLUX"
525   P_f_max=MAX(P_f(*))
526   Qti_f_max=MAX(Qti_f(*))
527   FOR I_p=1 TO N_case*2+1
528     X_data(I_p)=O2_flow_step*(N_case-ABS(I_p-N_case-1))+O2_flow_int
529     Y_data(1,I_p)=Th_f(I_p)
530     Y_data(2,I_p)=P_f(I_p)/P_f_max
531     Y_data(3,I_p)=Qti_f(I_p)/Qti_f_max
532   NEXT I_p
533   N_case=N_case*2+1
534   RETURN
535   !
536   !*******************************************************************
537   !*       PLOT DATA                                                *
538   !*******************************************************************
539   !
540 Plot_data:  !
541   !
542   !
543   !
544   CLEAR SCREEN
545   GINIT                                            !GRAPHICS INITIALIZE
546   Plot_flag=Plot_flag1
547   SELECT Plot_flag1
548   CASE 0
549     GOTO Select_plotter
550   CASE 1
551     PLOTTER IS CRT,"INTERNAL"
552     GOTO Draw_graph
553   CASE 2
554     PLOTTER IS 705,"HPGL"
555     GOTO Draw_graph
556   END SELECT
557 Select_plotter:  !
558   GINIT                                            !GRAPHICS INITIALIZE
559   REPEAT
560     PRINT TABXY(10,10);"PLOT ON CRT(1),  PLOTTER(2),  BOTH(3) OR END(0)"
561     INPUT A
562   UNTIL A=1 OR A=2 OR A=3 OR A=0
563   !
564   CLEAR SCREEN
565   SELECT A
566   CASE =1
567     PLOTTER IS CRT,"INTERNAL"
568     Plot_flag=1
569     GOTO Draw_graph
570   CASE =2
571     PLOTTER IS 705,"HPGL"
572     Plot_flag=2
573     GOTO Draw_graph
574   CASE =3
575     PLOTTER IS CRT,"INTERNAL"
576     Plot_flag=1
577     GOTO Draw_graph
```

```
578     DISP "plot"
579     PLOTTER IS 705,"HPGL"
580     Plot_flag=2
581     GOTO Draw_graph
582   CASE =0
583     GOTO Plot_end
584   CASE ELSE
585     GOTO Select_plotter
586   END SELECT
587        !
588     !
589 Draw_graph:    !
590   INTEGER Screen(1:12480)
591   KEY LABELS OFF
592   GRAPHICS ON
593   DEG                                   !SET ANGULAR MODE TO DEGREES
594   IF Plot_flag=2 THEN
595     OUTPUT 705;"VS10"                   ! PEN SPEED 10CM/SEC
596     OUTPUT 705;"SP2"
597   END IF
598   CSIZE 4                               !CHARACTER SIZE
599   LORG 6                                !CHARACTER ORIGINAL POINT
600   X_gdu_max=100*MAX(1,RATIO)            !X AXIS GDU MAX VALUE
601   Y_gdu_max=100*MAX(1,1/RATIO)          !Y AXIS GDU MAX VALUE
602   FOR I=-.1 TO .1 STEP .1                 !PLOT TITLE
603     MOVE X_gdu_max*.35+I,Y_gdu_max*.98    !
604     LABEL Graph_title$                        !
605   NEXT I                                !
606   LDIR 90                               !CHARACTER ROTATION
607   LORG 6                                !CHARACTER ORIGIN POINT
608   CSIZE 4.0                             !CHARACTER CELL SIZE 4*GDU HEIGHT
609   FOR I=-.1 TO .1 STEP .1
610     MOVE 0,Y_gdu_max*.5+I
611     LABEL "O"                            !Y-AXIS LABEL
612     MOVE 0,Y_gdu_max*.5+I
613     LABEL "-"                            !Y-AXIS LABEL
614   NEXT I
615   LORG 1
617   FOR I=-.1 TO .1 STEP .1
618     MOVE X_gdu_max*.13,Y_gdu_max*.4+I
619     LABEL "P"                             !Y-AXIS LABEL
620     MOVE X_gdu_max*.13,Y_gdu_max*.428+I
621     CSIZE 2.5
622     LABEL "O2"                            !Y-AXIS LABEL
623     MOVE X_gdu_max*.13,Y_gdu_max*.457+I
624     CSIZE 4
625     LABEL "(a.u.)"                        !Y-AXIS LABEL
626   NEXT I
627   LORG 6
629   FOR I=-.1 TO .1 STEP .1
630     MOVE X_gdu_max*.620,Y_gdu_max*.5+I
631     LABEL Y_label_3$                      !Y-AXIS LABEL
632   NEXT I
633   LDIR 0                                !CHARACTER ROTATION
634   LORG 5
635   FOR I=-.1 TO .1 STEP .1
636     MOVE X_gdu_max*.4+I,Y_gdu_max*.12         !1/2 X-WIDTH, 7/100 Y-HEIGHT
637     LABEL X_label$                        !X-AXIS LABEL
638   NEXT I
639   CSIZE 3.0,.6
```



```
640   LORG 2
641 ! MOVE X_gdu_max*.665,Y_gdu_max*.90
642 ! LABEL DATE$(TIMEDATE)
643 ! MOVE X_gdu_max*.665,Y_gdu_max*.85
644 ! LABEL TIME$(TIMEDATE)
645   MOVE X_gdu_max*.665,Y_gdu_max*.80
646   LABEL USING "8A,X,3D,X,5A";"PUMP :",Sp,"(L/S)"
647   MOVE X_gdu_max*.665,Y_gdu_max*.75
648   LABEL USING "8A,X,3D,X,5A";"GETTER :",Sg_0,"(L/S)"
649   MOVE X_gdu_max*.665,Y_gdu_max*.70
650   LABEL USING "8A,X,3D,X,5A";"ADSORP :",St_0,"(L/S)"
651   MOVE X_gdu_max*.665,Y_gdu_max*.65
652   LABEL USING "8A,D.DD,X,5A";"I sp :",I_sp,"(A)"
653   !
654   FOR I=1 TO Data_num
655     IF Plot_flag=2 THEN
656       OUTPUT 705;"SP"&VAL$(2+I)
657     END IF
658     LINE TYPE 1
659     MOVE X_gdu_max*.7,Y_gdu_max*(.4-.05*(I-1))
660     IF Plot_flag=2 THEN
661       OUTPUT 705;"SP"&VAL$(I+2)
662     END IF
663     LORG 2
664     CSIZE 4
665     SELECT I
666     CASE 1
667       IDRAW X_gdu_max*.05,0
668       LABEL " O"
669     MOVE X_gdu_max*.75,Y_gdu_max*(.4-.05*(I-1))
670     LABEL " -"
671     CASE 2
672       IDRAW X_gdu_max*.05,0
673       LABEL " P"
674     MOVE X_gdu_max*.785,Y_gdu_max*(.4-.05*(I-1))
675     CSIZE 2.5
676     LORG 3
677     LABEL "O2"
678     CASE 3
679       IDRAW X_gdu_max*.05,0
680       LABEL Line_3$
681     CASE 4
682       IDRAW X_gdu_max*.05,0
683       LABEL Line_4$
684     END SELECT
685   NEXT I
686   LINE TYPE 1
687   VIEWPORT .2*X_gdu_max,.6*X_gdu_max,.2*Y_gdu_max,.8*Y_gdu_max  !VIEWING ARE
A 20-60% OF X-WIDTH, 20-60% OF Y-HEIGHT
688   Xrange=Xmax-Xmin
689   Dx=Xrange/5
690   Yrange=Ymax-Ymin
691   Dy=Yrange/6
692   WINDOW Xmin,Xmax,Ymin,Ymax
693   IF Plot_flag=2 THEN
694     OUTPUT 705;"SP2"
695   END IF
696   AXES Dx/5,Dy/5,Xmin,Ymin,5,5,3
697   AXES Dx/5,Dy/5,Xmax,Ymax,5,5,3
698   IF Plot_flag=2 THEN
```

```
699     OUTPUT 705;"SP1"
700    END IF
701 !  GRID Dx,Dy,0,0,1,1                   ! GRID
702    CLIP OFF
703    FOR I=0 TO 30
704      MOVE Xmin-.3*Xrange,Ymin+Dy/5*I
705      IDRAW .015*Xrange,0
706    NEXT I
707    IF Plot_flag=2 THEN
708      OUTPUT 705;"SP2"
709    END IF
710    MOVE Xmin-.30*Xrange,Ymin
711    DRAW Xmin-.30*Xrange,Ymax
712    FOR I=0 TO 6
713      MOVE Xmin-.30*Xrange,Ymin+Dy*I
714      IDRAW .03*Xrange,0
715    NEXT I
716    IF Plot_flag=2 THEN
717      OUTPUT 705;"SP2"
718    END IF
719    FOR X=Xmin TO Xmax STEP Dx           ! LABEL UNIT FOR X AXIS
720      LORG 6
721      CSIZE 3.5
722      MOVE X,Ymin-Yrange*.025
723      LABEL X
724    NEXT X
725    FOR Y=Ymin TO Ymax STEP Dy           ! LABEL UNIT FOR Y AXIS
726      CSIZE 3.5
727      LORG 8
728      MOVE Xmin-Xrange*.02,Y
729      LABEL USING "#,Z.D";Y
730    NEXT Y
731    FOR Y=Ymin TO Ymax STEP Dy           ! LABEL UNIT FOR Y AXIS
732      CSIZE 3.5
733      LORG 8
734      MOVE Xmin-Xrange*.32,Y
735      LABEL USING "#,Z.D";Y
736    NEXT Y
737    FOR Y=Ymin TO Ymax STEP Dy           ! LABEL UNIT FOR Y AXIS
738      CSIZE 3.5
739      LORG 8
740      MOVE Xmax+.15*Xrange,Y
741      LABEL USING "#,Z.D";Y
742    NEXT Y
743    !
744    !
745    CLIP ON
746    CSIZE 2
747    LORG 5
748    IF Plot_flag=2 THEN
749      OUTPUT 705;"VS10"
750      OUTPUT 705;"SP2"
751    END IF
752    FOR I=1 TO Data_num
753      LINE TYPE 1
754      IF Plot_flag=2 THEN
755        OUTPUT 705;"SP"&VAL$(2+I)
756      END IF
757      FOR J=1 TO N_case
758        X=X_data(J)
```



```
759        Y=Y_data(I,J)
760        IF J=1 THEN
761          MOVE X,Y
762        END IF
763        DRAW X,Y
764      NEXT J
765      IF Data_num=1 THEN
766        GOTO Select_ploter
767        IF Plot_flag=2 THEN
768          OUTPUT 705;"SP0"
769        END IF
770      END IF
771    NEXT I
772    IF Plot_flag=2 THEN
773      OUTPUT 705;"SP0"
774    END IF
775    GOTO Select_plotter
776 Plot_end:  !
777    RETURN
778        !
779        !
780    !************************************************************************
781    !*     ERROR TRAP                                                      *
782    !************************************************************************
783    !
784 Error_trap:  !
785    !
786    IF Print_freq>0 THEN
787      PRINTER IS PRT
788      PRINT CHR$(12)
789      PRINTER IS CRT
790    END IF
791    DISP ERRN,ERRLN
792    KEY LABELS ON
793    END
     >>>>   Cross Reference   <<<<

*   Numeric Variables
A                      561  562  565
Abo                    282  332  442  447  453  464  466  476
Data_num               521  654  752  765
Dx                     689  696  697  719
Dy                     691  696  697  704  713  725  731  737
E                      280  331
Flux_ar                318  331  402  472  474
I                      151  173  175  186  219  328  358  367  368  369
                       370  371  372  373  435  436  437  439  440  442
                       445  446  448  453  460  461  464  466  472  473
                       474  475  476  482  483  499  602  603  605  609
                       610  612  614  617  618  620  623  626  629  630
                       632  635  636  638  654  656  659  661  665  669
                       674  685  703  704  706  712  713  715  752  755
                       759  771
I_p                    140  141  188  334  367  368  369  370  371  372
                       373  409  410  413  414  527  528  529  530  531
                       532
I_sp                   236  238  278  305  331  389  652
J                      757  758  759  760  764
Kb                     281
Max_run                151  277
```

```
N_case          137  140  141  334  409  410  527  528  533  757
N_o_in          317  332  401
O2_flow         141  217  309  330  332  393  410  412
O2_flow_int     137  141  245  247  410  528
O2_flow_max     137  249  251  514
O2_flow_step    137  141  253  255  375  410  528
P               125 <-DEF 345  358  368  435  436  437  499
P_f             126 <-DEF 368  413  525  530
P_f_max         525  530
Plot_flag       546  568  572  576  580  594  655  660  693  698
                707  716  748  754  767  772
Plot_flagl      198  265  267  546  547
Print_final     191  262  264
Print_freq      143  177  218  219  258  260  786
Q_in            342  345  358  435  452  455  478  499
Q_in_0          316  330  342  400  452
Qg              125 <-DEF 437  453  464  466
Qg_o            453  454  455  463  464  477
Qgs             476  477  478
Qt              125 <-DEF 436  442
Qt_a            446  447
Qti             125 <-DEF 346  358  373  453  460  464  466  472
                499
Qti_f           126.<-DEF 373  526  531
Qti_f_max       526  531
Ra              125 <-DEF 358  372  461  464  466  499
Ra_f            126 <-DEF 372  413
Screen          590 <-DEF
Sg              125 <-DEF 344  358  371  435  437  483  499
Sg_0            278  307  391  483  648
Sg_f            126 <-DEF 371  413
Site_t          291  442  446  474  476
Sp              239  241  306  345  390  435  646
St              125 <-DEF 343  358  370  435  436  448  482  499
St_0            242  244  308  343  392  482  650
St_f            126 <-DEF 370  413
Temp            289
Th              125 <-DEF 335  338  439  440  442  445  446  448
                472  473  474  475  476  482  483
Th_a            125 <-DEF 175  336  339  358  369  473  476  499
Th_f            126 <-DEF 369  413  529
Tm              126 <-DEF 367  413
X               719  722  723  724  758  761  763
X_data          127 <-DEF 528  758
X_gdu_max       600  603  618  620  623  630  636  645  647  649
                651  659  667  669  672  674  679  682  687
Xmax            514  688  692  697  719  740
Xmin            513  688  692  696  704  710  711  713  719  728
                734
Xrange          688  689  704  705  710  711  713  714  728  734
                740
Y               725  728  729  730  731  734  735  736  737  740
                741  742  759  761  763
Y_data          127 <-DEF 529  530  531  759
Y_gdu_max       601  603  610  612  618  620  623  630  636  645
                647  649  651  659  669  674  687
Yg_c            287  313  397  474
Ym_c            286  312  396  472  483
Ym_m            285  311  395  472  483
Ymax            512  690  692  697  711  725  731  737
```



```
Ymin            511  690  692  696  704  710  713  722  725  731
                737
Yrange          690  691  722

*  String Variables
Graph_title$    128 <-DEF 520  604
Line$           128 <-DEF
Line_1$         522
Line_2$         523
Line_3$         524  680
Line_4$         683
X_label$        128 <-DEF 516  637
Y_label_1$      128 <-DEF 517
Y_label_2$      128 <-DEF 518
Y_label_3$      128 <-DEF 519  631

*  Line Labels
Calculation     154  214 <-DEF
Data_transfer   176  366 <-DEF
Data_treat      200  509 <-DEF
Data_typein     135  234 <-DEF
Declaration     124 <-DEF
Det_speed       481 <-DEF
Draw_graph      552  555  569  573  577  581  589 <-DEF
Error_trap      121  784 <-DEF
Init_valiables  142  327 <-DEF
Main_cal_loop   139 <-DEF
Main_programm   133 <-DEF
Plot_data       201  540 <-DEF
Plot_end        583  776 <-DEF
Press           434 <-DEF 449
Print_condition 145  299 <-DEF
Print_data_0    146  354 <-DEF
Print_data_f    190  193  383 <-DEF
Print_out       216  221  496 <-DEF
Select_ploter   766
Select_plotter  549  557 <-DEF 585  775
Set_const       136  276 <-DEF
Sputter         470 <-DEF
Target          215  432 <-DEF

*  Line Numbers
   188          182

Unused entries =   13
```